

u^b

b
UNIVERSITÄT
BERN

Graduate School for Cellular and Biomedical Sciences

University of Bern

Artificial Intelligence in Neurodegenerative Diseases: Advancing Diagnosis and Prognosis

PhD Thesis submitted by

Leonor Serrano Lopes

for the degree of

Doctor of Medicine and Philosophy (MD,PhD)

Supervisor

Prof. Dr. Kuangyu Shi

Department of Nuclear Medicine

Faculty of Medicine of the University of Bern

Co-advisor

Prof. Dr. Claudio Bassetti

Department of Neurology

Faculty of Medicine of the University of Bern

Accepted by the Faculty of Medicine, the Faculty of Science and the Vetsuisse Faculty of the University of Bern at the request of the Graduate School for Cellular and Biomedical Sciences

Bern, Dean of the Faculty of Medicine

Bern, Dean of the Faculty of Science

Bern, Dean of the Vetsuisse Faculty Bern

Thesis Supervisor

Prof. Dr. Kuangyu Shi

Department of Nuclear Medicine

Inselspital, Bern University Hospital, University of Bern

Thesis Co-advisor

Prof. Dr. Claudio Bassetti

Department of Neurology

Inselspital, Bern University Hospital, University of Bern

Thesis Mentor

Prof. Dr. Anna Oevermann

Division of Neurological Sciences

Vetsuisse Faculty, University of Bern

External co-referee

Prof. Dr. Philipp Meyer

Department of Nuclear Medicine

Medical Center, University of Freiburg

“The enigma I will not explain – its ‘dark saying’ must be left unguessed... through and over the whole set another and larger theme ‘goes,’ but is not played.”

– Edward Elgar, 1899, about the *Enigma Variations*, Op. 36

The brain remains an enigma, its earliest signs of degeneration echoing a hidden theme, subtle, silent, and yet shaping the entire course of disease.

Abstract

Artificial Intelligence in Neurodegenerative Diseases:
Advancing Diagnosis and Prognosis

By Leonor Lopes

Neurodegenerative disorders are the major cause of disease and disability worldwide, with increasing prevalence and major social and economic impacts. Parkinson's Disease (PD) is the fastest growing neurodegenerative disorder. With the accelerated ageing of the population, there is a growing need for more accurate diagnostic methods at early stages of the disease and especially to predict its future development before the first symptoms appear. Isolated REM Sleep Behaviour Disorder (iRBD), being one of the most important prodromal markers of PD, is the ideal condition to study the disease progression and final phenoconversion.

This thesis aims to develop artificial intelligence (AI)-based biomarkers for PD and iRBD using both molecular imaging (PET and SPECT) and wearable actigraphy.

The work began by addressing a critical barrier in multicenter imaging studies: the incompatibility between PET and SPECT modalities. A CycleGAN-based domain adaptation model was developed to translate dopaminergic PET into synthetic SPECT images, enabling data harmonization and downstream AI-based diagnostic tasks across imaging platforms. Building on this harmonized imaging foundation, pretrained deep learning models were applied to longitudinal DAT and FDG PET scans of patients with iRBD. These models produced deep imaging risk scores that quantified the likelihood of phenoconversion and captured disease progression over time. Finally, to explore scalable and non-invasive biomarker alternatives, wearable actigraphy data were analyzed using both traditional machine learning and deep learning methods (including a pretrained transformer) with the aim of classifying PD subtypes and explore application to iRBD individuals.

CycleGAN-generated synthetic SPECT images preserved disease-relevant information and enabled accurate downstream PD classification, demonstrating effective cross-modality

translation. The PET-based DIRS models predicted phenoconversion of iRBD with high accuracy, particularly for DAT PET ($AUC > 0.93$ up to 8 years). Actigraphy-based models, especially the transformer model, achieved excellent classification performance ($AUC > 0.96$) and successfully distinguished PD subtypes. Scores for iRBD patients suggested the potential utility of the model in identifying individuals at high risk for PD conversion.

This thesis demonstrates that AI models applied to multimodal data – molecular imaging and wearable sensor recordings – can serve as effective and interpretable biomarkers for early detection, diagnosis, and prognosis of Parkinson's disease. By addressing modality harmonization, longitudinal prediction, and remote digital monitoring, the findings support the development of personalized, and scalable tools for clinical use in neurodegenerative disease management.

Keywords: Parkinson's Disease; Isolated REM Sleep Behavior Disorder; PET; SPECT; Actigraphy; Artificial Intelligence; Deep Learning; Biomarker; Phenoconversion; Domain Adaptation.

Acknowledgements

My PhD journey was a vast, complex and memorable symphony, with many movements, different tempos, rhythms, melodies, harmonies and disarmonies. Born in a family of musicians, I learned that every great symphony cannot be played without a fantastic orchestra behind, composed of amazing people. My PhD symphony could not have been played without the help from many, to whom I would like to express my sincere gratitude.

First and foremost, I would like to thank my supervisor, Prof. Kuangyu Shi, for his support, guidance, and always enthusiastic encouragement throughout the course of my PhD. I am also grateful to my co-advisor, Prof. Claudio L.A. Bassetti, my mentor Prof. Anna Oevermann, and my external co-referee, Prof. Philipp Meyer, for their valuable feedback and thoughtful discussions. A special thanks to Dr. Carolin Schäfer and Dr. Robert Seifert for the great collaborations, incredibly useful scientific and clinical inputs as well as encouragement and friendship over the last years.

Entering a new field can be challenging, but the journey is made infinitely better with a great and supportive group. To all my colleagues and friends from the AITT group, specially Song, Christoph, Carlos, Jiaxi, Marc, Jiaying and Yizhou, a big thanks for accompanying me during this journey, for the academic and life discussions, for the dinners and parties, but specially for all the help along the way. To Jimin and Lara, thank you for the long conversations, for listening to my complaints and complaining back, for the welcome distractions, and most of all, for always being there. To the new AITT colleagues, specially Kaly, Alex, Narendra and August, thanks for your instant friendship and warmth these past months.

A big *obrigada* to all my friends and family from Portugal, that however far away in distance, always make me feel close. From my oldest friends from Aveiro – Inês, Mariana, Carolina, Gabriel, Melly, Sérgio, Iscas, Bernardo, Quina, Jorge, Elitza e António – to my friends from Coimbra – Bogdana, Filipa, Berna, Rita, Fred, Joana Sayal, Inês Sequeira, Inês Pereira, Júlio, Gatões e Chichorro – thanks for keeping the friendship alive, for the dinners, coffees,

beers, concerts... To my family from São Pedro, specially Susana, Conceição, Adelino, Fernando, Marta, Mariana and Afonso, I thank for the constant support and proudness, but also for all the fun camping trips and delicious lunches that go until nightfall. To Lio, thank you for the closest and most magical friendship I could have asked for during the last 25 years. Your unconditional presence and support, specially in the darkest times, has always remind me to turn on the light. Mischief managed.

Arriving in a new country is never easy. Finding home in a new country is even harder. For this, I send a big thanks to all the friends I made here in Switzerland that made me feel welcome and at home during the last almost 4 years, specially Samuel, Raúl, Ana Rita, André, Cata, Raquel Calçada, Daniela, Raquel Mendes, Beatriz, António. Thank you for all the crazy hikes, fun board game nights and tasty portuguese dinners, but also for the interesting discussions and support during this journey. To Ahmed, Anil, Pragnya and Jöel, thank you for teaching me so much about the world and for being among the kindest people I've had the privilege to meet. A special thanks goes to Samuel and Raúl for the close and constant friendship over the past years and also for taking the time to review parts of this thesis.

Of course this thesis would not be possible without the unconditional support from my family. To my mother, Ana, my father Domingos and my grandmother Céu, I express my deepest gratitude. Your strength, perseverance, and the way you've built a beautiful life through determination and love continue to inspire me every day. Thank you for all the celebrations, dinners, movies (more known as "sleep in the sofa" sessions), evening walks, life advice, passionate discussions. Thank you for your patience, for embracing both my highs and lows, and most of all, for shaping the life I'm so lucky to have. To Ricardo, for the love, dedication, and trust that I have only found with you. For making me keep going, for believing in me, and for standing by me with strength and conviction. You are the most brilliant and dedicated person I know, unafraid to live by your values. What we share goes beyond words, but I thank you for everything, and for more than I could ever say.

Table of Contents

1.	<i>Introduction</i>	1
1.1.	Brain Health	1
1.2.	Neurodegenerative Disorders.....	3
1.3.	Parkinson's Disease	8
1.4.	Prodromal Parkinson's Disease	19
1.5.	Isolated REM Sleep Behaviour Disorder	20
1.6.	Prediction and Prevention	23
1.7.	Molecular Imaging	24
1.8.	Actigraphy	41
1.9.	Artificial Intelligence.....	46
2.	<i>Hypothesis and Aims</i>	65
3.	<i>Results</i>	69
3.1.	Cross-Modality Translation of Dopaminergic Imaging for AI-based Biomarker Development.....	69
3.2.	Prediction of iRBD conversion using PET-based Deep Learning	95
3.3.	Diagnosis and Prediction of PD on Actigraphy	119
4.	<i>Discussion and Outlook</i>	145
4.1.	Discussion.....	145
4.2.	Outlook.....	152
5.	<i>Bibliography</i>	157

Table of Figures

Figure 1.1. Infographic depicting the burden of neurological disorders in Europe and globally.....	4
Figure 1.2. Hallmarks of neurodegenerative disorders.	7
Figure 1.3. Braak stages of Parkinson's Disease Pathology	12
Figure 1.4. Hypothetical sequences of signs and biomarkers in PD stages	15
Figure 1.5. Scheme of a SPECT scanner design and functionality.....	25
Figure 1.6. Scheme of a PET scanner design and functionality.....	26
Figure 1.7. Typical 18F-FDG PET findings in individual patients with parkinsonism as depicted by the currently used image analysis methods	30
Figure 1.8. Schematic presentation of the Scaled Subprofile Model to calculate the disease-related patterns..	36
Figure 1.9. Dopaminergic scans of normal subject and Parkinson's disease patient.	39
Figure 1.10. Actigraphy representation	43
Figure 1.11. Evolution of AI in nuclear medicine	50
Figure 1.12. Convolutional Neural Networks operations	56
Figure 1.13. Schematic representation of ResNet architecture.....	57
Figure 1.14. Schematic representation of the Transformer's architecture.	58
Figure 1.15. Schematic figure of the basis of foundation models.	63
Figure 2.1. Schematic figure of the aims of this PhD thesis.....	65
Figure 3.1. Scheme of our Cycle GAN model	77
Figure 3.2. Performance of the DL classification model in NC vs PD classification in the real SPECT test set.....	82
Figure 3.3. Average Specific Binding Ratios of the synthetic SPECT, real SPECT, and real PET test datasets	84
Figure 3.4. Average contrast-to-noise (CNR) of the synthetic SPECT, real SPECT, and real PET test datasets.	85
Figure 3.5. Differences in Visual Grading Analysis Score (VGAS) between real and synthetic SPECT images....	86
Figure 3.6. Example of images of normal controls and Parkinson's disease from real PET, real SPECT, and synthetic SPECT	88
Figure 3.7. A schematic detailed explanation of the study pipeline	107
Figure 3.8. Longitudinal progression of FDG-based scores with iRBD disease progression until conversion	109
Figure 3.9. Longitudinal progression of DAT-based scores with iRBD disease progression until conversion....	109

Figure 3.10. FDG-based Models Prediction Performance for Disease Conversion.....	111
Figure 3.11. DAT-based Models Prediction Performance for Disease Conversion	112
Figure 3.12. 3D t-SNE representation of the features from the last layer of the DAT DL model.....	113
Figure 3.13. Actigraphy features per group.....	133
Figure 3.14 Classification performance of all methods in controls vs PD task.	135
Figure 3.15. Model interpretability for controls vs PD task.....	136
Figure 3.16. Classification performance of all methods in PD-noRBD vs PD-RBD task.....	138
Figure 3.17. Model interpretability for PD-noRBD vs PD-RBD task	139
Figure 3.18. PAT model scores for the 6 iRBD patients	140
Figure 4.1. α -synuclein PET imaging with [18F]ACI-12589 tracer in participants with α -synucleinopathies.....	154

Table of Tables

Table 3.1. Huashan Parkinsonian PET Imaging (HPPI) and Parkinson's Progression Markers Initiative (PPMI) datasets' size and corresponding training and testing splits' size per class/disease	78
Table 3.2. Diagnostic performance in terms of AUC, sensitivity, specificity, PPV, and NPV of individual readers on real and synthetic SPECT images.....	87
Table 3.3. Demographic data of all iRBD patients and subgroups.....	102
Table 3.4. Demographic data of all patients and subgroups	131

1. Introduction

1.1. Brain Health

Brain health can be pictured as the harmonious interplay of instruments within an orchestra, where each region of the brain contributes its unique melody, rhythm, and tone. In a healthy brain, these elements play together in a coordinate way, creating a balanced composition that supports individual physical and mental well-being, emotional resilience, and meaningful interpersonal social connections.^{1,2} Just as harmony in music elevates the collective beauty of a performance, nurturing brain health enhances the cohesion, vibrancy, and resilience of entire communities.

This comprehensive view aligns with the World Health Organization's (WHO) definition, which describes brain health as encompassing cognitive, sensory, social-emotional, behavioural, and motor domains, enabling individuals to achieve their full potential throughout life.³ Importantly, brain health is shaped by various factors, including physical health, safe environments, lifelong learning, social connection, and access to quality services, which influence how the brain develops, adapts, and responds to stress and adversity. Optimizing these factors not only promotes mental and physical health at an individual level but also generates positive social and economic impacts, ultimately benefiting society as a whole.⁴

Prevention, in particular, has gained increased attention in recent years, shifting the traditional medical focus from managing neurological diseases to proactively protecting brain health. Recent studies indicate that up to 40% of dementia cases could be prevented through effective interventions and lifestyle modifications, highlighting the critical importance of that proactive measures and health promotion strategies play in preserving brain health and preventing disease onset.^{5,6}

Despite these efforts, conditions affecting the brain and nervous system may still emerge throughout life. Effectively addressing the previously mentioned challenges requires multisectoral and interdisciplinary collaboration, embracing a holistic approach focused on promotion, prevention, treatment, care, rehabilitation, and active engagement with affected individuals, their families, and caregivers.

As societies worldwide experience longer lifespans and aging populations, maintaining brain health has become increasingly crucial to ensure that individuals remain productive, independent, and actively engaged across their lifespan.

1.2. Neurodegenerative Disorders

Neurodegenerative disorders represent a heterogeneous group of neurological conditions characterized primarily by the progressive degeneration and loss of neurons within the central or peripheral nervous system. This neuronal loss, together with the deterioration of the structure and function of neural networks, severely disrupts critical communication pathways within the brain, ultimately impairing cognitive, sensory, motor, behavioral, and emotional functions.⁷

1.2.1. Epidemiology

Neurological and neurodegenerative disorders immensely impact global health, contributing to worldwide mortality and disability. These conditions are now the leading cause of disease and disability globally. Collectively, neurological disorders affect approximately 3.40 billion people worldwide, representing about 43.1% of the population. Specifically, Alzheimer's disease (AD) and other dementia affects 56.9 million individuals, while Parkinson's disease (PD) impacts approximately 11.8 million people. Neurological disorders are responsible for around 11.1 million deaths, with dementia alone contributing to nearly 2 millions of these deaths. These conditions are the top contributor of global disability-adjusted life years, with about 443 million years of life lost due to disease in 2021.⁸

The societal and economic repercussions of neurodegenerative diseases are extensive, as displayed in Figure 1.1. The global costs associated with dementia alone increased 35% from 2010, with \$604 billion, to 2015, with \$818 billion US dollars. In 2030, the costs are expected to increase to approximately \$2 trillion dollars, highlighting the substantial economic burden posed by these conditions.⁹ Comparable increases are anticipated for other neurodegenerative disorders. Thus, there is an urgent need for effective prevention strategies, improved diagnostic approaches, and comprehensive management frameworks that can mitigate the considerable personal, familial, and societal burdens associated with neurodegeneration.



Definitions: * Years of Life Lost (YLL) and Disability adjusted Life Years (DALY)

NCDs: Noncommunicable Diseases

YLL: YLLs are calculated from the number of deaths multiplied by a global standard life expectancy at the age at which death occurs.

DALY: One DALY represents the loss of the equivalent of one year of full health. DALYs for a disease or health condition are the sum of the years of life lost due to premature mortality (YLLs) and the years lived with a disability (YLDs) due to prevalent cases of the disease or health condition in a population.

** Age standardised rate per 100,000 is used.

Figure 1.1. Infographic depicting the burden of neurological disorders in Europe and globally. From Bassetti et al., European Journal of Neurology, 2022.¹

1.2.2. Hallmarks of Neurodegenerative Disorders

Neurodegeneration is a complex process characterized by the progressive dysfunction and loss of neurons, typically associated with aging. Several interrelated hallmarks define the neurodegenerative process, which include pathological protein aggregation, synaptic and neuronal network dysfunction, aberrant proteostasis, cytoskeletal abnormalities, altered energy homeostasis, DNA and RNA defects, inflammation, and ultimately neuronal cell death.⁷ A summary of the hallmarks of the most common neurodegenerative diseases is given in Figure 1.2.

Pathological protein aggregation is a defining feature of various neurodegenerative diseases (NDDs), such as AD, PD, amyotrophic lateral sclerosis (ALS) or Huntington's disease (HD). The aggregation process involves misfolded proteins forming toxic assemblies that disrupt cellular function, either through gain-of-toxic-function mechanisms or by impairing

the protein's normal physiological roles.^{10,11} Nevertheless, protein aggregation alone cannot explain all the disease process.

Synaptic dysfunction, frequently occurring before noticeable neuronal loss, contributes significantly to the clinical symptoms of NDDs and results from disrupted neurotransmission, impaired calcium homeostasis, mitochondrial dysfunction, and energy deficits. A complex pattern of synaptic malfunctioning can be observed, both with hyper and hypo functioning synapses. Additionally, the previously mentioned protein aggregation can also accumulate inside synapses, both at pre or postsynaptic locations, leading to adverse effects.¹²

Furthermore, impaired protein clearance mechanisms, such as the ubiquitin-proteasome system and autophagy pathways, leads to the harmful accumulation of misfolded proteins and damaged organelles, exacerbating neuronal injury. These dysregulated systems are known to influence cell death pathways, eventually leading to neuronal death.¹³

Dysfunctions in axonal transport and cytoskeletal dynamics have been linked to neurodegeneration. Cytoskeletal abnormalities affect neurons' structural integrity and intracellular transport, leading to compromised energy metabolism, mitochondrial dysfunction, and impaired synaptic maintenance.¹⁴

Altered energy homeostasis, particularly involving mitochondrial dysfunction and reduced ATP availability, underlies many NDDs, causing neuronal stress through oxidative damage and disrupted metabolic processes, eventually leading to cell death. Energy homeostasis can be detectable through functional imaging modalities like FDG-PET, which is altered in almost all NDD.¹⁵

Genetic and epigenetic disturbances manifesting as DNA damage and dysregulated RNA metabolism further disrupt cellular homeostasis, promoting neuronal vulnerability and death.^{16,17} As known, RNA malfunctions can lead to disrupted protein production and aggregation.

Neuroinflammation, mediated by chronic activation of microglia and astrocytes, plays a critical role, exacerbating neuronal damage, disrupting synaptic connections, and fueling ongoing neurodegenerative processes. Neuroinflammation, driven by the persistent activation of microglia and astrocytes, is a key contributor to neurodegenerative process, amplifying neuronal injury, impairing synaptic integrity, and sustaining neurodegenerative

mechanisms. Activated astrocytes influence synaptic activity, regulate energy balance, promote protein misfolding, and contribute to neuronal loss, while also interacting with and modulating microglial behavior. In turn, activated microglia are implicated in aberrant synapse pruning in neurodegenerative diseases, which may lead to disturbances in neuronal network function.^{11,14}

Ultimately, the convergence of these hallmarks overwhelms neuronal resilience mechanisms, resulting in irreversible neuronal cell death – the defining endpoint of neurodegeneration. Understanding these interconnected pathological processes is crucial for developing targeted preventive and diagnostic strategies and also therapies capable of modifying the disease course and improving clinical outcomes across various neurodegenerative disorders.

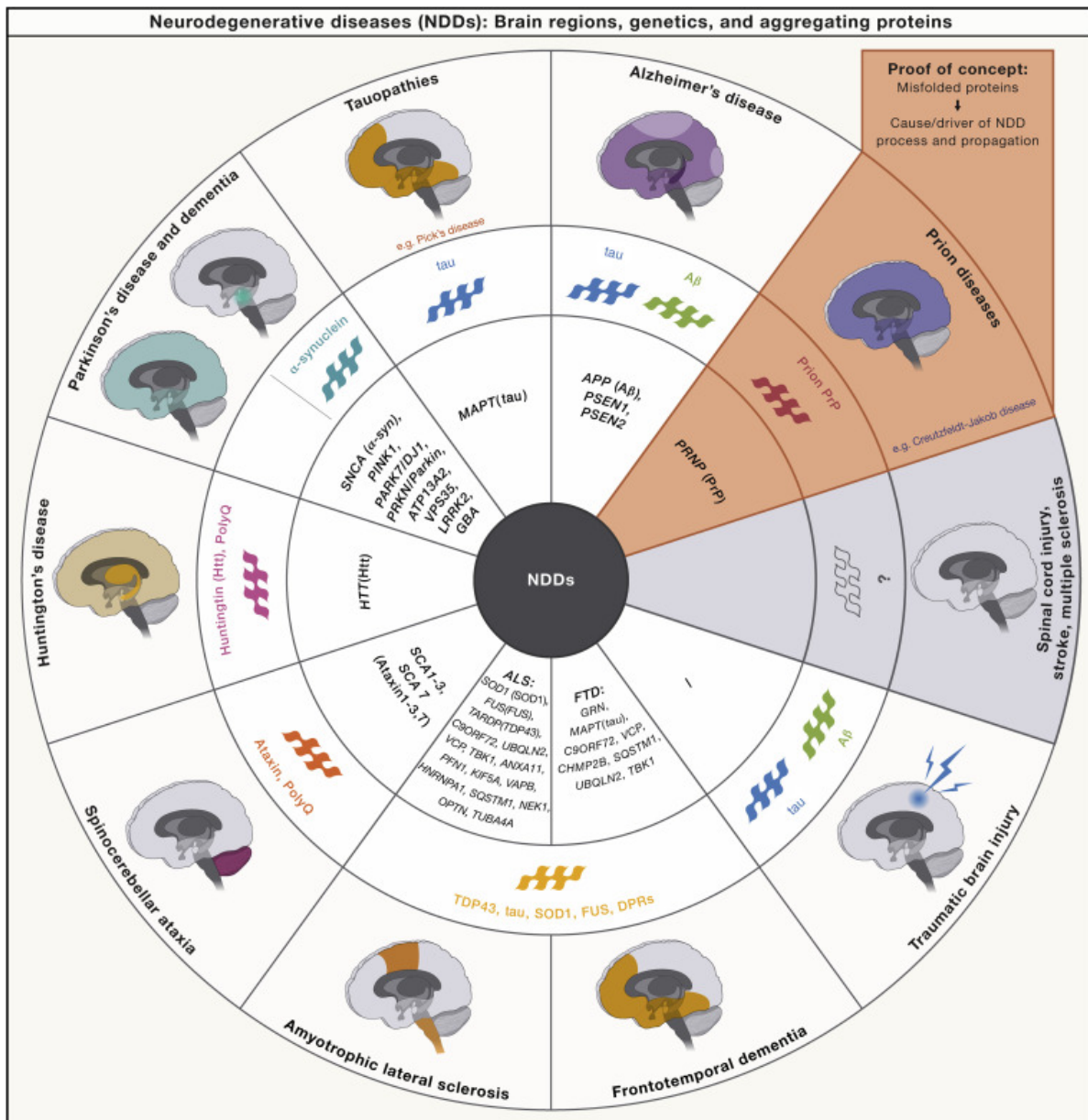


Figure 1.2. Hallmarks of neurodegenerative disorders. From Wilson et al., Cell, 2023.⁷

1.3. Parkinson's Disease

The first formal description of PD was already two centuries ago.¹⁸ Since then, our understanding of this prevalent neurodegenerative disorder has substantially evolved, encompassing detailed clinical and imaging phenotyping, precise neuropathological characterization, and genetic investigation.

The earliest systematic description of PD described patients exhibiting a unique pattern of clinical signs, including resting tremor, pronounced slowness (bradykinesia), rigidity or lack of voluntary movements, postural instability and freezing.¹⁹ Only half a century later, PD was established as a distinct neurological entity and recognized as the second most common neurodegenerative disorder after AD.²⁰

1.3.1. Epidemiology

PD is the second most common neurodegenerative disorder globally and the fastest-growing neurological condition in terms of prevalence. According to the Global Burden of Disease Study, the number of individuals living with PD worldwide reached approximately 11.8 million in 2021, reflecting a dramatic 273.9% increase since 1990.⁸ The median age at onset is approximately 66 years,²¹ with the incidence significantly rising with age.²² The incidence, prevalence, and mortality associated with PD are higher in men than in women, with a male-to-female ratio of about 1.4:1.²³

The causes underlying PD are multifactorial, involving a complex combination of genetic and environmental influences. Intrinsic determinants include genetic factors, metabolic conditions, and comorbidities like diabetes. Extrinsic determinants comprise environmental exposures, lifestyle behaviors, physical trauma, and infectious agents. Interactions between intrinsic and extrinsic factors – through mechanisms like epigenetic modifications, microbiome alterations, and additional comorbidities – further complicate disease etiology and progression.²⁴

Several risk and protective factors have been identified in PD. Factors associated with an increased risk include a positive family history of PD or dementia, depression, daytime somnolence, epilepsy, earlier menarche in women, non-smoking, and low alcohol consumption. In contrast, protective factors such as coffee and tea consumption (particularly in men), anti-inflammatory drug use, and regular physical activity are linked to a lower risk of developing PD.²¹ Among environmental risk factors, exposure to toxicants (including pesticides, solvents, and air pollution) has been consistently associated with an increase risk of PD.

Genetic factors play a crucial role in PD, with both familial and sporadic forms exhibiting genetic contributions. More than 20 genes have been identified in familial PD, while genome-wide association studies have uncovered over 200 genetic loci associated with sporadic PD, highlighting the complex genetic architecture of the disease. Among the well-established monogenic causes, three autosomal dominant genes – SNCA, LRRK2, and VPS35 – and three autosomal recessive genes – PRKN, PINK1, and DJ1 (PARK7) – have been linked to PD.²⁵ The identification of the SNCA gene led to the identification of α -synuclein as the hallmark of PD.²⁶ Indeed, an increased expression of SNCA mRNA and its encoded protein, α -synuclein, is sufficient to trigger neurodegeneration, emphasizing its central role in PD pathogenesis.²⁷ Mutations in LRRK2, particularly the common G2019S variant, are the most frequent cause of familial PD in Europe and the United States and are also found in sporadic cases.²⁸ In Japan, PRKN gene is the most frequent cause. It encodes an E3 ubiquitin-protein ligase, Parkin, that is important for the degradation of damaged mitochondria.^{29,30} While these genetic forms of PD provide valuable insights into disease mechanisms, they account for only a minority of total cases. The majority of genetic risk variants has incomplete penetrance and modest individual effects, highlighting the combined interaction between genetic predisposition and environmental or epigenetic factors.^{25,27}

1.3.2. Pathophysiology

α -Synuclein and Lewy bodies are the pathological hallmarks of PD. α -Synuclein is a protein that can bind lipid membranes and that is normally present in the synaptic terminals

of neurons. Its functions are, among others, vesical transport and neurotransmitter release.³¹ In PD, initially, α -synuclein forms small aggregates in the cytoplasm. These eventually coalesce into diffuse pale bodies that aggregate into filaments. These filaments will then form the Lewy body. The filaments are trap organelles such as mitochondria and lysosomes leading to synaptic dysfunction, cellular toxicity and death.²⁵

But why does α -synuclein accumulates and aggregates? This can result from a combination of genetic, environmental, and cellular factors that disrupt its normal homeostasis. As mentioned before, genetic mutations (e.g., in the SNCA gene) increase its propensity to aggregate. Impaired protein degradation pathways, including dysfunction of the ubiquitin-proteasome system (UPS) and autophagy-lysosomal pathway (ALP), contribute to its accumulation by reducing its clearance.³² Mitochondrial dysfunction, characterized by reduced complex I activity, abnormal calcium homeostasis, increased reactive oxygen species (ROS), and reduced ATP production, creates a cellular environment that promotes oxidative stress and facilitate the formation of soluble α -synuclein oligomers and insoluble fibrils.³³ Additionally, chronic immune activation and neuroinflammation is triggered by alpha-synuclein aggregates, mitochondrial antigens, and gut bacterial endotoxins, exacerbating neuronal toxicity.³⁴

Moreover, toxic forms of alpha-synuclein propagate between anatomically connected cells or spread over longer distances, potentially via extracellular vesicles, further amplifying pathology. Several studies have been performed in animal models where the injection of alpha synuclein in the periphery (for example the gut) is able to induce lesions in the brain and vice-versa.^{35,36}

Together, these mechanisms create a vicious cycle of alpha-synuclein accumulation, aggregation, and neuronal death in PD.

The characteristic motor symptoms arise when there is a compromise of a region called substantia nigra pars compacta (SNpc). This region has the cell bodies of neurons that project to the striatum, in the so called, nigrostriatal dopaminergic pathway.³⁷ With the loss of SNpc neurons there is a depletion of striatal dopamine. The striatum has 2 major pathways: a “direct pathway” to the substantia nigra pars reticulata and an “indirect pathway” to output

nuclei through the globus pallidus and subthalamic nucleus. The first one is thought to support initiation and performance of movement actions and the second one inhibits competing movements, but inconsistent evidence exists. Nevertheless, disruptions in both these pathways results in lack of voluntary movements in PD.³⁸

According to the Braak staging system,³⁹ and as displayed in Figure 1.3, the pathology originates in the dorsal motor nucleus of the vagus nerve (IX/X) and the anterior olfactory nucleus (Stage 1), regions that are highly interconnected with the peripheral nervous system. As the disease progresses, the pathology ascends the brainstem, affecting the locus coeruleus, raphe nuclei and other pontine nuclei (Stage 2), followed by the substantia nigra and basal forebrain (Stage 3), where the characteristic motor symptoms of PD begin to emerge. Further progression involves the anteromedial temporal mesocortex, including the transentorhinal and entorhinal cortices (Stage 4), leading to early cognitive deficits. Eventually, Lewy pathology goes into the neocortex, first affecting high-order sensory association and prefrontal areas (Stage 5) before spreading to primary sensory, motor, and premotor cortices (Stage 6), contributing to widespread cognitive and motor dysfunction. This stepwise progression suggests that PD may originate outside the dopaminergic system and only later involve the substantia nigra, reinforcing the hypothesis that non-motor symptoms such as autonomic dysfunction, olfactory impairment, and sleep disturbances may precede the classical motor phenotype by years or even decades. Despite being useful and explaining some of the progressive pathology in PD, many cases do not follow this proposed system.⁴⁰

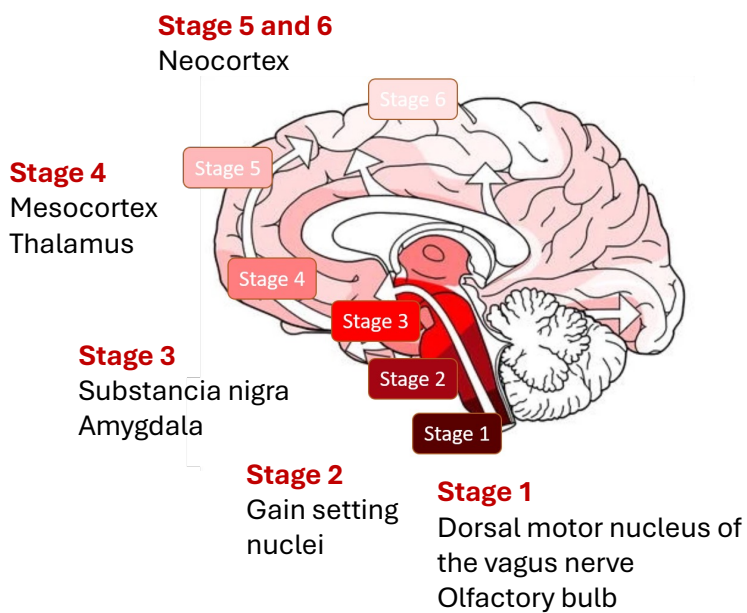


Figure 1.3. Braak stages of Parkinson’s Disease Pathology. Adapted from Braak et al., Neurobiology of Aging, 2003.³⁹

To address these inconsistencies, a new model was recently proposed. The body-first and brain-first hypothesis proposes that PD may develop through two distinct pathways, differing in the initial site of α -synuclein pathology and its subsequent spread throughout the nervous system. In the body-first subtype, pathology originates in the enteric or peripheral autonomic nervous system, propagating through autonomic pathways to the brainstem before affecting the substantia nigra and cortical structures.^{41,42} This progression aligns with post-mortem findings of caudo-rostral Lewy pathology, where the lower brainstem and autonomic structures exhibit greater pathological burden in early stages.⁴² Notably, patients with REM sleep behavior disorder (RBD) are more frequently associated with this subtype, as the pathology reaches the pons – a key structure in REM sleep regulation – before advancing to the nigrostriatal system.⁴³ Conversely, in the brain-first subtype, α -synuclein pathology emerges within the central nervous system, particularly in the olfactory bulb, limbic structures, or substantia nigra, before spreading to the peripheral autonomic nervous system.^{41,42} This pattern correlates with an amygdala-centered distribution of Lewy pathology, where the limbic system and dopaminergic structures show more pronounced degeneration than autonomic regions.⁴²

In summary, the pathophysiology of PD is characterized by the accumulation and aggregation of α -synuclein, leading to the formation of Lewy bodies, synaptic dysfunction,

and progressive neuronal loss – most notably in the nigrostriatal dopaminergic system. While the classical Braak staging framework highlights a stereotyped, ascending pattern of pathology, other studies supports a more heterogeneous disease process, as captured by the body-first and brain-first hypothesis. These findings clearly show the complex interaction of genetic, environmental, and systemic factors contributing to disease onset and progression, and help explain the wide variability in clinical presentation. A deeper understanding of these mechanisms is essential not only for early identification and classification of disease subtypes, but also for the development of more targeted diagnostic tools and disease-modifying therapies.

1.3.3. Diagnosis

The diagnosis of PD begins with establishing the presence of parkinsonism, characterized clinically by bradykinesia, plus at least one additional sign – tremor or rigidity.⁴⁴ Bradykinesia, a hallmark feature, presents as difficulty in fine motor tasks, reduced facial expression (hypomimia), reduced arm swing during gait, small handwriting (micrographia), and progressively slower and smaller movements upon repetitive tasks.⁴⁵ Tremor in PD typically occurs at rest, classically presenting as a low-frequency (4–6 Hz), asymmetric “pill-rolling” movement of the hands, though it may also affect other regions such as the jaw or legs. It usually starts in one side and progresses to involve both. Importantly, tremor is not mandatory for diagnosis, as a subset of patients never develop it.⁴⁶ Rigidity is detected through passive joint movements and characterized by a uniform and velocity-independent increased muscle tone. It is usually described as “lead-pipe” resistance or “cogwheel rigidity”. Patients frequently report associated unilateral pain or stiffness, commonly misdiagnosed initially as orthopaedic conditions such as frozen shoulder.^{46,47}

Non-motor symptoms, though often subtle or nonspecific, provide additional diagnostic support; these include early anosmia, constipation, depression, RBD, cognitive impairments (particularly affecting attention, executive function, visuospatial skills, and memory), autonomic dysfunction (urinary urgency, orthostatic hypotension), and neuropsychiatric manifestations like anxiety or psychosis.⁴⁸ The presence of these symptoms, along with a positive clinical response to levodopa (especially improvement in bradykinesia and rigidity)

reinforces the diagnosis of PD.⁴⁴ Additionally, dyskinesias or choreiform movements arising with ongoing dopaminergic therapy further confirm this clinical suspicion.

Finally, disease progression is integral to diagnosis. A hypothetical diagram of PD disease progression with corresponding signs and biomarkers is shown in Figure 1.4. PD typically evolves gradually, with symptoms steadily worsening over years. Although the rate varies significantly among individuals, the presence of progressive deterioration, such as increased gait impairment, festination, freezing episodes, postural instability, and greater dependency, confirms a diagnosis of PD.⁴⁹ Regular monitoring to ensure a characteristic trajectory of progression is therefore essential in affirming and maintaining an accurate clinical diagnosis.

For more objective clinical assessments and for longitudinal monitoring of the disease, clinical rating scales are commonly used. One of first well validated scales was the Unified Parkinson's Disease Rating Scale version 3.0 (UPDRS), published in 1987.⁵⁰ It evaluates impairment and disability related to PD and combines the most important aspects of previous used scales. It allowed for comparability between clinical trials. In the earliest 2000s, the Movement Disorder Society (MDS) reviewed the previous guideline and improved it, creating the MDS-UPDRS.⁵¹ The official English version was published in 2008 along with extensive clinical validation, and since then, MDS-UPDRS is the official benchmark clinical scale used in PD.⁵² The Hoehn and Yahr Staging Scale (HY) is also widely used, due to its simplicity. It classifies patients into one of five stages of disease - 1 (unilateral involvement, usually with minimal or no functional impairment) to 5 (confined to bed or wheelchair unless aided).⁵³ Other scales with different goals exist, such as the Clinical Impression of Severity Index (CISI-PD), to assess disease severity,⁵⁴ the Scales of Outcomes in Parkinson's Disease-Motor (SCOPA-Motor), for motor assessment,⁵⁵ the Self-Assessment Parkinson's Disease Disabilities Scale (SPDDS), to assess the patients' ability to perform daily activities,⁵⁶ and many more. A review can be found in Bhidayasiri and Martinez-Martin, 2017.⁵⁷

Imaging modalities play a supportive but crucial role in the diagnosis and differential diagnosis of PD. Brain MRI is recommended early in the disease course.⁵⁸ Transcranial sonography may further aid differentiation by assessing characteristic echogenic patterns in structures like the substantia nigra, nucleus lentiformis, and third ventricle.⁵⁹ Dopamine transporter SPECT (DaT-SPECT) is useful for detecting nigrostriatal dopamine deficits,

particularly in clinically ambiguous parkinsonian or tremor syndromes.⁶⁰ FDG-PET imaging can also be considered in cases suggestive of atypical parkinsonian disorders or when evaluating dementia risk in PD.^{61,62}

Following the clinical identification of parkinsonism, other potential causes must be excluded through careful examination and patient history, looking specifically for atypical features that might suggest alternative diagnoses.

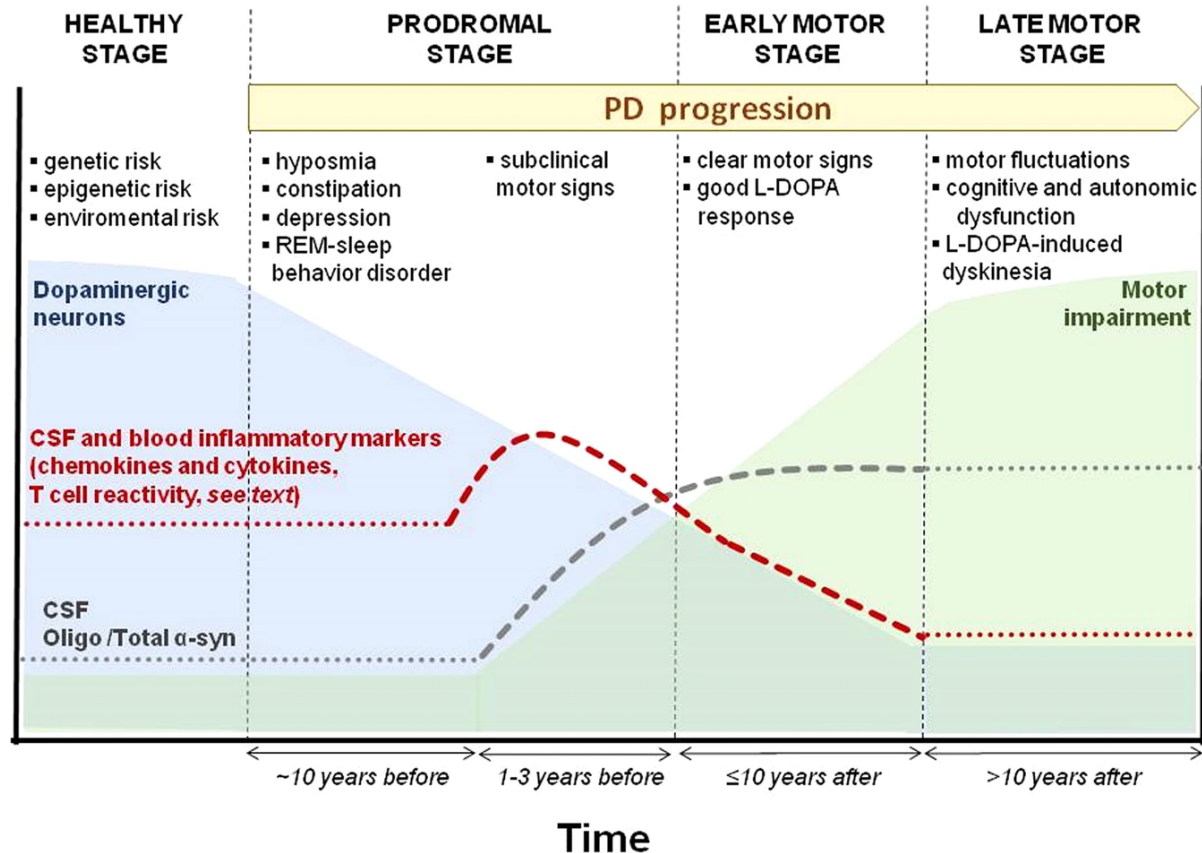


Figure 1.4. Hypothetical sequences of signs and biomarkers in PD stages. In Calabresci et al., Cell Death & Disease, 2023.³⁴

1.3.4. Differential Diagnosis

PD shares clinical features with several other neurological disorders, making differential diagnosis critical yet often challenging, particularly in early stages.

Dementia with Lewy Bodies (DLB) represents one of the most common mimics of PD. DLB is characterized by early cognitive impairment, marked fluctuations in attention, visual hallucinations, RBD, and parkinsonism. The key distinguishing feature is the timeline of cognitive decline; cognitive symptoms precede or appear concurrently with motor symptoms within the first year, distinguishing DLB from Parkinson's disease dementia (PDD), where dementia develops after established parkinsonism.⁶³

Multiple System Atrophy (MSA) is another α -synucleinopathy often confused with PD. It features rapidly progressive parkinsonism poorly responsive to levodopa, significant autonomic dysfunction (orthostatic hypotension, urinary disturbances, erectile dysfunction), cerebellar ataxia, and corticospinal signs. Unique features include pronounced early autonomic symptoms, respiratory stridor, cerebellar symptoms, and a positive Babinski sign. MRI findings, such as the “hot cross bun” sign, can support this diagnosis. It can be divided into 2 types: MSA with predominant parkinsonism (MSA-P) and MSA with predominant cerebellar ataxia (MSA-C).⁶⁴

Progressive Supranuclear Palsy (PSP), a tauopathy, typically presents with symmetrical parkinsonism involving axial rigidity, early falls (often backwards), and characteristic abnormalities of vertical eye movements (particularly slowed vertical saccades). PSP also involves early cognitive deficits, predominantly affecting executive function, apathy, and impulsivity. Poor levodopa responsiveness and imaging findings such as midbrain atrophy (the “hummingbird sign”) further support the diagnosis.⁶⁵

Corticobasal Degeneration (CBD), another tauopathy, is marked by strongly asymmetric rigidity and bradykinesia, usually accompanied by cortical dysfunction such as apraxia, aphasia, cortical sensory loss, alien limb phenomena, dystonia, and myoclonus. This combination of extrapyramidal symptoms and cortical dysfunction, coupled with poor levodopa responsiveness, distinguishes CBD from typical PD.⁶⁶

Drug-induced Parkinsonism is a common secondary cause, typically arising from dopamine receptor-blocking medications such as antipsychotics and certain antiemetics. Symptoms usually appear symmetrically, and most importantly, symptoms often resolve after discontinuation of the causative drug, although some patients might unmask underlying idiopathic PD.⁶⁷

Vascular Parkinsonism arises from cerebrovascular lesions affecting basal ganglia structures or their connections, frequently resulting in bilateral lower-limb predominant symptoms, with a characteristic wide-based gait and minimal tremor. MRI showing extensive vascular lesions and a normal dopamine transporter scan help differentiate this from idiopathic PD.⁶⁸

Essential Tremor (ET) is a common tremor disorder characterized by bilateral, predominantly upper limb tremor occurring during sustained postures or voluntary movements, such as writing or holding objects. ET typically progresses slowly and may begin at any age, though incidence increases with advancing age. Unlike the classical rest tremor of PD, ET improves temporarily with small amounts of alcohol and worsens with anxiety, fatigue, or illness. ET frequently has a strong familial component. Although usually distinct from PD, differentiation can become challenging, especially since some patients with PD may also exhibit postural action tremors. In ambiguous cases, dopamine transporter imaging can be useful, as it is typically normal in patients with ET but abnormal in PD.⁶⁹

Some other non-neurological causes that can mimic some of PD symptoms include arthritis, due to pain and joint stiffness mimicking PD rigidity and bradykinesia, depression, due to psychomotor slowing, reduced facial expression, fatigue, and apathy, and psychogenic parkinsonism, a somatoform disorder characterized by effortful motor slowing and rigidity that improve significantly with distraction.

1.3.5. Treatment

Treatment strategies for PD primarily focus on symptom management, given the current lack of proven disease-modifying therapies. Pharmacological therapy is adapted based on the patient's age, symptom severity, comorbidities, side-effect profiles, and psychosocial considerations.

Levodopa remains the most effective medication for controlling PD symptoms but can lead to early motor fluctuations, particularly at higher doses or in younger patients. Therefore, younger patients are often started on alternative treatments, such as dopamine agonists (e.g., pramipexole, ropinirole, rotigotine) or MAO-B inhibitors (selegiline, rasagiline), to delay

motor complications. When initial monotherapy is insufficient, combination therapy with levodopa, dopamine agonists or MAO-B inhibitors is considered.⁷⁰

To manage motor fluctuations, adjusting levodopa dosing frequency or adding extended-release or rapidly soluble levodopa forms, dopamine agonists, MAO-B inhibitors, or COMT inhibitors is recommended. Amantadine is indicated for treating levodopa-induced dyskinesias. Severe or refractory tremor may require dosage adjustments of levodopa or dopamine agonists, cautious use of anticholinergics, or advanced therapies such as deep brain stimulation (DBS).⁷⁰

Additionally, non-motor symptoms should be addressed accordingly, namely pain, autonomic dysfunctions, sleep problems, cognitive disorders and psychiatric conditions, among others. A review can be found in Seppi et al., 2018.⁷¹

Invasive procedures are indicated when medication-optimized patients continue to experience significant levodopa-dependent motor fluctuations. DBS of the subthalamic nucleus is recommended for patients whose symptoms show at least 33% improvement in standardized levodopa testing and who lack contraindications such as cognitive impairment, severe psychiatric symptoms, or other significant comorbidities. In cases where DBS is unsuitable, pallidotomy may be considered for advanced PD with difficult-to-control motor complications.^{70,72} Treatment decisions should always consider motor and non-motor symptom profiles, patient characteristics, and individual preferences.

1.4. Prodromal Parkinson's Disease

As mentioned before, the pathological process of PD is thought to start years before the main motor symptoms arise and before the substantia nigra is affected. The prodromal phase represents an early stage of the disease, during which underlying neurodegeneration is already occurring but has not yet progressed enough to meet clinical diagnostic criteria for PD. During this period, non-motor symptoms—such as hyposmia, constipation, and RBD—can emerge, often preceding motor symptoms by years or even decades.⁷³ This is supported by Braak's hypothesis suggesting that PD pathology originates in extranigral structures, such as the olfactory system, lower brainstem, and autonomic nervous system, before spreading to the substantia nigra.³⁹

To better identify individuals at risk for developing PD, the Movement Disorder Society (MDS) prodromal criteria were developed.⁷⁴ These criteria estimate an individual's likelihood of prodromal PD based on a Bayesian classification system that integrates age-based baseline probability with additional risk factors. These include environmental exposures, genetic predisposition, and diagnostic biomarkers. When the calculated probability exceeds 80%, the individual is classified as having probable prodromal PD.

Olfactory dysfunction has been reported in up to 80% of PD patients, and large population studies have shown that individuals with impaired olfaction have a significantly increased risk of developing PD within three to four years. However, this association weakens over longer timeframes.⁷⁵

Constipation is another well-established prodromal feature, affecting up to 61% of PD patients. The Honolulu-Asia Aging study found that individuals with bowel movements less than once per day had increased risk of developing PD. Moreover, post-mortem studies have linked constipation with an increased presence of incidental Lewy bodies in the substantia nigra.⁷⁶ Emerging evidence also suggests that α -synuclein pathology in the enteric nervous system may contribute to bowel dysmotility in PD.⁷⁷

RBD is a highly predictive biomarker of prodromal PD and it will be discussed in the next chapter.

1.5. Isolated REM Sleep Behaviour Disorder

RBD is characterized by abnormal behaviors, such as repetitive dream enactments, including motor behaviors, jerks, and/or vocalizations during REM sleep. These episodes are often associated with REM sleep-related dream content and result from an excess of muscle tone and/or phasic muscle twitching during REM sleep. These episodes typically occur during the latter half of the sleep period when REM sleep is more prevalent. The hallmark feature of RBD is REM sleep without atonia (RSWA), in which the typical muscle paralysis of REM sleep is absent.⁷⁸

According to current knowledge, RBD can manifest in two forms. It can appear as an isolated form (isolated RBD, iRBD), which is recognized as an early stage of α -synucleinopathy. Alternatively, RBD may be associated with other diseases, such as overt α -synucleinopathies, including PD, DLB and MSA. In these cases, it is referred to as secondary RBD.⁷⁹

The iRBD patients are usually diagnosed at 50-80 years-old, documenting a history of about 1-10 years of symptoms. The prevalence of iRBD in the general population is documented to be approximately 1%,^{80,81} with a male to female ratio of 2:1.⁸² However, in neurodegenerative disorders, particularly in its secondary form, the prevalence is significantly higher. It occurs in 25–58% of patients with PD, 70–80% of patients with DLB, and 90–100% of patients with MSA. Additionally, the use of certain medications can trigger RBD or RSWA.^{83–85} Most patients don't seek medical attention (as they believe it is normal and benign or are unaware of the behaviors) so the prevalence is thought to be higher.

Diagnosis involves a thorough clinical history and is confirmed through polysomnography (PSG) with video recording, which documents the loss of REM-related muscle atonia and the presence of abnormal behaviors during sleep, according to the International Classification of Sleep Disorders, Third Edition (ICSD-3).⁸⁶ As patients may act out violent dreams, exhibiting behaviors such as punching, kicking, and shouting, these episodes can cause injuries to themselves or bed partners, sometimes leading to abrasions, fractures, or other trauma.

RBD is also often associated with early motor and non-motor abnormalities characteristic of neurodegeneration. Patients may exhibit mild bradykinesia and subtle

hypomimia, suggesting early motor impairment. Additionally, asymptomatic cognitive dysfunction, hyposmia, autonomic disturbances such as constipation, urinary dysfunction, and erectile dysfunction, as well as psychiatric symptoms, including depression and anxiety, are commonly observed.^{79,87} In PD, the presence of RBD is linked to a more severe disease course. Patients with both PD and RBD frequently exhibit the rigid-akinetic form of parkinsonism, experience more non-motor symptoms and hallucinations, and demonstrate a more rapid progression to dementia, motor disability, and increased risk of falls.^{88–90}

Despite its clinical significance, the mechanisms underlying RBD remain incompletely understood. Given that the disorder is defined by the loss of REM sleep atonia, the brainstem circuits responsible for REM sleep muscle inhibition are believed to play a central role in its pathophysiology. The key neural structures involved include the subcoeruleus nucleus (sublaterodorsal tegmental nucleus, SLD, in mice) and the nuclei in ventral medial medulla (VMM). RBD is hypothesized to result from synucleinopathic degeneration affecting these REM sleep circuits. Pathological α -synuclein accumulation is thought to originate in the caudal brainstem and progress rostrally over time. In the early, prodromal stages of disease, pathology develops in the brainstem regions that regulate REM atonia, particularly the SLD neurons and VMM neurons. Under normal conditions, SLD cells activate VMM neurons, which in turn inhibit spinal motoneurons to induce REM sleep muscle atonia. However, in RBD, α -synuclein-mediated dysfunction in these cells disrupts this pathway, leading to the characteristic loss of REM sleep atonia and the emergence of dream enactment behaviors.⁹¹ As the disease progresses, pathology spreads to regions traditionally affected in α -synucleinopathies, including the substantia nigra and corticolimbic circuits, contributing to the motor and non-motor impairments observed in PD, DLB, and MSA.⁹²

iRBD is now recognized as one of the strongest clinical predictors of future neurodegeneration. Studies indicate that up to 80–90% of iRBD patients will develop a neurodegenerative disorder within 10–15 years. The conversion rate to an overt α -synucleinopathy is about 6.3% per year. Several clinical and neurobiological markers have been identified as potential predictors of conversion to PD or DLB. Abnormal motor function, olfactory dysfunction, mild cognitive impairment, erectile dysfunction and evidence of dopaminergic dysfunction detected by DAT-SPECT or PET imaging are among the strongest

indicators of disease progression. Additionally, increased RSWA severity on PSG, constipation, colour vision problems, and age, have been linked to a higher risk of conversion.⁹³

Management of RBD focuses on ensuring safety and alleviating symptoms. Physical safeguards include modifying the sleep environment to prevent injury, such as removing dangerous objects and placing barriers around the bed. Pharmacological treatments commonly involve clonazepam, which has been shown to effectively reduce symptoms. However, clonazepam may cause side effects such as daytime sleepiness and decreased balance. Melatonin is also used as a treatment option and may have fewer side effects.⁸³

1.6. Prediction and Prevention

We can now identify patients at risk of developing PD. But the key question remains: should we?⁹⁴ As previously mentioned, no disease-modifying treatment is currently available for PD, meaning there is no specific therapy to offer these patients. Furthermore, the psychological burden and potential distress associated with such a diagnosis, along with the risk of false positives, must be carefully weighed when considering the overall benefit of early disclosure.

On the other hand, waiting until clinically definite symptoms appear may be too late to stop disease progression, as significant brain pathology and dysfunction have already occurred at that stage. Identifying individuals in the prodromal phase is also crucial for targeted recruitment into disease-modifying trials.⁹⁵ Additionally, symptomatic treatments are improving and can help maintain a good quality of life.

There is also growing evidence supporting non-pharmacological interventions, such as increased physical activity, for individuals with prodromal features of PD, including iRBD. Research suggests that intense physical activity may have disease-modifying effects, while the associated risks and costs remain low.⁹⁶

Ultimately, the benefits of identifying the prodromal stage and predicting future disease must be carefully balanced against potential drawbacks. This decision should be individualized and guided by shared decision-making principles, applying the ethical values of autonomy, beneficence, and non-maleficence. The goal should not necessarily be an "early" diagnosis, but rather a "timely" one.

What is clear, however, is that we must have the necessary methods in place for when the time comes—when early identification and intervention become the standard approach to stopping disease progression.

1.7. Molecular Imaging

Imaging has long been the primary method for visualizing the inside of the human body. Anatomical imaging reveals the basic structure and location of organs and lesions based on their physical properties, such as density or water content. This field began with Wilhelm Roentgen's groundbreaking discovery of X-rays and has since evolved to include more advanced techniques like Computed Tomography (CT) and Magnetic Resonance imaging (MRI). While these methods are essential for many diagnostic workflows, they primarily provide structural information and do not directly assess organ or tissue function.

Over the past decades, molecular imaging has reshaped healthcare as it allows the visualization and quantify several biological processes. This is achieved by labelling a biologically active molecule—such as glucose—with a radioactive isotope. The resulting compound, called a radiotracer, is injected into the body, where it behaves according to the biological activity of the labelled molecule. As the radioisotope decays, it emits radiation that can be detected externally, allowing the reconstruction of functional or molecular images that reflect physiological processes.

The two main modalities of molecular imaging are Positron Emission Tomography (PET) and Single Photon Emission Computed Tomography (SPECT). Both were developed in the 1950s and 1960s along similar timelines. Interestingly, their first clinical applications were in brain imaging, particularly for assessing brain tumors and cerebral perfusion. These techniques initially lacked precise anatomical localization, and to address this, hybrid imaging systems such as PET/CT and SPECT/CT were introduced in the late 1990s, combining anatomical and functional imaging in a single session. This integration enables the accurate localization of functional activity within specific anatomical structures.⁹⁷

1.7.1. SPECT imaging

SPECT imaging is a nuclear medicine technique that uses gamma-emitting radioisotopes to visualize physiological processes in the body. The most common ones include ^{99m}Tc , ^{123}I , ^{131}I and ^{67}Ga .⁹⁸ After the radiotracer is administered, it emits gamma photons, which are detected by a gamma camera. This camera uses a collimator to allow only photons

traveling in specific directions to reach the detector, forming a projection of the radiotracer distribution. A schematic representation of SPECT scanner is given in Figure 1.5. The image quality is largely determined by the design of the collimator. To generate three-dimensional images, the gamma camera head is rotated around the patient, collecting projection data from different angles. These data are then reconstructed into tomographic images of the tracer's distribution in tissues, similar to the process used in CT imaging. SPECT imaging is often performed with a full 360-degree rotational scan and is now commonly integrated with CT in SPECT/CT systems. The CT component provides anatomical reference, improving localization and interpretation of the functional data obtained from SPECT.^{97,99}

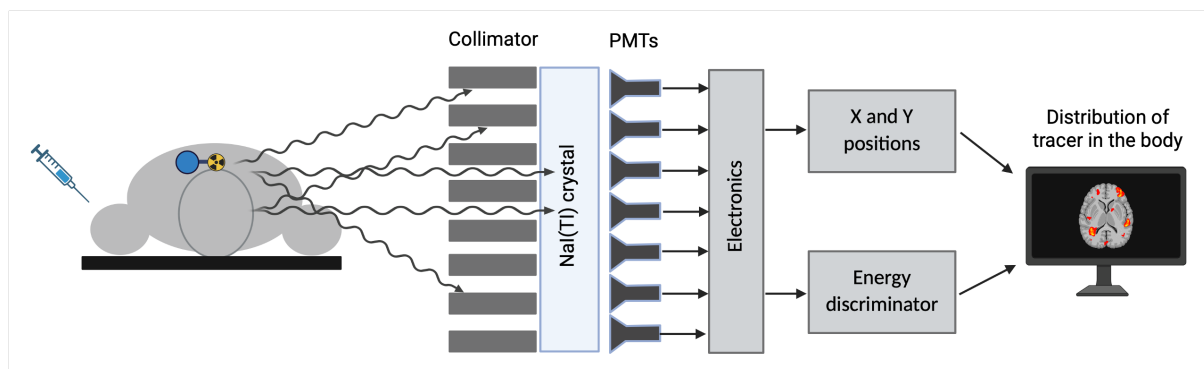


Figure 1.5. Scheme of a SPECT scanner design and functionality. Created in BioRender.

1.7.2. PET imaging

PET is a more sensitive and quantitatively accurate molecular imaging technique that utilizes positron-emitting radioisotopes. The most common ones are ^{11}C and ^{18}F .^{98,100} When these isotopes decay, they emit positrons that travel a short distance before encountering electrons in the tissue. The resulting annihilation event produces a pair of gamma photons that travel in opposite directions (180 degrees apart). A schematic image of a PET scanner is displayed in Figure 1.6. These photons are detected in coincidence by a ring of detectors surrounding the patient. The collected data are reconstructed into detailed three-dimensional (3D) maps of the radiotracer distribution, enabling precise measurement of biological processes such as glucose metabolism, receptor binding, or protein aggregation.

PET is also routinely combined with CT or MRI to create hybrid PET/CT or PET/MRI systems that provide both functional and anatomical information in a single imaging session.^{99,101}

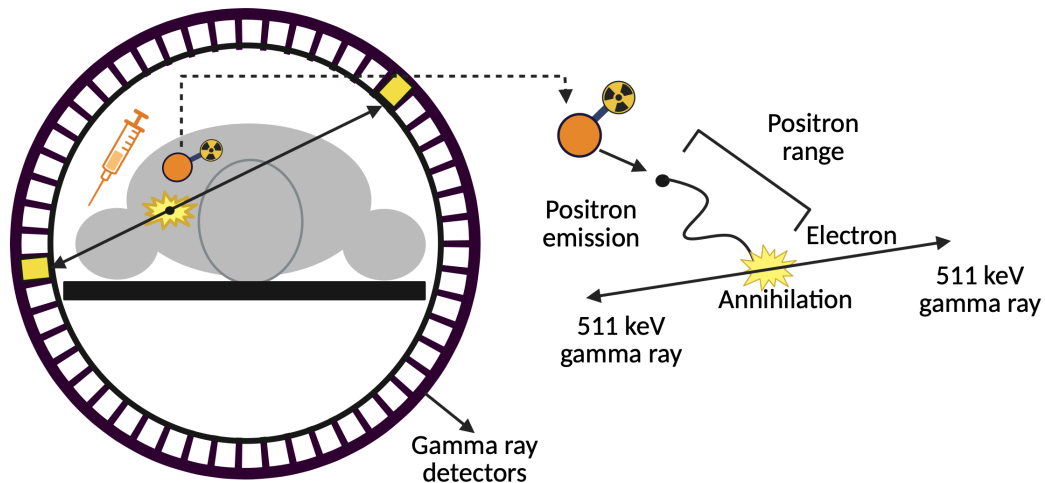


Figure 1.6. Scheme of a PET scanner design and functionality. Created in BioRender.

While both SPECT and PET are nuclear imaging techniques designed to measure physiological function and molecular processes *in vivo*, they differ in key technical and practical aspects. One of the main differences lies in the type of radioactive decay they detect: SPECT detects single gamma photons emitted directly by the tracer, whereas PET detects pairs of gamma photons resulting from positron-electron annihilation events. This fundamental distinction affects both sensitivity and image quality. Because SPECT relies on mechanical collimators to spatially filter incoming photons, its sensitivity and resolution are inherently limited. PET, by contrast, uses electronic coincidence detection without collimators, resulting in higher sensitivity and better spatial resolution.¹⁰² Quantitatively, PET is more accurate than SPECT and is often preferred in applications requiring precise measurement of tracer uptake. However, SPECT remains more available, less expensive, and is still widely used in clinical practice, particularly in cardiology, bone imaging, and certain neurological applications such as dopamine transporter imaging. PET is more commonly used in oncology, neurology, and cardiology, particularly in imaging metabolic activity or specific molecular targets such as amyloid or tau proteins in AD. Furthermore, PET tracers typically

have shorter half-lives and often require on-site or nearby cyclotron facilities for production, whereas many SPECT tracers have longer half-lives and are easier to distribute.¹⁰³

In summary, PET offers superior image quality, sensitivity, and quantification, making it especially valuable in research and precision diagnostics. SPECT, on the other hand, offers a more accessible and cost-effective solution for a wide range of established clinical applications. Both modalities are complementary, and the choice between them often depends on clinical needs, availability, and specific diagnostic questions.

1.7.3. Applications and Potential of PET and SPECT

It is important to highlight the enormous potential of PET and SPECT imaging. These techniques are continuously evolving, driven not only by advances in imaging technology—such as improved detector sensitivity, resolution, and quantification methods—but also by the ongoing development of novel radiotracers. The discovery of new biological targets has propelled a parallel effort in tracer design, allowing researchers to probe an ever-widening range of physiological and pathological processes, including metabolism, receptor binding, neurotransmission, inflammation, and protein aggregation. This molecular specificity makes PET and SPECT uniquely suited to address unmet needs in both clinical and research settings.⁹⁹

Building upon the diagnostic power of PET and SPECT, the field of Theranostics—a fusion of therapy and diagnostics—is rapidly gaining prominence. However the concept has been here since 1940s, with the first treatment of thyroid cancer with radioactive iodine,¹⁰⁴ it has recently gained momentum with the approvals of lutetium 177 (¹⁷⁷Lu) tetraazacyclododecane tetraacetic acid octreotate (DOTATATE), for neuroendocrine tumors, and ¹⁷⁷Lu–prostate-specific membrane antigen (PSMA), for prostate cancer.¹⁰⁵ Theranostics uses the same molecular targeting principles as in imaging to deliver therapeutic radionuclides directly to disease sites. In radiopharmaceutical therapy (RPT), the radiotracer acts not just as a marker but as a treatment agent, enabling highly targeted interventions. Traditionally, RPT is administered using standardized activity doses, but recent efforts are shifting toward personalized treatment planning.¹⁰⁶ By incorporating quantitative imaging data on disease burden and tracer pharmacokinetics, clinicians can tailor therapy regimens to

the individual, optimizing efficacy while minimizing toxicity. This paradigm represents a compelling step toward precision medicine and emphasizes the broader potential of molecular imaging beyond diagnosis.

In parallel to advances in therapeutic nuclear medicine, and among the many applications of diagnostic molecular imaging, neuroimaging represents a particularly rich and evolving field, offering unique information into the functional and biochemical processes of the brain. Several PET and SPECT tracers have been developed to target specific aspects of brain function, helping in the diagnosis and understanding of a wide range of neurological disorders. In the following sections, this work focus on three key neuroimaging modalities that are widely used in both clinical and research settings: FDG PET, which measures cerebral glucose metabolism as a proxy for neuronal activity; DAT PET, which assesses dopamine transporter availability and serves as a marker of presynaptic dopaminergic function; and DAT SPECT, a more accessible and widely used alternative for evaluating the integrity of the dopaminergic system. Each of these techniques provides distinct but complementary information, and together, they play a central role in the assessment of neurodegenerative diseases such as PD and related disorders.

1.7.4. FDG-PET imaging

2-[¹⁸F]fluoro-2-deoxy-D-glucose positron emission tomography (FDG PET) is one of the most widely used molecular imaging techniques in clinical medicine and research. After intravenous injection, [¹⁸F]FDG is transported into cells via glucose transporters and phosphorylated by hexokinase, forming [¹⁸F]FDG-6-phosphate, which becomes metabolically trapped due to its inability to proceed through the glycolytic pathway. The accumulation of this radiolabeled compound reflects cellular glucose uptake and phosphorylation rates, serving as a surrogate for metabolic activity. FDG PET is extensively used in oncology for tumor detection, staging, and therapy monitoring, as many cancers exhibit increased glycolytic activity. In addition to its oncological applications, FDG PET plays a central role in the evaluation of infectious, inflammatory, and neurodegenerative diseases.¹⁰⁷

In neurology, FDG PET provides a unique window into brain function by mapping regional cerebral glucose metabolism. Although the adult human brain accounts for only

about 2% of body mass, it consumes approximately 20–25% of the body's glucose. Remarkably, around 95% of the ATP required for sustaining neuronal activity is derived from glucose metabolism.¹⁰⁸

It is important to clarify what does higher or lower FDG uptake actually indicate in terms of brain function. Neuronal energy is primarily used for signaling and information transmission. Most of the brain's glucose consumption is linked to synaptic transmission—particularly the generation of synaptic currents and action potentials. Indeed, studies have demonstrated increased glucose uptake in axon terminals during neuronal stimulation. As a result, the FDG PET signal largely reflects synaptic and neuronal activity.¹⁰⁹ Consequently, alterations in neuronal and synaptic integrity due to brain disease often lead to regional changes in glucose metabolism, which can be detected using FDG PET.

In addition to neurons, glucose is also metabolized by astrocytes, which convert it into lactate—a key energy source for neurons.^{110,111} Moreover, microglial activation, such as during inflammation, has been shown to significantly impact both glucose metabolism and FDG uptake.¹¹² Thus, it is clear that not only neuronal but also glial activity and other factors further shape FDG uptake patterns.

Some studies also suggest that FDG PET can offer more than regional metabolic quantification.^{113,114} For instance, deformation-based morphometry applied to FDG PET data has been shown to reveal hippocampal atrophy in AD.¹¹⁴ This approach correlates with cognitive performance and may be used as a complementary biomarker of neurodegeneration alongside conventional FDG PET analysis.

Image Acquisition, Processing and Interpretation

For diagnostic purposes, FDG PET imaging typically begins between 30 and 60 minutes post-injection. Modern PET/CT and PET/MRI systems typically acquire data in list mode and 3D format. After acquisition, attenuation correction is applied to compensate for photon loss due to tissue density, using either simultaneous CT or MRI scans. Images are then reconstructed using ordered subset iterative reconstruction, incorporating time-of-flight (TOF) data when available, with voxel size under 2 mm in all directions.¹¹⁵ The interpretation of images can be performed by visual assessment, semiquantitative methods, or voxel-based analyses. Other methods include multivariate analyses, such as the scaled subprofile model.

Visual Assessment

Visual evaluation requires careful examination of motion or attenuation artifacts. Figure 1.7 shows typical FDG PET findings in PD and other parkinsonian disorders. To assist in interpretation of findings, it is helpful to have a well-matched (same type of camera, and acquisition and processing methods) normal database. Adjustments to color scale and contrast can improve interpretation, which should consider both global and regional alterations in FDG uptake. Increased uptake may indicate tumors, inflammation, epileptogenic activity, or normal physiological activation, while hypometabolism is commonly seen in neurodegenerative diseases. Anatomical context, such as atrophy, should also be considered, with image fusion (e.g., PET/MRI or PET/CT) improving localization.¹¹⁵

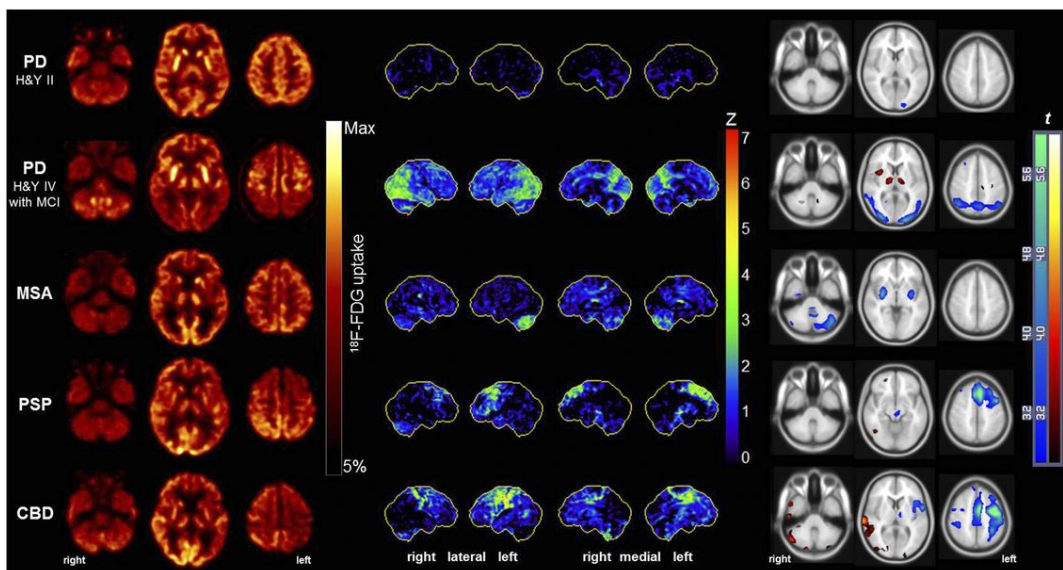


Figure 1.7. Typical 18F-FDG PET findings in individual patients with parkinsonism as depicted by the currently used image analysis methods. Adapted from Philipp T. Meyer et al., *J Nucl Med*, 2017. Copyright © Society of Nuclear Medicine and Molecular Imaging.

Semiquantitative and Voxel-Based Analysis

Semiquantitative approaches in FDG PET analysis aim to complement visual interpretation by providing objective, reproducible metrics that highlight regional deviations in glucose metabolism. They include region-of-interest (ROI)-based methods, commonly used in oncology, or voxel-wise methods. The latest can be either univariate, such as Statistical

Parametric Mapping (SPM), or multivariate, such as the Scaled Subprofile Model and Principal Component Analysis (SSM-PCA).¹¹⁶

A fundamental metric used in semiquantitative PET analysis is the Standardized Uptake Value (SUV). The SUV represents the tissue radioactivity concentration at a given time point, normalized for the injected dose and the patient's body weight, lean body mass, or body surface area. It is a practical and widely used measure to assess the relative glucose metabolism in different brain regions. However, SUV can be affected by various factors including patient physiology, scanner calibration, and uptake time, limiting its comparability across subjects or sessions.¹¹⁷ To address these limitations, SUV ratios (SUVr) are often used, where uptake in a target region is normalized to that in a reference region presumed to be unaffected by pathology. This normalization mitigates inter-subject and technical variability and allows for more reliable comparisons between individuals or groups.¹¹⁵

Univariate voxel-wise statistical methods such as SPM generate individual Z-score or t-score maps by comparing the patient's scan to the age-matched normative database. These maps show regions of significantly increased or decreased uptake compared to controls and can be overlaid on anatomical images to improve localization and interpretation. These tools can assist clinicians in interpreting complex patterns of hypo- or hypermetabolism, especially in early or atypical disease presentations. Many software tools—both commercial and freeware—offer pipelines for these analyses, often including options for spatial normalization, smoothing, and statistical thresholding.^{115,116} The SSM-PCA method is described in detail in the following section.

A critical step in semi-quantification is intensity normalization, which corrects for global signal variability caused by technical or physiological factors unrelated to disease. Normalization can be done using the whole brain or reference regions, such as the cerebellum, occipital cortex or pons. The reference region should be carefully chosen based on the clinical context to ensure it is not affected by pathology or methodological artifacts.¹¹⁸

These automated methods have shown increased sensitivity and specificity in clinical studies, particularly in early or atypical cases of neurodegenerative diseases.¹¹⁹ However, the accuracy of voxel-based analyses heavily depends on harmonization between the patient scan and the normal database in terms of acquisition protocol, attenuation correction, reconstruction parameters, and preprocessing steps. Inconsistent parameters can lead to

artifacts or false findings. The growing availability of large, high-quality normal databases through research consortia is helping to standardize these methods and promote their clinical adoption.^{116,120}

While semiquantitative tools are not a replacement for expert visual interpretation, they provide valuable support, especially for less experienced readers or in centers without access to specialized neuroimaging expertise.

Scaled Subprofile Model and the Spatial Covariance Patterns

The Scaled Subprofile Model (SSM) is a multivariate analytic method that identifies major sources of variation in functional brain image data of controls and diseased patients, corresponding to spatial covariance patterns of disease. These patterns are composed of positive and negative deviations from the subject's global mean uptake and group values. It was developed to overcome limitations of traditional statistical methods, such as assumptions of group homogeneity and fixed correlational structures.^{121,122}

At its core, SSM is based on Principal Component Analysis (PCA), which decomposes the variance in brain PET data into orthogonal principal components (PCs), each representing an independent spatial pattern of metabolic variation. The key innovation of SSM is in its preprocessing steps: the data goes through a log transformation and “double centering” (subtracting the mean across both rows – subjects mean – and columns – group means – of the subject-by-voxel matrix), which normalizes for global subject and regional effects. This preprocessing ensures that the analysis is robust and does not change with inter-subject and inter-regional factors, allowing for the detection of subtle, disease-specific deviations in glucose metabolism.^{123,124}

SSM produces a limited set of principal components, each representing a spatial pattern of metabolic covariance. The first few PCs typically explain the majority of the variance in the dataset. Importantly, only those PCs that discriminate effectively between patients and controls, or correlate with independent measures of disease severity, are retained as disease-related covariance patterns. Each subject's expression of a given pattern is quantified by a scalar score (or pattern expression score), which reflects how closely the subject's brain metabolism conforms to that spatial pattern.^{123,124} These scores have been shown to correlate

strongly with clinical markers of disease severity and progression, offering a powerful tool for biomarker development.^{125,126}

By highlighting disease-related network alterations rather than isolated regional changes, SSM provides a biologically meaningful representation of the functional topography of brain disorders. Z-scored maps of voxel weights can be visualized to identify spatially distributed networks that are pathologically altered in conditions such as PD, AD, and other neurodegenerative disorders.^{125,127,128}

The description of the method with mathematical formulation is given below:

1) Registration to a Common Space - All brain images are spatially normalized to a standard anatomical template (e.g., Montreal Neurological Institute – MNI – space) to ensure voxel-wise correspondence across subjects.

2) Intensity Normalization - To reduce inter-subject variability not related to disease, images may be intensity-normalized. This is typically done by dividing voxel intensities by the mean uptake in a reference region (e.g., cerebellum or whole brain):

$$I_{\text{norm}}(x) = \frac{I(x)}{\bar{I}_{\text{ref}}}$$

where, I is the intensity in each voxel x , and \bar{I}_{ref} , is the mean intensity in the reference region, and I_{norm} is the normalized image.

3) Brain Masking - To restrict analysis to brain regions of interest, a binary brain mask is applied. This can be predefined or generated by thresholding each scan and combining them:

$$I_{\text{masked}}(x) = I(x) \cdot M(x)$$

where $M(x) \in \{0,1\}$ is the binary mask and I_{masked} the resulting masked image.

The resulting registered, normalized and masked images of all subjects are flatten and stacked in an array, further defined as X .

4) Log Transformation - A log transformation is applied to all voxel intensities to convert multiplicative effects into additive components, aiding in variance normalization:

$$L_{i,j} = \log(X_{i,j})$$

where $X_{i,j}$ is the intensity of voxel j in subject i, and $L_{i,j}$ the resulting log transformed subjects matrix.

5) Row Centering (Subject Mean Removal) - Each subject's data is centered by subtracting their mean uptake value, μ_i , across all voxels, removing global subject-level effects:

$$\mu_i = \frac{1}{V} \sum_{j=1}^V L_{i,j}$$

$$L'_{i,j} = L_{i,j} - \mu_i$$

where V is the number of voxels, $L_{i,j}$ is the previously log transformed matrix and $L'_{i,j}$ the resulting row centered matrix.

6) Column Centering (Voxel Mean Removal) - Each voxel is then centered by subtracting the mean voxel value across all subjects, \bar{L}_j , also called Group Mean Profile, thus removing global voxel-level effects. This yields the Subject Residual Profile (SRP):

$$\bar{L}_j = \frac{1}{N} \sum_{i=1}^N L'_{i,j}$$

$$\text{SRP}_{i,j} = L'_{i,j} - \bar{L}_j$$

where N is the number of subjects.

7) Compute the Covariance Matrix - The covariance matrix C is calculated from the SRP to capture the similarity in spatial patterns across subjects:

$$C = \text{SRP} \cdot \text{SRP}^T$$

This results in a subject-by-subject matrix describing shared variation in brain activity profiles.

8) Eigen Decomposition – Principal Component Analysis (PCA) is applied to the covariance matrix by solving for eigenvalues λ_k and eigenvectors v_k :

$$Cv_k = \lambda_k v_k$$

where $v_k = [v_{1,k}, v_{2,k}, \dots, v_{N,k}]^T$ and λ_k its corresponding eigenvalue. Each eigenvector represents a dominant mode of intersubject variability.

9) Compute Subject Scores (SSF) - Eigenvectors are scaled by the square root of their corresponding eigenvalues to form the Subject Scaling Factors (SSF) or score matrix S:

$$S_{i,k} = v_{i,k} \cdot \sqrt{\lambda_k}$$

10) Compute Voxel Pattern Vectors (GIS) - The voxel-wise spatial covariance patterns (also known as Group Invariant Subprofiles, GIS) are obtained by projecting the transpose of SRP onto the score matrix:

$$\text{GIS} = \text{SRP}^T \cdot S$$

Each GIS vector represents a disease-related spatial pattern of metabolism. The proportion of variance explained by component k (VAF_k) is:

$$VAF_k = \left(\frac{\lambda_k}{\sum_{j=1}^K \lambda_j} \right) \times 100$$

To be considered disease-related, a single GIS component k or a linear combination must show significant group separation (e.g., $p \leq 0.001$ in a two-sample t-test on $S_{i,k}$).

11) Subject Score alternative calculation - Thanks to orthogonality, the subject score $S_{i,k}$ for GIS k can be computed as the dot product between the subject's SRP vector and the GIS vector:

$$S_{i,k} = \text{SRP}_i \cdot \text{GIS}_k$$

This equation allows for forward application of SSM-derived GIS patterns to new subjects by computing pattern expression scores—an approach historically termed Topographic Profile Rating (TPR). This enables assessment of individuals or replication of group results in independent cohorts.

12) New Subject Score calculation - To obtain subject's score for new subjects, the previously determined Group Mean Profile, \bar{L}_J , can be used to get the new subject SRP:

$$\text{SRP}_{i,j} = L_{i,j} - \mu_i - \bar{L}_J$$

and the voxel-wise spatial covariance pattern, GIS_k , and this subject's SRP, can be used to calculate the single score that quantifies pattern k expression in the new subject – TPR_k .

$$TPR_k = \text{SRP} \cdot \text{GIS}_k$$

A schematic presentation of SSM-PCA method is shown in Figure 1.8.

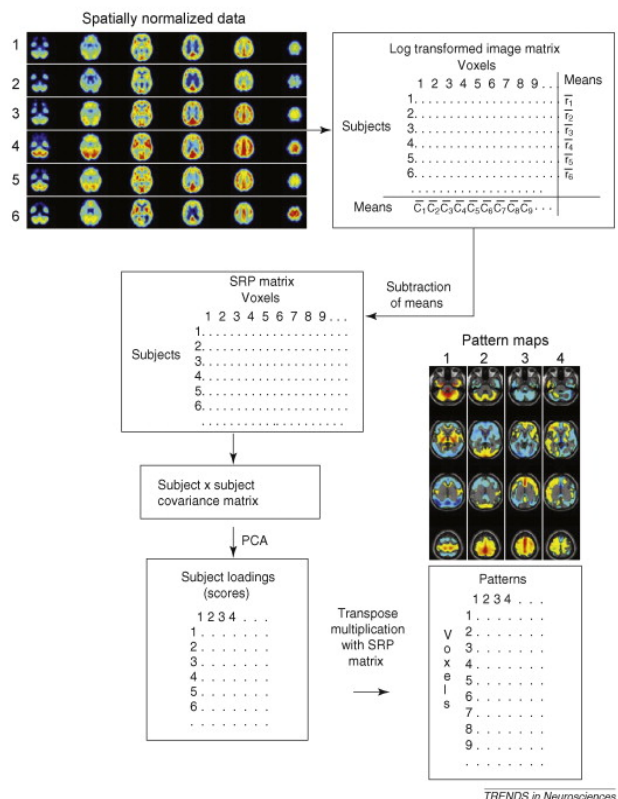


Figure 1.8. Schematic presentation of the Scaled Subprofile Model to calculate the disease-related patterns. From Eidelberg et al., Trends in Neurosciences, 2009. Copyright © 2009 Elsevier Ltd.¹²⁴

In conclusion, SSM-PCA represents a robust and interpretable approach for uncovering disease-related patterns of brain activity, offering both group-level insights and subject-level applicability. Its ability to transform complex brain imaging data into reproducible, quantifiable network signatures makes it particularly valuable for studying neurodegenerative diseases and for advancing biomarker-based precision medicine in neurology.

As part of this work, to facilitate the use of this methodology, a dedicated Python package that implements the full SSM-PCA pipeline was developed and published, enabling reproducible analysis of FDG brain PET data (available at: <https://github.com/lopes-leonor/Scaled-Subprofile-Model>).

1.7.5. Dopaminergic Imaging

Dopaminergic imaging using nuclear medicine techniques offers valuable insight into the functional integrity of the dopaminergic system and plays a central role in the evaluation of parkinsonian syndromes. Currently, both presynaptic and postsynaptic components of dopaminergic neurotransmission can be assessed using PET and SPECT tracers targeting different aspects of the synapse function.¹²⁹

Dopamine synthesis begins with the amino acid L-tyrosine, which is hydroxylated to L-dihydroxyphenylalanine (DOPA) and then decarboxylated by the enzyme aromatic L-amino acid decarboxylase (AADC) to form dopamine. The newly synthesized dopamine is transported into intracellular vesicles by vesicular monoamine transporter type 2 (VMAT2), where it is stored until neuronal depolarization triggers its release into the synaptic cleft. Once released, dopamine binds to postsynaptic dopamine receptors to exert its physiological effects. Dopamine that remains in the synaptic cleft is then cleared via reuptake into the presynaptic terminal through the dopamine transporter (DAT).¹³⁰

Presynaptic dopaminergic imaging focuses on the function of dopaminergic neurons and their terminals. It includes tracers that bind to the DAT (e.g. [¹²³I]FP-CIT SPECT or [¹¹C]CFT PET), to VMAT2 (e.g. [¹⁸F]-FP-DTBZ PET), or enzymes such as AADC (e.g. [¹⁸F]-DOPA PET). This type of imaging is particularly useful for differentiating neurodegenerative parkinsonian syndromes—such as PD, MSA or PSP—from conditions not primarily associated with dopaminergic degeneration, such as essential tremor or drug-induced parkinsonism. A reduction in presynaptic tracer uptake typically reflects degeneration of the nigrostriatal pathway.^{129,131}

In contrast, postsynaptic dopaminergic imaging assesses the integrity and density of dopamine D₂/D₃ postsynaptic receptors, primarily located on striatal neurons. It is typically used to distinguish between parkinsonian syndromes with presynaptic dysfunction and those with combined pre- and postsynaptic involvement.^{129,131}

While both pre- and postsynaptic imaging contribute valuable diagnostic information, this section will focus exclusively on presynaptic dopaminergic imaging, which is the most widely used modality for assessing nigrostriatal degeneration. Interpretation of these scans involves both visual assessment and, increasingly, semi-quantitative analysis.

Visual Assessment

Prior to interpretation, rigorous quality control is essential to identify motion artifacts, attenuation correction issues, or PET-MRI/PET-CT fusion misregistration. Structural imaging aids in identifying concurrent abnormalities such as infarcts, atrophy (e.g., cerebellar atrophy in MSA, midbrain atrophy in PSP), or white matter changes (as seen in vascular parkinsonism). PET images should be displayed with optimized color scaling, typically setting the highest uptake voxel within the striatum as the maximum value. Proper head positioning is also crucial to avoid artificial asymmetries in tracer distribution.⁶⁰

In healthy individuals, presynaptic dopaminergic PET demonstrates symmetric bilateral uptake in the caudate and putamen, with gradual color gradation and relative preservation of background uptake in cortex and cerebellum. Non-neurodegenerative parkinsonian conditions such as drug-induced parkinsonism, psychogenic parkinsonism, and essential tremor typically exhibit normal scans. Vascular parkinsonism can be variable – showing either normal uptake or focal deficits aligned with structural lesions.⁶⁰

In PD, a characteristic posterior-to-anterior gradient of dopaminergic loss is typically observed, starting in the posterior putamen contralateral to the clinically affected side, with relative sparing of the caudate. Left-right asymmetry and bilateral reductions can be seen even in early-stage PD. Young-onset PD tends to show more uneven patterns with greater caudate sparing, while late-onset PD may exhibit more uniform reductions. However, dopaminergic PET cannot definitively diagnose PD, as similar patterns may be present in other neurodegenerative diseases. MSA presents with symmetric presynaptic dopaminergic reductions, often with a clear posterior-to-anterior gradient in the parkinsonian subtype. Cerebellar subtype tends to show milder reductions or even normal scans. PSP and CBD also show bilateral dopaminergic loss, but often with early caudate involvement and, in the case of CBD, pronounced left-right asymmetry. DLB shares imaging features with PD, though a minority of DLB patients may show normal scans.^{60,132}

Figure 1.9 shows examples of scans with different types of tracers of dopaminergic imaging in both PD and control.

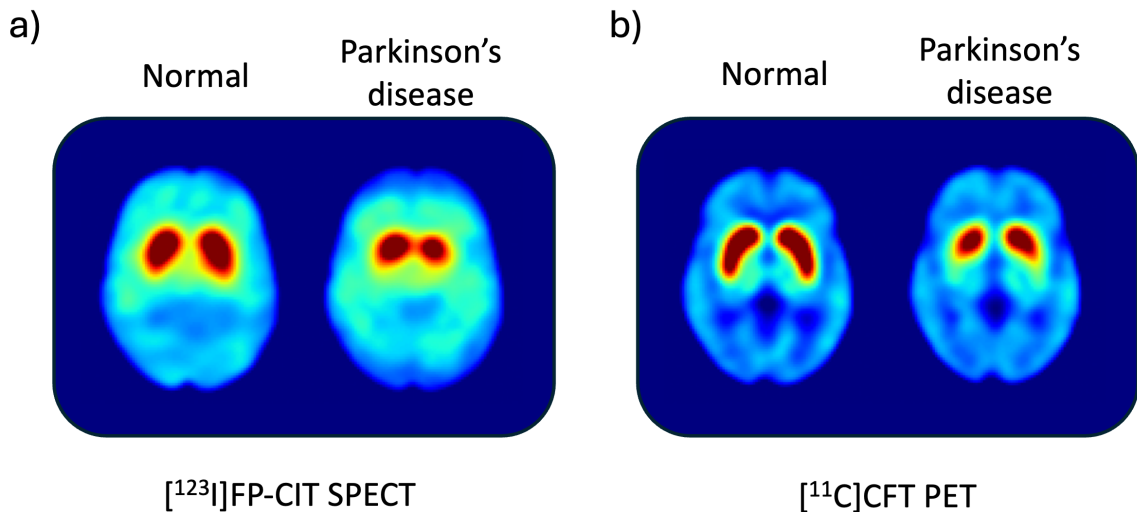


Figure 1.9. Dopaminergic scans of normal subject and Parkinson's disease patient. a) [¹²³I]FP-CIT SPECT scan; b) [¹¹C]CFT PET scan.

Semiquantitative Analysis

Although visual reading remains the main method of dopaminergic PET interpretation, semi-quantitative analysis can offer additional sensitivity, especially for early-stage detection and longitudinal monitoring.¹³³

The most widely used semiquantitative metric is the specific binding ratio (SBR), which provides an estimate of DAT availability by comparing tracer uptake in striatal regions to a reference region with minimal or absent DAT expression. While not a direct measure of DAT density, under near-equilibrium conditions, the simple ratio of striatal-to-background activity can serve as a surrogate marker proportional to DAT density. The SBR is calculated as:

$$SBR = \frac{\text{Mean Counts}_{ROI} - \text{Mean Counts}_{background}}{\text{Mean Counts}_{background}}$$

with the occipital cortex or cerebellum as a reference regions.

However, SBR is still influenced by multiple biological and technical factors, highlighting the need for consistent acquisition protocols and, ideally, site-specific or database-calibrated reference values. Normative databases such as ENC-DAT¹³⁴ and PPMI have been instrumental in accounting for age and sex effects in SBR interpretation, supporting its integration in both clinical and research settings.

In the absence of a normal database, asymmetry indices and within-subject comparisons (e.g., between caudate and putamen or between hemispheres) can help identify abnormal patterns. In institutions with established reference databases, SBR values can be compared to age- and sex-matched healthy controls to determine the presence and extent of dopaminergic neurodegeneration. Furthermore, semi-automated algorithms are increasingly used in clinical research to standardize SBR computation and improve reproducibility. This has enhanced the value of dopaminergic imaging not only in diagnosis but also in tracking disease progression and evaluating treatment effects in clinical trials.^{60,135}

1.8. Actigraphy

Many neurological disorders—including PD, AD and other dementias, and a variety of sleep disorders—are associated with abnormal motor activity and disrupted rest-activity cycles. In clinical practice, it is essential to monitor these symptoms both to diagnose, assess disease severity and to evaluate the efficacy of pharmacological or behavioural interventions. Clinical scores are helpful tools for this purpose, but have limitations such as being subjective, measuring the score in only a point in time, requiring the visit of the patient to the clinic.¹³⁶

Actigraphy can be a complementary solution to improve performance of the other methods. It is easily accessible, non-invasive and allows for a continuous and objective measurement of activity for several days.

Actigraphy is the record of physical movement by small, lightweight, watch-like wearable devices equipped with triaxial accelerometers. These devices are typically worn on the non-dominant wrist and allow for monitoring of rest-activity cycles and sleep-wake behavior for extended periods of time in the patient's natural sleeping environment. In addition to motion sensing, modern actigraphs often include auxiliary sensors to record ambient light exposure, temperature (to detect device removal), and an event-marker button for the subject to annotate events such as bedtime, waking, naps, or medication intake.^{136,137}

The raw movement data captured by the accelerometer can be processed in several ways, depending on the device and the device settings. For example, zero-crossing mode (ZCM), where each axis registers a count whenever acceleration crosses a preset threshold. These zero-crossing counts are integrated over time (often in 1-minute epochs) and stored internally for later download to a computer. In addition to the commonly used zero-crossing mode (ZCM), some actigraphy devices, such as the MotionWatch, utilize an alternative method based on raw acceleration magnitude. In this approach, for each second, the peak acceleration (positive or negative) is recorded and compared against a predefined threshold (approximately 0.1 g) to exclude periods of inactivity. Only values exceeding this threshold are retained, and the resulting per-second values are then summed over each epoch (e.g., 30 or 60 seconds) and scaled using calibration data from standardized testing.^{137–139}

Actigraphy has become a widely used method for long-term, real-world monitoring of sleep and activity, especially valuable in neurological populations where rest-activity and sleep disruptions are common. While polysomnography (PSG) remains the gold standard for evaluating sleep architecture and diagnosing sleep disorders, it presents several limitations—being expensive, intrusive, logistically challenging, and impractical for repeated or large-scale assessments. In contrast, actigraphy offers a non-invasive, cost-effective, and ecologically valid alternative, allowing for continuous monitoring in the subject's natural environment over multiple days or weeks.

Several features can be extracted from Actigraphy records to assess sleep and activity patterns. These include basic variables like the time the individual went to bed, woke up, sleep midpoint, and total duration spent in bed. More advanced features can be derived using sleep detection algorithms, which classify time segments as either sleep or wake. Two common algorithms for this purpose are those developed by Cole-Kripke¹⁴⁰ and Sadeh.¹⁴¹ From these classifications, key sleep metrics can be calculated, including total sleep time, sleep efficiency (the percentage of time in bed spent asleep), sleep onset latency, wakefulness after sleep onset, and the frequency and duration of awakenings.^{142–144}

Circadian rhythm metrics offer a broader view of the daily rest-activity cycle and its consistency. These features can be extracted using both model-based and model-free approaches. In parametric analyses, such as COSINOR modeling, a cosine curve is fitted to the activity data to estimate rhythm parameters, including the average level (MESOR), amplitude, phase timing (acrophase), and period. Non-parametric analyses, on the other hand, focus on rhythm fragmentation and regularity without assuming a fixed waveform. Key measures include intradaily variability (IV), which reflects rhythm fragmentation; interdaily stability (IS), which indicates how consistent the rhythm is from day to day; relative amplitude (RA), showing the contrast between most and least active periods; and specific metrics such as the least active 5-hour period (L5) and the most active 10-hour period (M10).^{137,143} An example of an actigraphy record and some features is displayed in Figure 1.10.

Several studies have confirmed that actigraphy can reliably estimate key sleep parameters—such as total sleep time, sleep efficiency, and wake after sleep onset—when compared to the gold-standard measure, PSG. However, the accuracy of actigraphy in determining sleep onset latency appears to be more limited.^{139,145–147} Reported correlations

between actigraphy-derived and PSG-derived total sleep time are high, with reliability coefficients ranging from 0.89 to 0.98.¹⁴⁸

Recent advances in software and signal processing have led to the development of open-source Python packages (e.g. PyActigraphy) that enable automated, standardized extraction of actigraphy features. These tools are expanding the accessibility of actigraphy analysis for clinical and research use, while supporting reproducibility across studies.

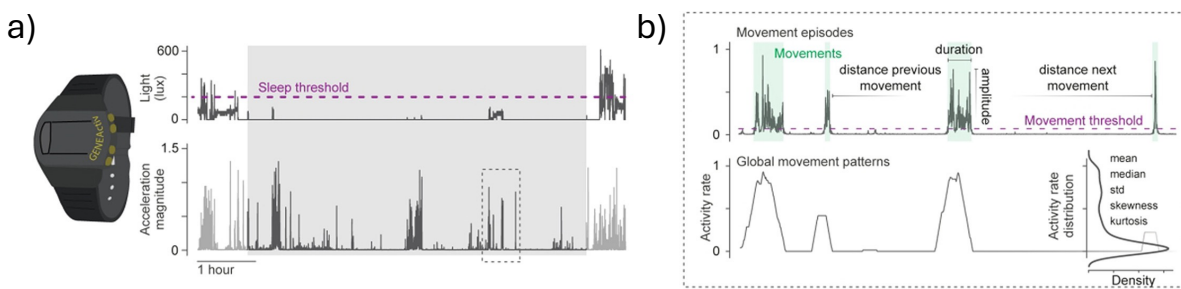


Figure 1.10. Actigraphy representation. a) Movement wrists actigraphy and light sensor recordings; b) Features of nocturnal actigraphy record. Adapted from Raschellà et al., Annals of Neurology, 2023.¹⁴⁹

1.8.1. Applications in PD

Recent studies in large cohorts have demonstrated that actigraphy-derived measures—particularly sleep efficiency and sleep onset latency—are associated with the risk of progression to cognitive impairment.¹⁵⁰ These findings highlight the potential of actigraphy as a sensitive, non-invasive tool for detecting early changes in neurodegenerative conditions.

In PD, actigraphy has similarly revealed distinctive alterations in circadian and sleep-related parameters. Compared to healthy controls, individuals with PD have lower circadian amplitude, an advanced acrophase (earlier timing of peak activity), shorter total sleep time and lower sleep efficiency.¹⁴⁷ As PD progresses, these disruptions become more pronounced, with further declines in amplitude and robustness (i.e., how closely activity patterns follow a 24-hour rhythm), as well as increased time wake after sleep onset and fragmentation of the rest-activity cycle.^{151,152} In fact another study showed significant correlation between UPDRS and measures of physical activity, captured by actigraphy.¹⁵¹ Importantly, these actigraphic

features not only reflect disease severity but may also serve as early indicators of risk: decreasing circadian amplitude, mean activity level, and rhythm robustness have been linked to a higher likelihood of developing PD in older adults.¹⁵³

Beyond characterization and risk prediction, actigraphy is also being explored as a tool to evaluate therapeutic interventions in PD. For example, subthalamic deep brain stimulation (DBS) has been associated with improvements in both motor function and sleep-related outcomes. Actigraphy revealed significantly longer time spent in bed after DBS, with no evidence of circadian phase shifts. Polysomnography confirmed increased sleep efficiency, more time spent in deep sleep, and a progressive accumulation of slow-wave activity overnight.¹⁵⁴ These findings suggest that actigraphy can capture sleep–wake improvements following neuromodulation therapy.

Pharmacological therapies have also been examined through actigraphy. In PD patients reporting sleep disturbances, melatonin supplementation led to a modest but statistically significant increase in total sleep time with a 50 mg dose compared to 5 mg or placebo. While the improvement was relatively small, subjective sleep quality also improved, suggesting that actigraphy can capture subtle treatment effects.¹⁵⁵ Meanwhile, dopaminergic therapy has been associated with shifts in circadian timing, including earlier waking and immobility offset times. These changes appear to be independent of disease stage and may instead reflect treatment-related effects. Patients on dopaminergic medication who reported greater daytime sleepiness and nighttime psychotic symptoms also tended to go to bed and wake up earlier, pointing to complex interactions between medication, circadian rhythms, and non-motor symptoms.¹⁵⁶

Together, these findings support the role of actigraphy to assist clinicians, together with clinical evaluation and scores (such as UPDRS), in monitoring disease-related changes, disease progression and therapeutic outcomes in PD, specifically in outpatient settings.

Changes in physical activity, as captured by actigraphy, are associated with increased severity in clinical symptoms of PD over time. This suggests that, when used in conjunction with the conventional UPDRS measure, an actigraphic measure of physical activity may provide clinicians with an adjunct measurement approach to monitor activity-based disease progression or responses to treatment in outpatient clinic settings.¹³⁶

1.8.2. Application in RBD

Actigraphy has shown significant promise as a non-invasive tool for detecting and characterizing RBD, particularly in its isolated form (iRBD), which is considered a prodromal stage of synucleinopathies such as PD. The combination of seven or more nights of home actigraphy data with a nine-item questionnaire—including the Innsbruck RBD Inventory and questions on prodromal symptoms like hyposmia, constipation, and orthostatic dizziness—yielded an actigraphy-based classifier with 95.2% sensitivity and 90.9% precision in identifying iRBD patients. When actigraphy and questionnaire predictions were concordant, specificity and precision reached 100%, outperforming individual screening tools.¹⁵⁷ Additional actigraphy metrics—such as the imbalance between nocturnal and diurnal motor activity ($I < O$ index), reduced relative amplitude, increased time in bed and sleep latency, and decreased sleep efficiency—can distinguish iRBD from other sleep disorders and healthy controls with accuracy comparable to expert visual scoring.¹⁵⁸

In PD patients, actigraphy has been used to identify RBD with high specificity (95.5%) using the number of nocturnal wake bouts, though sensitivity remained low (20.1%), suggesting it may be most effective when paired with sensitive screening questionnaires.¹⁵⁹ One study has though employed machine learning approaches to classify RBD on PD patients based on actigraphy features and achieved both high sensitivity ($94.9 \pm 7.4\%$) and specificity ($92.7 \pm 13.8\%$). However, sample size was very limited.¹⁴⁹

Moreover, actigraphy may offer prognostic insights into disease progression. Significant increases in probable napping behavior, activity fragmentation, and physical inactivity during active periods have been observed across the continuum from healthy controls to iRBD to overt α -synucleinopathies. In a longitudinal study of iRBD patients, baseline actigraphy data from individuals who later converted to a defined α -synucleinopathy were compared to those who did not convert. Converters showed more frequent probable napping episodes and, even after adjusting for napping, exhibited significantly lower levels of daytime activity.¹⁶⁰ These findings position actigraphy not only as a tool for RBD detection but also as a potential biomarker for disease progression and phenoconversion risk.

1.9. Artificial Intelligence

Today, we are living through a transformative era with the rise of artificial intelligence (AI). As radioactivity significantly improved the healthcare practice in the 20th century, AI is and will redefine the landscape of medicine in the 21st century. Parts of the following section were published in the review article by Lopes et al., 2025.¹⁶¹

“Artificial Intelligence” as a term was reportedly used for the first time in Dartmouth Summer Research project¹⁶² in 1956. AI algorithms can be defined as models that learn from data and perform intelligent tasks, such as data analysis, pattern finding, image recognition or text understanding and production. Machine learning (ML) is a branch of AI where models are able to learn without being explicitly programmed, by finding patterns in data and using them to make their predictions. ML still needs some help from humans to extract features from the data that are the inputs given to the model. An example would be to cluster data based on similarities between features. Deep learning is a branch of machine learning that uses deep neural networks to perform several more sophisticated tasks. In this case, there is less human preparatory work needed, as the inputs to these networks can be raw image values or text. As these models learn how to solve tasks from data (used to train them), data availability is one of the most important aspects in the development of the models. With the development of deep learning, computation resources also moved into focus.

In the medical field, data is also what allows physicians to diagnose (from symptoms and signs) or treat (from guidelines and clinical studies’ data) patients. Physicians are trained and learn (also from previous data) that some conjunction of features is associated with specific conditions. Physicians then use more data, such as complementary diagnostic methods (blood tests, scans, etc.) to adapt the hypothesis and make a more aligned diagnosis. Physicians use data and pattern recognition to make their decisions, which is why AI-based methods appear to be particularly applicable in the medical domain.

1.9.1. AI in Nuclear Medicine

Nuclear medicine is no exception given its dependency on images, an extremely complex type of data (with great granularity of information, visible and hidden). Since the

beginnings of AI, it has been applied in several nuclear medicine areas, with promise in improving diagnosis, prognosis and therapy, especially by more personalized approaches. Early applications in the 1990s and 2000s focused on diagnostics, demonstrating the potential of AI to analyse and interpret complex medical imaging data, as shown below:

In terms of diagnostic capabilities, mostly classification models were used. These use several clinical parameters or imaging features, and more recently full images as input, and as output, they classify each case into several categories, for example diseases or stages. Early works include neural network classifiers that were used to distinguish between normal and Alzheimer's disease FDG PET scans based on uptake values of different brain regions.¹⁶³ Others use machine learning methods such as decision trees for diagnosis of coronary artery disease from both clinical and imaging inputs.¹⁶⁴ These early studies showed the ability of AI to complement clinical decision-making with data-driven insights. The development of Convolutional Neural Networks (CNNs) minimized the need for manual extraction of features from images, as these models are designed to process grid-like high dimensional data, such as images. The principle of CNNs is to use filters for the extraction of spatial features like edges, textures, and shapes. Since then, a lot more was accomplished and new models, new approaches, new disease, new applications of AI in diagnosis continue to arise.

AI's role in prognosis is another important development, with models designed to predict outcomes and treatment responses. Early studies used Bayesian networks and support vector machines to predict two-year survival in lung cancer patients.¹⁶⁵ Machine learning frameworks were also utilized for cancer response assessment in PET/CT scans,¹⁶⁶ prediction of myocardial perfusion SPECT outcomes,¹⁶⁷ or predicting the progression from mild cognitive impairment to Alzheimer's disease using FDG-PET brain imaging.¹⁶⁸

Advancements in image segmentation and lesion detection followed, with AI models enabling precise identification and delineation of physiological anatomical structures and pathological lesions in nuclear medicine scans. Initial models were based on simple statistical analysis and machine learning, with the need for handcrafted features. Examples are the automated segmentation of whole-body bone scintigrams for diagnostic purposes¹⁶⁹ and neural network-based systems for PET volume segmentation.¹⁷⁰ More recent models and now widely used, such as U-Net¹⁷¹ and nnU-Net,¹⁷² achieve remarkable performance in medical image segmentation directly from images. They are based on CNNs and have an encoder-

decoder structure, i.e. first there is a contracting pathway to extract high-level, abstract features of the image, and then a decoder to reconstruct a desired output with high spatial resolution, like a tumour segmentation.

In addition to image interpretation, AI has also been used for enhanced image quality, including reconstruction, attenuation correction, and denoising. Techniques that model PET image intensity based on prior information for image reconstruction,¹⁷³ and the generation of attenuation correction for PET/MRI scans¹⁷⁴ are early examples. Since then, many other methods have arisen, such as image-to-image AI methods, that enable CT synthesis from MR¹⁷⁵ and deep learning methods for low-dose PET imaging.¹⁷⁶ The goal for most AI-driven improvements in image quality is exactly to enhance diagnostic accuracy while reducing radiation exposure.

More recently, in theranostics, AI has enabled more precise dosimetry, important for treatment planning. Approaches use machine-learning and deep learning for organ-based¹⁴ and voxel-based¹⁷⁷ post-therapy dose prediction in treatments like Lutetium-177 PSMA therapy, facilitating personalized care.

In addition to analysing or improving nuclear medicine images, text-processing AI is becoming increasingly relevant. Since the release of the transformer model¹⁷⁸ in 2017, Large Language Models and generative AI have flourished, opening new possibilities also for nuclear medicine. The transformer architecture is a powerful AI tool that uses a mechanism called self-attention to focus on the most important parts of the input. For example, when understanding the sentence, "The patient with diabetes needs insulin," the transformer would pay more attention to "diabetes" and "insulin" when deciding the meaning of "needs." Unlike older models that work step-by-step, the transformer analyses data in parallel, making it faster and more efficient. Initially, transformer models were designed for sequence-to-sequence tasks, such as machine translation. But soon it was applied in generative tasks. Generative models can generate data that is similar to the data they were trained on. This can be both text, images or any other kind of data. This novel architecture was so efficient that concepts of it were also used and merged with other models, such as Vision Transformer¹⁷⁹ and U-Net Transformer,¹⁸⁰ allowing not just for text generation but also for image generation, classification and segmentation, text-to-image generation, etc.

The presented advancements provide an overview of the evolution of AI in nuclear medicine, displayed in Figure 1.11, from its initial diagnostic applications to its transformative impact on data generation.

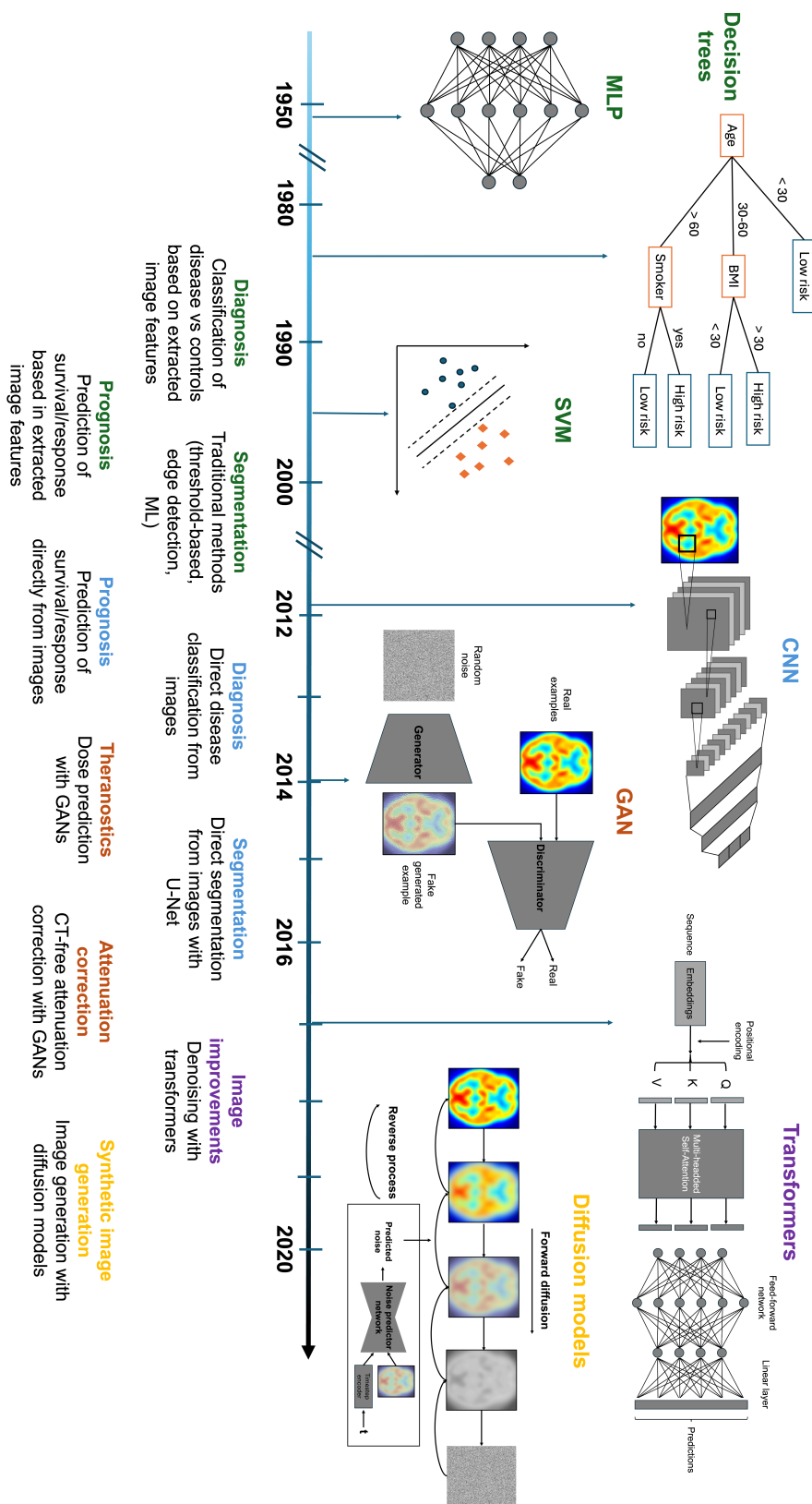


Figure 1.11. Evolution of AI in nuclear medicine. On top the AI model development is shown with some of the relevant corresponding nuclear medicine use cases on the bottom. AI: Artificial Intelligence; CNN: Convolutional Neural Network; GAN: Generative Adversarial Network; ML: Machine-learning; MLP: Multi-layer Perceptron; SVM: Support Vector Machine.

1.9.2. Applications in neurology

Many AI-based tools for disease diagnosis on nuclear medicine scans have been dedicated to neuroimaging, particularly in distinguishing neurodegenerative disorders. For example, initial works used machine learning and neural networks, trained with extracted imaging features such as regional brain uptake or standardized uptake value ratio (SUVR). For instance, Kippenhan et al.¹⁸¹ demonstrated the feasibility of using these extracted features from FDG-PET images for Alzheimer's disease classification (vs normal scans; AUC 0.85), influencing subsequent works. Several following studies also used extracted imaging features for AD classification, often in combination with clinical or other parameters.^{182–187} Studies, like from Suk et al.¹⁸⁸, marked the transition to deep learning, by using autoencoders and support vector machines for AD and mild cognitive impairment (MCI) classifications, with accuracies > 0.90 for AD and 0.85 for MCI classification.

In PD, several studies^{189,190} used machine learning techniques (e.g., SVM and logistic regression) for disease subtyping with ROI or voxel intensity data from FP-CIT SPECT images or other imaging modalities¹⁹¹ (for example, PD vs vascular parkinsonism or dopaminergic degeneration vs non-degeneration, the last with an AUC of 0.96 in an external dataset). Deep learning enabled more robust and generalizable models: Wenzel et al.¹⁹² used CNNs for FP-CIT SPECT image classification, achieving robust accuracy across multi-site datasets and varied acquisition protocols. Models like Choi et al.¹⁹³ utilized transfer learning, showing adaptability of models trained on one disease, such as AD (with AUC 0.94), to another, such as MCI converters (AUC 0.82) or PD with dementia (AUC 0.81). Recent advancements include 3D CNNs and deeper architectures (i.e. with more hidden layers and some adaptations to allow for that), exemplified by Wu et al.,¹⁹⁴ Zhao et al.,¹⁹⁵ or Etminani et al.,¹⁹⁶ which achieved multiclass classification with remarkable accuracies, for example above an AUC > 0.97 in cross-validation even when distinguishing between very similar conditions in FDG PET, such as PD, multiple system atrophy and progressive supranuclear palsy. However, performances decrease in external testing cohorts.

Complete reviews of AI applications in AD and PD can be found on Kaur et al.,¹⁹⁷ and Dzialas et al.,¹⁹⁸ respectively. Other applications include rarer neurodegenerative disorders,^{199,200} stroke,²⁰¹ epilepsy,^{202–204} and brain injury.²⁰⁵ More studies are though needed

to fully evaluate the relevance of these methods for routine clinical practice. There is however growing evidence for clinical applicability, like a study by Kim et al.,²⁰⁶ who demonstrated that incorporating deep learning-based SUVR assessments in amyloid PET imaging increased inter-reader agreement from 0.46 to 0.76 (calculated by Fleiss kappa coefficients) and confidence among physicians.

1.9.3. AI in Actigraphy

Actigraphy, the continuous recording of movement over time using wearable sensors, provides a rich source of time-series data that reflects patterns of activity, rest, and sleep. Given its complexity and relevance for health monitoring, actigraphy has become a natural domain for the application of AI. Since early studies, AI has shown potential to transform actigraphy analysis from manual and rule-based to automated, data-driven ways. These advancements started with traditional machine learning approaches, with the need for feature extraction to recent deep learning and generative AI models. These advanced models have applications in diagnostics, sleep analysis, behavioural phenotyping, and even mental health prediction.

Early applications of AI in actigraphy focused on sleep/wake classification, a fundamental task in sleep research and clinical monitoring. Traditional rule-based algorithms such as those by Cole-Kripke¹⁴⁰ or Sadeh¹⁴¹ were eventually complemented by machine learning approaches that leveraged handcrafted features from raw acceleration data. For example, Trevenen et al. used a Hidden Markov Model with features extracted from triaxial wrist accelerometry to classify not only wakefulness and sleep, but also discriminate rapid eye movement sleep, stage one sleep, stage two sleep and deep sleep.²⁰⁷ Other models employed random forests using engineered features from multiple statistical measures across accelerometer axes, achieving sleep/wake classification with F1 scores around 74%.²⁰⁸

As access to richer sensor data grew, so did model complexity. Studies incorporating both acceleration and photoplethysmography-derived heart rate data from consumer wearables, like the Apple Watch, explored multiple classifiers (logistic regression, k-NN, random forest, neural networks), with neural networks achieving the best performance—

90% accuracy in sleep-wake classification and around 72% accuracy in classifying wake, REM, and NREM.²⁰⁹ Another study using ActiWatch devices reported high sensitivity for sleep epochs (~96%), but significantly lower for wake (~39%).²¹⁰

More recent developments use deep learning architectures tailored to time-series data. A prominent example is SLAMSS (Sequence-to-Sequence LSTM for Automated Mobile Sleep Staging), which achieves 79% accuracy and a weighted F1 score of 0.80 in three-class classification (wake, NREM, REM), and comparable performance in four-class staging.²¹¹ Similarly, self-supervised learning techniques have emerged, allowing deep neural networks to learn meaningful representations directly from large-scale accelerometry datasets without requiring labelled data. These models demonstrate fair to moderate agreement with polysomnography.²¹²

Beyond sleep-wake classification, AI has also played a growing role in diagnostics and disease classification using actigraphy. As mentioned in chapter 1.8, movement and circadian rhythm patterns can reveal subtle changes associated with neurological, psychiatric, and chronic health conditions.

One such application is in the identification of chronic insomnia. In a recent study, researchers trained machine learning models —namely random forests and support vector machines — to classify individuals as having chronic insomnia or not. A set of nonlinear and dynamic time-domain features extracted from actigraphy signals recorded across multiple nights were used to train the models. The best-performing model, based on a random forest classifier, achieved an accuracy of approximately 80%, demonstrating that machine learning can reliably distinguish individuals with insomnia from healthy sleepers using passive, at-home monitoring data.²¹³

In the context of RBD, AI methods have shown significant promise. As mentioned previously, in one approach, movement features extracted from wearable devices were used to train classifiers capable of distinguishing iRBD from other sleep disorders and healthy controls. When predictions from both the actigraphy model and a dedicated questionnaire were concordant, the system reached nearly perfect specificity and precision, indicating strong potential for high-confidence pre-screening of iRBD in the general population.¹⁵⁷ Additionally, one study also used machine learning to classify patients into PD with RBD or without RBD based on actigraphy.¹⁴⁹

AI has also been applied to motor symptom monitoring in PD. Models using data from multiple body-worn accelerometers and gyroscopes have been developed to detect freezing of gait (FoG) episodes, a common and disabling symptom in PD. Both traditional machine learning approaches, such as random forests, and deep learning models—such as convolutional neural networks—have shown high accuracy, with some models reaching over 95% specificity and up to 81–88% sensitivity in detecting FoG events, even in naturalistic or unscripted environments.²¹⁴ Deep learning solutions like DeepFoG, using CNNs and only a wrist-worn device, also showed high sensitivity and specificity in classifying FoG from normal walking and turning.²¹⁵

AI systems have further been developed to differentiate essential tremor from PD based on gait and balance data from multiple wearable sensors,²¹⁶ and assess motor fluctuations ("on"/"off" states) using deep learning.²¹⁷ These methods often outperform classical machine learning models (e.g., SVM, logistic regression) in terms of F1-score, accuracy, and perform better on unseen data.

AI has also shown excellent results in detecting tremor and quantifying its severity. CNN-based approaches trained on accelerometer data have achieved accuracies up to 97% for distinguishing PD patients with hand tremor and healthy subjects,²¹⁸ and can also estimate tremor severity levels outperforming previously used machine learning models.²¹⁹ Other motor symptoms like bradykinesia can also be detected more accurately with deep learning methods than with traditional pipelines,²²⁰ and models have demonstrated promising performance in classifying PD motor states (OFF, ON, DYSKINETIC) using a single wrist-worn sensor.²²¹

Taken together, these developments demonstrate that AI-powered actigraphy analysis extends far beyond sleep studies, offering powerful tools for diagnosing and phenotyping a wide range of motor and sleep-related disorders in real-world settings.

1.9.4. Classification Models

Among the most widely used architectures for classification tasks are Convolutional Neural Networks (CNNs), Residual Networks (ResNets), and more recently, Transformers.

These models have demonstrated remarkable performance in automatically extracting and learning hierarchical features – low-level patterns first, then higher-level concepts – from raw data, often surpassing traditional machine learning methods in accuracy and generalizability, by performing well on unseen data.

Convolutional Neural Networks (CNNs)

CNNs are specifically designed to process structured grid-like data, such as images or time series.²²² The core building block of a CNN is the convolutional layer, which applies a set of learnable filters (kernels) across the input. For a 2D input image x and a 2D kernel w , the convolution operation producing output y can be written as:

$$y(i, j) = \sum_{m=0}^{M-1} \sum_{n=0}^{N-1} w(m, n) \cdot x(i + m, j + n)$$

Here, $M \times N$ is the size of the kernel, and $y(i, j)$ is the output at location (i, j) in the resulting feature map, which is smaller than the original image. CNNs are composed of multiple layers of convolutional filters that slide across the input to detect local patterns, such as edges or textures, interleaved with non-linear activation functions (e.g., ReLU) and followed by pooling layers that reduce spatial dimensions while retaining the most salient information. The final feature maps are flattened and passed through fully connected layers for classification. By stacking several convolutional and pooling layers, CNNs can capture increasingly abstract features, enabling them to classify complex inputs with minimal manual feature engineering. Visual representations of convolution and pooling are shown in Figure 1.12.

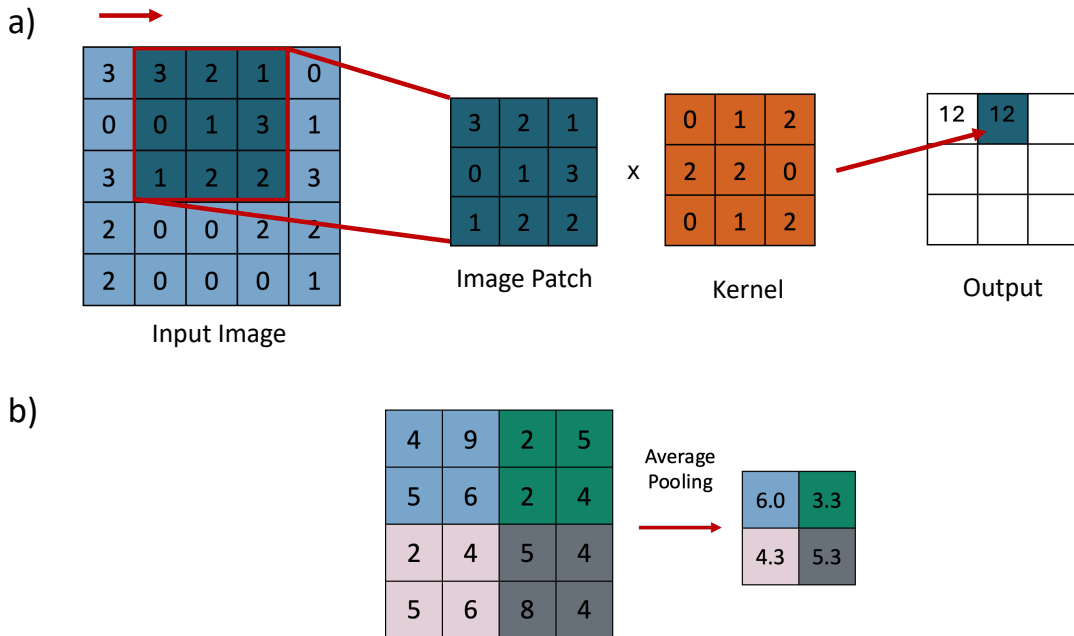


Figure 1.12. Convolutional Neural Networks operations. a) Convolution example; b) Average pooling example.

Residual Networks (ResNets)

Residual Networks represent a significant evolution of CNN architecture. By introducing skip connections (also known as residual connections), these models enable information to bypass one or more layers,²²³ which has a substantial impact on gradient flow during backpropagation and effectively mitigates the vanishing gradient problem. In a ResNet block (visually represented in Figure 1.13), the output is defined as:

$$y = \mathcal{F}(x) + x$$

where x is the input, $\mathcal{F}(x)$ is the transformation learned by a series of layers (typically convolution, batch normalization, and ReLU), and y is the output.

The addition of the input x through a shortcut connection facilitates the learning of identity mappings and improves the propagation of gradients throughout the network. This architectural innovation enables the training of significantly deeper networks—such as ResNet-50 or ResNet-101—without suffering from performance degradation commonly encountered in very deep CNNs.

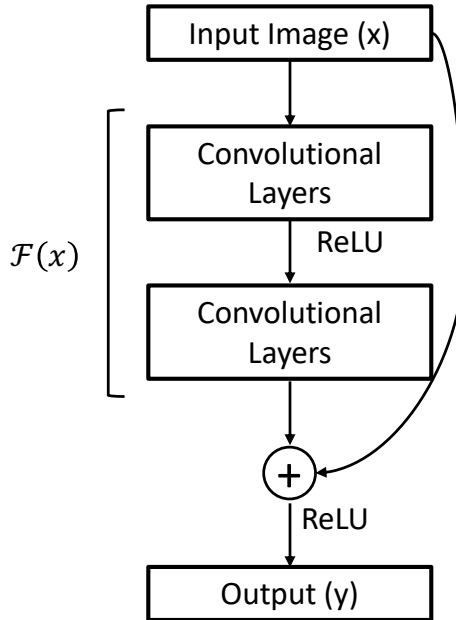


Figure 1.13. Schematic representation of ResNet architecture.

ResNets are known for their robustness, high accuracy, and ability to generalize across complex datasets, making them a popular choice in medical imaging and signal classification tasks.

Transformers

Transformers, originally developed for sequence modeling,²²⁴ have recently been adapted for time series data and also to image classification – the later, through the Vision Transformer (ViT) architecture.²²⁵ Unlike CNNs, which operate through local receptive fields, Transformers use self-attention mechanisms to capture global dependencies across the entire image. In ViTs, an image is divided into a sequence of non-overlapping patches, each flattened and linearly projected into a vector embedding. These embeddings are processed as a sequence $X \in \mathbb{R}^{T \times d}$, where T is the number of patches and d is the embedding dimension.

The core of the Transformer is the self-attention mechanism, defined as:

$$\text{Attention}(Q, K, V) = \text{softmax}\left(\frac{QK^T}{\sqrt{d_k}}\right)V$$

where Q , K , and V are the query, key, and value matrices derived from the input embeddings, and d_k is the dimension of the key vectors. This mechanism enables the model to assign dynamic importance to each patch based on its relationship to all others, allowing it to model global context effectively. Transformers have shown impressive results in many domains and are already being adopted for tasks involving medical signals, such as actigraphy^{226,227} or EEG²²⁸, where temporal and contextual relationships are critical, as well as in imaging applications. A visual representation of the architecture is displayed in Figure 1.14.

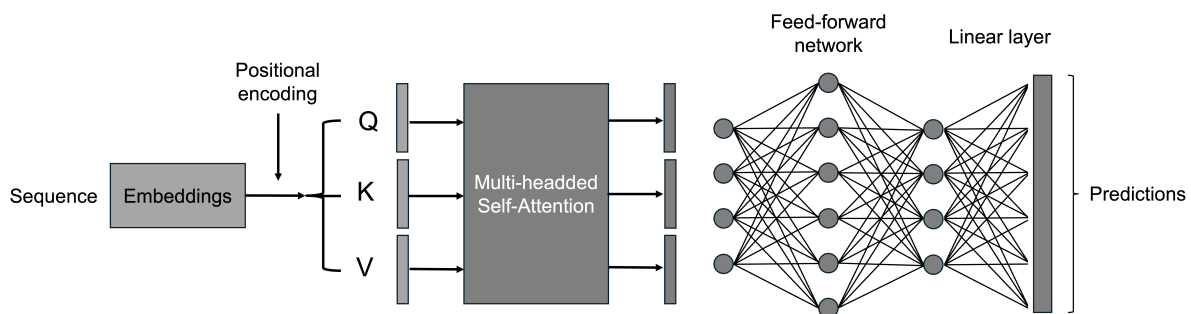


Figure 1.14. Schematic representation of the Transformer’s architecture.

Each of these architectures—CNNs, ResNets, and Transformers—has distinct strengths and computational characteristics. CNNs are efficient and effective for capturing local structure; ResNets facilitate deep representation learning through residual connections; and Transformers provide powerful mechanisms to model long-range dependencies across input regions/sections. In this work, these models are implemented for classification of medical data, specifically PET images and actigraphy recordings, to evaluate their performance and interpretability in the context of neurological disorder assessment.

1.9.5. Generative Models

Generative models are a class of machine learning methods that aim to learn the underlying data distribution and generate new samples that resemble the original data. They have become central to many advances in artificial intelligence, particularly in the context of Transformer-based architectures and large language models (LLMs) such as GPT, which generate coherent text, code, and even images through learned probability distributions.²²⁹

While Transformers and LLMs have gained significant attention in natural language and multimodal tasks, generative modeling has also made substantial progress in the field of computer vision and medical imaging through architectures such as Generative Adversarial Networks (GANs)²³⁰ and, more recently, diffusion models.²³¹ These models play a key role in applications such as image synthesis, data augmentation, super-resolution, and denoising. In the context of biomedical data, generative models are particularly valuable for addressing challenges such as limited sample sizes, data imbalance, and missing or corrupted information.

Generative Adversarial Networks (GANs)

First introduced by Goodfellow et al. in 2014,²³⁰ GANs are composed of two neural networks—the generator G and the discriminator D —that are trained simultaneously. The generator attempts to create realistic synthetic samples from random noise, while the discriminator tries to distinguish between real and generated data. The two models are optimized with opposing objectives: the generator tries to fool the discriminator, and the discriminator tries to correctly identify real versus fake samples.

The original GAN objective can be formulated as:

$$\min_G \max_D E_{x \sim p_{\text{data}}(x)} [\log D(x)] + E_{z \sim p_z(z)} [\log (1 - D(G(z)))]$$

Here, $x \sim p_{\text{data}}(x)$ denotes samples from the true data distribution, and $z \sim p_z(z)$ is a latent variable (usually Gaussian noise). The function D outputs the probability that a given sample is real, aiming for high values on real data and low values on data generated by G . Meanwhile, the generator $G(z)$ learns to map latent vectors z to the data space in such a way that the generated samples are indistinguishable from real ones by the discriminator.

GANs have shown impressive results in high-quality image generation, including realistic synthesis of medical images such as brain MRIs, retinal fundus images, and PET scans.²³² Variants of the original GAN framework, such as CycleGANs and Wasserstein GANs,^{233,234} have further improved training stability and applicability in domain adaptation, image-to-image translation, and data augmentation tasks.²³²

Despite their strengths, GANs suffer from common training challenges such as mode collapse, instability, and the need for careful tuning of network architectures and loss

functions. Nevertheless, their ability to generate visually convincing outputs with sharp details has made them a dominant approach in generative modeling over the past decade.

Cycle GAN

As CycleGAN was one of the main methods used in section 3.1 and corresponding paper, an introduction and mathematical formulation of its architecture is given below.

Cycle GAN²³⁴ is a type of GAN designed for unpaired image-to-image translation. Unlike traditional GANs that require paired training examples, CycleGAN can learn to translate images between two domains without one-to-one correspondence between images. It achieves this by introducing a cycle-consistency loss, which ensures that translating an image from one domain to another and back again results in the original image. This approach enables a wide range of applications, such as style transfer and domain adaptation, especially in scenarios where paired data is scarce or unavailable. In the context of this work, a 3D CycleGAN was developed to make the image-to-image translation between two domains, PET imaging and SPECT imaging. A schematic representation of the architecture is presented in Figure 3.1 of section 3.1. The CycleGAN model includes two generators (G_{PS} - PET to SPECT- and G_{SP} – SPECT to PET) and two associated adversarial discriminators (D_P and D_S).

Each one of the discriminators encourages its corresponding generator to synthesize images similar to the original ones by minimizing an adversarial loss function, defined, for PET to SPECT translation, as:

$$\mathcal{L}_{adv}(G_{PS}, D_S, P, S) = \mathbb{E}_{S \sim p_{data}(S)}[\log D_S(S)] + \mathbb{E}_{P \sim p_{data}(P)}[\log(1 - D_S(G_{PS}(P)))]$$

where P and S are the sampled elements from each probability distribution of PET and SPECT images respectively, G_{PS} is the generator that translates PET to SPECT images and D_S the discriminator that distinguishes between real and synthetic SPECT. A similar adversarial loss for SPECT to PET translation, $\mathcal{L}_{adv}(G_{SP}, D_P, S, P)$, is used.

The synthesized SPECT images are then translated back to the original PET domain, with the G_{SP} (and vice-versa for the synthetic PET images). The cycle consistency loss, $\mathcal{L}_{cyc}(G_{PS}, G_{SP})$, helps ensure that the translated images are similar to the real ones:

$$\mathcal{L}_{cyc}(G_{PS}, G_{SP}) = \mathbb{E}_{P \sim p_{data}(P)}[\| G_{SP}(G_{PS}(P)) - P \|] + \mathbb{E}_{S \sim p_{data}(S)}[\| G_{PS}(G_{SP}(S)) - S \|]$$

The PET scan is inputted into the G_{SP} and vice-versa (SPECT to the G_{PS}) and the output image is compared to the real PET (and SPECT) image, through the identity loss:

$$\mathcal{L}_{id}(G_{PS}, G_{SP}) = \mathbb{E}_{P \sim p_{data}(P)}[\| G_{SP}(P) - P \|] + \mathbb{E}_{S \sim p_{data}(S)}[\| G_{PS}(S) - S \|].$$

The final and total cycleGAN loss is:

$$\begin{aligned} \mathcal{L}(G_{PS}, G_{SP}, D_P, D_S) = & \alpha_1 [\mathcal{L}_{adv}(G_{PS}, D_S, P, S) + \mathcal{L}_{adv}(G_{SP}, D_P, S, P)] + \\ & \alpha_2 \mathcal{L}_{cyc}(G_{PS}, G_{SP}) + \alpha_3 \mathcal{L}_{id}(G_{PS}, G_{SP}), \end{aligned}$$

where $\alpha_1, \alpha_2, \alpha_3$ weight the importance of each loss.

Diffusion Models

Diffusion models are a more recent family of generative models that take a fundamentally different approach. Instead of learning to generate data directly from random noise in a single step, diffusion models progressively learn to reverse a gradual noising process. The model is trained to reconstruct clean data from increasingly noisy versions over a series of timesteps, essentially modeling the data distribution as the reverse of a diffusion process.²³¹

The training objective of a basic diffusion model involves minimizing the difference between predicted and actual noise added to the data at each timestep:

$$\mathcal{L}_{diffusion} = E_{x,\epsilon,t}[\| \epsilon - \epsilon_\theta(x_t, t) \| ^2]$$

where x_t is the noisy image at timestep t , ϵ is the true noise, and ϵ_θ is the neural network's prediction of the noise. During generation, a sample is initialized with Gaussian noise and denoised step-by-step using the learned reverse process.

Diffusion models have achieved state-of-the-art performance in image synthesis tasks, often outperforming GANs in terms of sample diversity and fidelity.²³⁵ In the medical domain, diffusion models are emerging as promising tools for super-resolution, denoising, and data augmentation, although their computational demands and long sampling times remain active areas of research.²³⁶

In summary, generative models such as GANs and diffusion models are powerful tools for learning complex data distributions and generating realistic synthetic data. While GANs are known for producing sharp, high-fidelity samples, and are widely adopted in medical image synthesis, diffusion models offer greater stability and theoretical grounding, making them a compelling alternative for high-quality image generation. As the field evolves, both architectures are expected to play an increasingly important role in augmenting data-limited biomedical research and improving model generalizability in real-world clinical applications.

1.9.6. The next frontier of AI - Foundation and Multimodal Models

From simple statistical models to LLMs, the ultimate goal of those AI-tools is always to improve patient care. The scaling laws in LLMs say that the language modelling performance increases as we increase the model size, dataset size and computing power.²³⁷ This means that models will get better as more data and more effective computational resources are becoming available.

Recently, foundational models have gathered significant interest and excitement. A schematic image of these models is displayed in Figure 1.15. Foundation models are deep learning models that are very large and pretrained with vast amount of diverse data, so that they can perform a wide range of tasks with minimal fine-tuning in these specific tasks. For example, GPT-4,²³⁸ trained on diverse text data, has shown exceptional performance in generating medical summaries or answering diagnostic questions. Another example would be Segment Anything Model,²³⁹ which was trained on a wide variety of images and can perform organ or tumour segmentation in medical imaging. However, these models struggle in performing complex domain-specific tasks. That is why, once pre-trained, foundational models can then be further fine-tuned for specific applications, such as analysing medical images, predicting treatment outcomes, or automating reports, with relatively small amounts of task-specific data. In nuclear medicine, foundational models could enable quick adaptation to tasks like dosimetry prediction or image interpretation, offering a flexible and efficient approach to accelerate AI implementation in medical problems and clinical practice, where data availability is a bottleneck.

Other interest is being given to multimodal AI models.²⁴⁰ With the advancements of models that allow for integration of diverse data sources, for example models that combine data from diverse modalities - such as PET, SPECT, CT, MRI, genomics, and clinical records – it will be possible to create complete and comprehensive patient profiles. The next steps for AI in nuclear medicine will likely involve expanding its integration into clinical workflows, improving the robustness and generalizability of models, and fostering interdisciplinary collaboration.

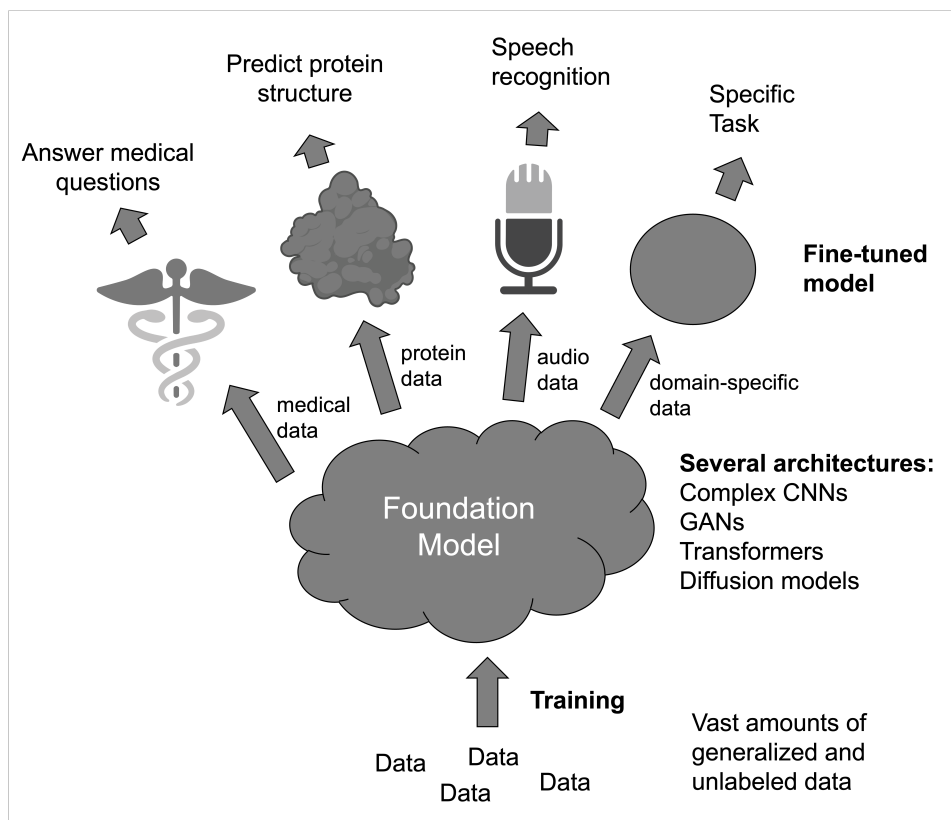


Figure 1.15. Schematic figure of the basis of foundation models.

2. Hypothesis and Aims

The overarching goal of this PhD thesis is to develop AI-based biomarkers for PD and its prodromal stage, iRBD, by integrating neuroimaging and digital health data. The thesis leverages both cross-sectional and longitudinal datasets comprising PET, SPECT, and actigraphy, aiming to improve diagnosis, disease stratification, and prediction of phenoconversion.

The research is structured around three complementary aims, as summarized in **Figure 2.1**. Each aim employs distinct data modalities and computational strategies, yet contributes to the unified goal of identifying early and robust biomarkers of PD progression.

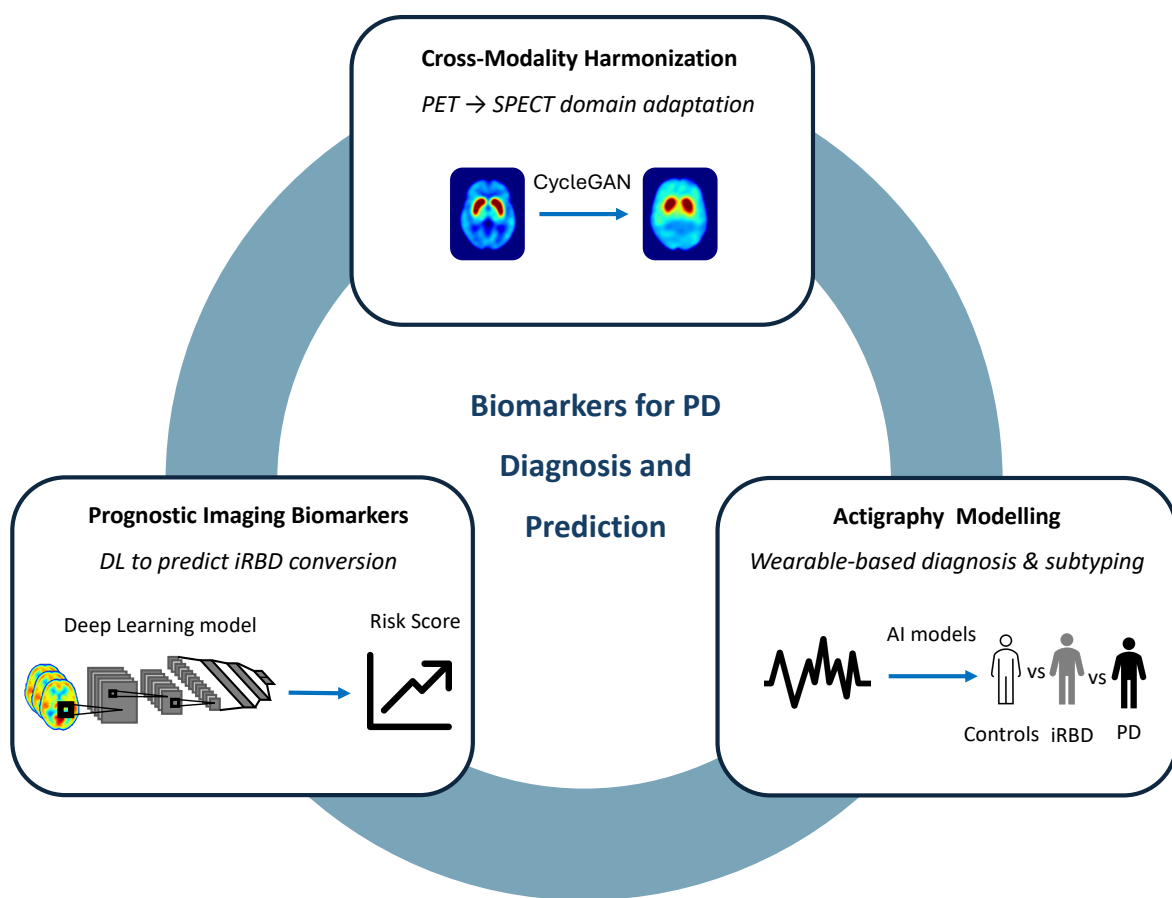


Figure 2.1. Schematic figure of the aims of this PhD thesis.

Aim 1: Cross-Modality Translation of Dopaminergic Imaging for AI-based Biomarker Development

This aim addresses the challenge of modality inconsistency between PET and SPECT in dopaminergic imaging across regions. A CycleGAN model is developed to translate [¹¹C]CFT PET images to [¹²³I]FP-CIT SPECT images, enabling harmonization of datasets across imaging centers. The hypothesis is that synthetic SPECT images retain disease-relevant information sufficient for downstream AI-based diagnostic tasks, thus facilitating the use of large-scale PET data in SPECT-centric clinical frameworks.

Tools & Data: CycleGAN, classification networks, [¹¹C]CFT PET (n=602), [¹²³I]FP-CIT SPECT (n=1152)

Key Metric: Diagnostic performance of classifiers trained on synthetic SPECT

Aim 2: Prediction of Phenoconversion in iRBD using PET-based Deep Learning

This aim focuses on developing deep learning-based prognostic biomarkers to predict phenoconversion of iRBD to PD or dementia with Lewy bodies. Using pre-trained classifiers on DAT and FDG PET images of overt PD and controls, deep imaging risk scores (DIRS) are computed to quantify the probability of conversion over time in iRBD patients. The central hypothesis is that these imaging-based risk scores increase with disease progression and outperform conventional metrics in predicting short- and long-term conversion.

Tools & Data: Transfer learning with 3D CNNs, DAT and FDG PET in iRBD (n=38)

Key Metric: Area under the ROC curve (AUC) for conversion prediction at 2–8 years

Aim 3: Actigraphy-Based AI Models for Non-Invasive Diagnosis of PD and RBD

The third aim explores actigraphy as a low-cost, scalable digital biomarker for PD diagnosis and stratification. Both traditional machine learning and deep learning models—including a pretrained transformer—are evaluated for classifying PD vs controls and PD with RBD (PD-RBD) vs PD without RBD (PD-noRBD). The models are tested on iRBD patients to assess their potential for early-stage detection. The hypothesis is that actigraphy-based AI

models can differentiate PD subtypes and identify prodromal individuals at risk of phenoconversion.

Tools & Data: PAT model, CNNs, ML classifiers, actigraphy in PD-RBD, PD-noRBD, RLS controls

Key Metric: Classification AUC, accuracy, and interpretability of extracted features

Underlying Assumptions

- PET/SPECT and actigraphy data contain complementary, clinically relevant information for diagnosis and prognosis.
- PD and iRBD represent a continuum, with iRBD as a prodromal stage of α -synucleinopathies.
- AI models trained on well-defined clinical groups can generalize to at-risk or prodromal individuals.
- Neurodegeneration in PD is progressive, with temporal patterns detectable in imaging and actigraphy data.

3. Results

3.1. Cross-Modality Translation of Dopaminergic Imaging for AI-based Biomarker Development

This chapter has been published as an original research article in the European Journal of Nuclear Medicine with the following reference²⁴¹:

Lopes L, Jiao F, Xue S, et al. Dopaminergic PET to SPECT domain adaptation: a cycle GAN translation approach. *Eur J Nucl Med Mol Imaging*. 2025;52(3):851-863. doi:10.1007/s00259-024-06961-x

Contributions:

My contributions for this article were the design and implementation of the deep learning pipeline, including the development and training of the CycleGAN model for cross-modality image translation between [¹¹C]CFT PET and [¹²³I]FP-CIT SPECT scans, based on previous work from Song Xue, co-author of the paper. The code for the CycleGAN is available at <https://github.com/leonorlopes96/DAT-cycle-gan.git>. Additionally, I performed comprehensive data preprocessing, including quality control, image normalization, and preparation of input-output pairs for model training. I also designed and executed the evaluation framework, which involved both quantitative assessments (e.g., Fréchet Inception Distance, classification performance, binding ratio analysis) and qualitative analyses (e.g., visual grading by experts). I also developed the controls vs PD classification model based on DAT imaging, available at <https://github.com/leonorlopes96/DAT-DL-classification.git>. In addition, I generated all figures and tables, contributed to the interpretation of results in the clinical context, and led the writing and revision of the manuscript.

Dopaminergic PET to SPECT Domain Adaptation:

A Cycle GAN translation approach

Leonor Lopes^{1,2}, Fangyang Jiao³, Song Xue^{1,4}, Thomas Pyka¹, Korbinian Krieger¹, Jingjie Ge^{3,5}, Qian Xu^{3,5}, Rachid Fahmi⁶, Bruce Spottiswoode⁶, Ahmed Soliman⁶, Ralph Buchert⁷, Matthias Brendel^{8,9,10}, Jimin Hong^{1,2}, Yihui Guan^{3,5}, Claudio LA Bassetti¹¹, Axel Rominger¹, Chuantao Zuo^{3,5}, Kuangyu Shi^{1,12} and Ping Wu^{3,5}

1 - Department of Nuclear Medicine, Inselspital, Bern University Hospital, University of Bern, Bern, Switzerland

2 - Graduate School for Cellular and Biomedical Sciences, University of Bern, Bern, Switzerland

3 - Department of Nuclear Medicine & PET Center, Huashan Hospital, Fudan University, Shanghai, China

4 - Department of Biomedical Imaging and Image-Guided Therapy, Division of Nuclear Medicine, Medical University of Vienna, Vienna, Austria

5- National Center for Neurological Disorders & National Clinical Research Center for Aging and Medicine, Huashan Hospital, Fudan University, Shanghai, China

6- Siemens Medical Solutions USA, Inc., Knoxville, Tennessee, United States

7 - Department of Diagnostic and Interventional Radiology and Nuclear Medicine, University Medical Center Hamburg-Eppendorf, Hamburg, Germany

8 - Department of Nuclear Medicine, University Hospital, Ludwig Maximilian University of Munich, Munich, Germany

9- Munich Cluster for Systems Neurology (SyNergy), Munich, Germany

10 - German Center for Neurodegenerative Diseases (DZNE), Munich, Germany

11 - Department of Neurology, Inselspital, Bern University Hospital, University of Bern, Bern, Switzerland

12 - Department of Informatics, Technical University of Munich, Munich, Germany

Abstract

Purpose: Dopamine transporter imaging is routinely used in Parkinson's disease (PD) and atypical parkinsonian syndromes (APS) diagnosis. While [¹¹C]CFT PET is prevalent in Asia with a large APS database, Europe relies on [¹²³I]FP-CIT SPECT with limited APS data. Our aim was to develop a deep learning-based method to convert [¹¹C]CFT PET images to [¹²³I]FP-CIT SPECT images, facilitating multicenter studies and overcoming data scarcity to promote Artificial Intelligence (AI) advancements.

Methods: A CycleGAN was trained on [¹¹C]CFT PET (n=602, 72%PD) and [¹²³I]FP-CIT SPECT (n=1152, 85%PD) images from PD and non-parkinsonian control (NC) subjects. The model generated synthetic SPECT images from a real PET test set (n=67, 75%PD). Synthetic images were quantitatively and visually evaluated.

Results: Fréchet Inception Distance indicated higher similarity between synthetic and real SPECT than between synthetic SPECT and real PET. A deep learning classification model trained on synthetic SPECT achieved sensitivity of 97.2% and specificity of 90.0% on real SPECT images. Striatal specific binding ratios of synthetic SPECT were not significantly different from real SPECT. The striatal left-right differences and putamen binding ratio were significantly different only in the PD cohort. Real PET and real SPECT had higher contrast-to-noise ratio compared to synthetic SPECT. Visual grading analysis scores showed no significant differences between real and synthetic SPECT, although reduced diagnostic performance on synthetic images was observed.

Conclusion: CycleGAN generated synthetic SPECT images visually indistinguishable from real ones and retained disease-specific information, demonstrating the feasibility of translating [¹¹C]CFT PET to [¹²³I]FP-CIT SPECT. This cross-modality synthesis could enhance further AI classification accuracy, supporting the diagnosis of PD and APS.

Keywords: CFT PET; FP-CIT SPECT; domain adaptation; Parkinson's disease; Cycle GAN

Background

Dopamine transporter (DAT) imaging, such as positron emission tomography (PET) with [¹¹C]2β-carbomethoxy-3β-(4-fluorophenyl) tropane ([¹¹C]CFT) and single photon emission computed tomography (SPECT) with [¹²³I]2β-carbomethoxy-3β-(4-iodophenyl)-N-(3-fluoropropyl) nortropane ([¹²³I]FP-CIT; DaTscan™, GE Healthcare), is a powerful tool in the differential diagnosis of idiopathic Parkinson's disease (PD) from essential tremor or other secondary parkinsonism without nigrostriatal degeneration. However, this imaging tool is currently unreliable for differentiating PD from atypical neurodegenerative parkinsonian syndromes (APS), such as multiple system atrophy (MSA) or progressive supranuclear palsy (PSP).²⁴²

In clinical practice, the use of visual interpretation and semi-quantitative analysis has demonstrated high diagnostic accuracy for PD and essential tremor differentiation.^{133,243–245} In research, semi-quantitative methods are generally preferred as they provide more objective measurements of DAT density.²⁴⁶ The striatal specific binding ratio (SBR) is the most commonly used semi-quantitative measure.^{246,247} However, the lack of consistency in SBR measurements across different research sites, image acquisition techniques, reconstruction processes, and data analysis methods poses a challenge in longitudinal/multicenter studies.

Recently, Artificial Intelligence (AI), especially deep learning (DL), could achieve similar, if not higher, diagnostic accuracy than previous conventional methods,¹⁹² even in differentiating PD from APS.^{248,249} [¹¹C]CFT PET is widely accessible in Asia and a substantial APS database was collected to support AI advancements.²⁴⁹ [¹²³I]FP-CIT SPECT is widely used in Europe,^{60,246} however, limited APS data is available. A cross-modality synthesis between the two imaging techniques is appealing as it could allow better reproducibility of SBR and other quantitative measures and assist in AI diagnosis in modalities with a lack of sufficient data.

Generative adversarial networks (GANs)²³⁰ have remarkable capabilities in cross-modality medical image synthesis.^{250–254} Moreover, GANs tackle various other medical challenges, such as image quality recovery²⁵⁵ or CT-free PET paradigm.²⁵⁶ These methods can alleviate data scarcity in medical research, by generating substantial quantities of realistic data. Cycle-consistency GAN (Cycle GAN)²³⁴ stand out in medical image-to-image synthesis,

as it does not need paired data for training, due to its cycle-consistency loss.^{257–260} Cycle GAN has also been successfully used in multi-modality synthesis. In our case, although the same target is used (DAT), the modalities can differ due to different half-lives of the labels Carbon-11 and Iodine-123 and the different acquisition times. Thus, as we are dealing with different modalities and no paired data is available, we aimed to develop a Cycle GAN-based approach for cross-modality synthesis to improve interchangeability between [¹¹C]CFT PET and [¹²³I]FP-CIT SPECT.

Materials and methods

Data

This retrospective study included [¹¹C]CFT PET brain images (DAT PET) from the Huashan Parkinsonian PET Imaging (HPPI) database and [¹²³I]FP-CIT SPECT brain images (DAT SPECT) openly available from Parkinson's Progression Markers Initiative (PPMI) database.

HPPI Data

The Normal Controls (NC) cohort included 43 DAT PET scans from healthy subjects and 142 from subjects with normal DAT imaging, with a total of 185 subjects. In the PD cohort, we included 484 DAT PET from patients diagnosed with PD.

All included patients from the HPPI performed a DAT PET and an MRI to exclude structural brain abnormalities at Huashan Hospital. Patients with PD were diagnosed by movement disorder specialists on their return visits after PET examination, according to the current diagnostic criteria.⁴⁴ The inclusion criteria for healthy controls and normal DAT subjects can be found in the supplementary materials.

DAT PET Acquisition and Reconstruction

DAT PET scans were all acquired with a Biograph™ 64 HD PET/CT (Siemens Medical Solutions USA, Inc., Molecular Imaging, Knoxville, TN), one hour after an intravenous injection of 333-407 MBq (9-11mCi) of [¹¹C]CFT. The duration of acquisition was 15 minutes. Low dose CT was performed previously for attenuation correction. Iterative 3D-ordered subset expectation maximization algorithm was used to reconstruct the images after corrections for scatter, dead time and random coincidences.

PPMI Data

The PPMI is a large, international multicenter clinical study that aims to identify various biomarkers for the progression of de novo PD.

We included 194 reconstructed [¹²³I]FP-CIT SPECT (DaTscan™) scans from the Healthy Controls Cohort – NC group – and 1086 from the PD cohort – PD group – from the PPMI initiative (www.ppmi-info.org/data).

Participants in this study were individuals diagnosed with PD who were at least 30 years old, regardless of gender. The PPMI study had specific criteria for participant eligibility that can be found at <https://www.ppmi-info.org/study-design/research-documents-and-sops>.

DAT SPECT Acquisition and Reconstruction

DAT SPECT scans are acquired four hours after injection of 3-5 mCi (111-185 MBq) of DaTscan™. CT was performed for attenuation correction and the Hermes (Hermes Medical Solutions, Stockholm) iterative ordered-subsets-expectation-maximization algorithm was used to reconstruct the images. The detailed PPMI [¹²³I]FP-CIT SPECT protocol can be found at <https://www.ppmi-info.org/study-design/research-documents-and-sops>.

Image preprocessing

Before inputting the images into the model, they were spatially normalized into the Montreal Neurological Institute (MNI) brain space using SPM 5 (<http://www.fil.ion.ucl.ac.uk/spm>), implemented in Matlab 7.4.0 (Mathworks Inc, Sherborn, MA). To facilitate the Cycle GAN training the images were then smoothed by a 3D Gaussian filter of 10 mm for PET and 6 mm for SPECT full width at half maximum (FWHM). Intensity normalization was performed by dividing each voxel by the maximum value of each training dataset (described below). We applied the SPM brain mask from the MNI brain space atlas before inputting the images into the CycleGAN.

Cycle GAN

Model

A 3D CycleGAN (20) was developed to make the image-to-image translation between two domains, DAT PET imaging and DAT SPECT imaging. The CycleGAN model includes two generators (G_{PS} - PET to SPECT- and G_{SP} – SPECT to PET) and two associated adversarial discriminators (D_P and D_S). Each of the discriminators encourages its corresponding generator to synthesize images similar to the original ones by minimizing an adversarial loss function. The synthesized SPECT images are then translated back to the original PET domain, with the G_{SP} (and vice-versa for the synthetic PET images). The cycle consistency loss helps ensure that the translated images are similar to the real ones. The PET scan is inputted into the G_{SP} and

vice-versa (SPECT to the G_{PS}) and the output image is compared to the real PET (and SPECT) image, through the identity loss.

Detailed formulas and networks structures are shown in the supplementary material.

Figure 3.1 shows a scheme of our cycle GAN model.

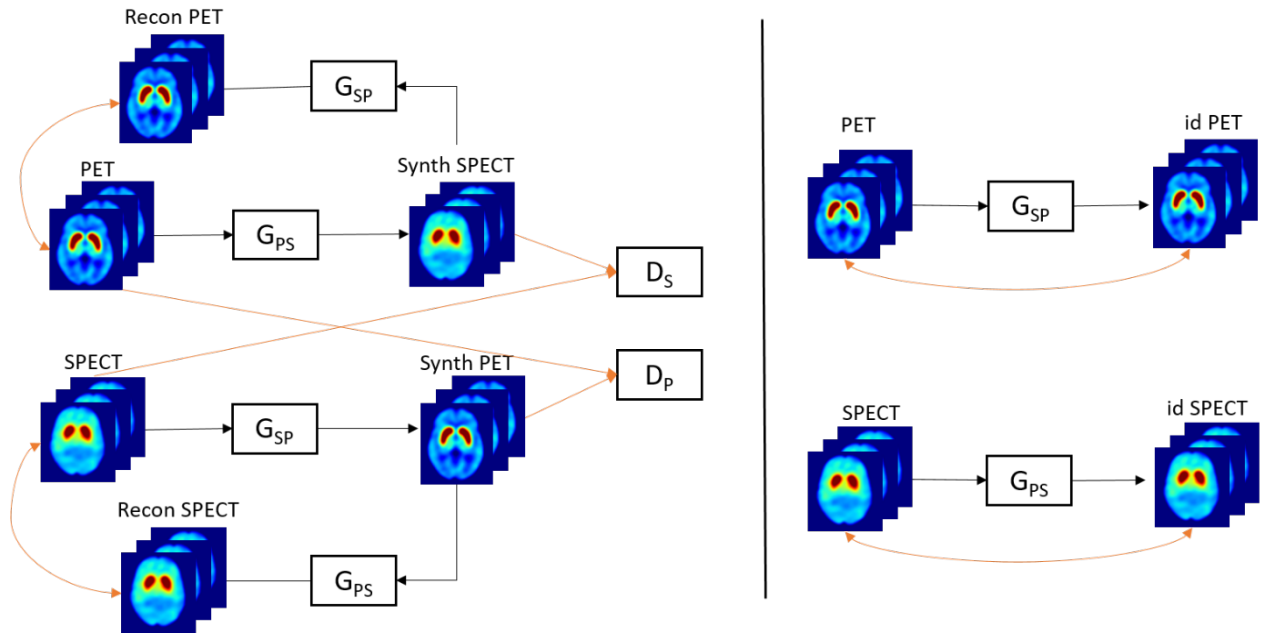


Figure 3.1. Scheme of our Cycle GAN model. G_{PS} : Generator of PET to SPECT; G_{SP} : Generator of SPECT to PET. D_P : Discriminator of real and synthetic PET; D_S : Discriminator of real and synthetic SPECT; Recon PET/SPECT: Reconstructed PET/SPECT back to original domain; Synth PET/SPECT: Synthetic PET/SPECT; id PET/SPECT: identity PET/SPECT that should be unchanged when passed through the G_{SP}/G_{PS} generators.

Training and image generation

We trained the CycleGAN with 90% of PPMI SPECT and HPPI PET and used the remaining 10% as testing datasets to evaluate the performance of the model. For these evaluations, we generated synthetic SPECT images from the real PET images in the testing dataset. We applied the SPM brain mask in the MNI space and a Gaussian filter of 1.7 FWHM before further analysis, to smooth the images with a grid-like texture (Supplementary Figure 2). Table 3.1 shows the number of scans from each dataset in training and testing procedures.

The model was trained in a NVIDIA GeForce RTX 2080 Ti GPU (NVIDIA Corporation, Santa Clara, CA, USA) for 200 epochs with a batch size of 1 due to memory constraints. We used binary cross entropy loss for the adversarial loss and L1 loss for the cycle consistency and

identity losses, with weights of 10 for the cycle consistency and 1 for the others. Adam optimizer was used with a learning rate of 2e-4.

Table 3.1. Huashan Parkinsonian PET Imaging (HPPI) and Parkinson’s Progression Markers Initiative (PPMI) datasets’ size and corresponding training and testing splits’ size per class/disease. NC: Normal controls; PD: Parkinson disease.

		HPPI PET data	PPMI SPECT data
Training dataset	NC	168	174
	PD	434	978
Testing dataset	NC	17	20
	PD	50	108
Total		669	1280

Evaluation of results

Fréchet Inception Distance

To assess the high-level perceptual image similarity between synthetic SPECT and real SPECT and PET, we calculated the Fréchet Inception Distance (FID). The FID, introduced by Heusel, M. et al. in 2017,²⁶¹ is a widely adopted metric to compare the quality of images synthesized by generative models, particularly when paired data is not available and thus, methods such as root-mean-square error (RMSE) and structural similarity index (SSIM) cannot be used. A lower FID value suggests greater similarity between the two datasets in terms of their statistical properties. FID is calculated as the Wasserstein-2 distance between the multi-variate Gaussians fitted to data embedded into a feature space, employing a pre-trained Inception V3 network. We performed bootstrapping with replacement to perform statistical comparison (Student’s t-test) between FIDs of synthetic SPECT with real SPECT and synthetic SPECT with real PET.

Deep-Learning Classification model

A classification network was trained using the synthetic SPECT data and tested on the real SPECT test set. A previously developed network, based on the ResNet architecture and

validated for the differential diagnosis between PD and APS, was used.²⁴⁹ The final linear layer of this network was modified to enable binary classification to differentiate between two classes (NC and PD) with log sigmoid activation. The highest log probability (NC or PD) determined the prediction for diagnostic evaluation. The model was trained for 50 epochs, with early stop if validation accuracy did not improve in 30 epochs. The initial learning rate was 1e-4 and was reduced by a factor of 0.5 when validation loss did not improve for 10 epochs. Adam optimizer and the negative log likelihood loss were used.

Semi-quantitative Analysis

We calculated the striatum specific binding ratio (SBR), caudate specific binding ratio (CBR) and putamen specific binding ratio (PBR) for each already preprocessed image in the synthetic SPECT, real SPECT, and real PET test datasets and then assessed the differences between test datasets. The regions of interest (ROI), including striatum, putamen or caudate, binding ratios were calculated as follows:

$$\frac{\text{mean counts of ROI} - \text{mean counts of background region}}{\text{mean counts of background region}},$$

where the background region corresponds to a region within the occipital lobe.

The ROI and occipital regions were obtained by applying the CerebrA template to each image after being registered to the MNI space.²⁶²

We also calculate the absolute differences between left (SBR_L) and right striatum (SBR_R) as $|\text{SBR}_L - \text{SBR}_R|$.

Contrast-to-noise ratio

To measure the image quality, we also calculated the contrast-to-noise ratio (CNR) for each already preprocessed image in the synthetic SPECT, real SPECT, and real PET test datasets and then assessed the differences between test datasets. The CNR was calculated as follows:

$$\text{CNR} = \frac{\text{mean counts of striatum} - \text{mean counts of background region}}{\text{standard deviation of counts of background region}}$$

Blind Visual Assessment

Four nuclear medicine physicians (T.P.: 5 years of experience; K.K.: 2 years of experience; J.G.: 6 years of experience F.J.: 7 years of experience) evaluated the quality of the synthetic images through absolute visual grading analysis (VGA).²⁶³ Ten synthetic SPECT images were generated from 10 real PET (5 NC and 5 PD) randomly selected from the HPPI test set. Additionally, 10 real SPECT images from the PPMI test set were chosen randomly. These 20 datasets were mixed and presented to the readers, who had no information about data source (synthetic or original) or diagnosis (NC or PD).

Readers, untrained in detecting synthetic images, assessed images based on four criteria using a 3-point Likert scale: level of noise (1=low, 2=medium, 3=high), presence of artifacts (1=absent, 2=uncertain, 3=present), synthetic appearance (1=real, 2=uncertain, 3=synthetic), and confidence in diagnosis (1=insufficient, 2=sufficient, 3=good/confident). VGA Scores (VGAS) for each of these four criteria were computed for each image dataset (real and synthetic SPECT) based on these assessments as:

$$\text{VGAS} = \frac{\sum_{O,I} S_c}{N_i N_o}$$

where S_c are the given individual scores for observer (O) and image (I), N_i is the total number of images and N_o is the total number of observers.

The physicians also made a diagnosis, as either NC or PD.

Statistical Analysis

Statistical analysis was performed using *Python* 3.11.4 with the libraries *Scipy* 1.11.1 and *Scikit-learn* 1.3.0. Cycle GAN was implemented using *Keras* 2.12.0 library and the DL classification model using *Pytorch* 1.13.0. Differences were considered significant for $p < 0.05$, using two-sided p-values. Effect size was calculated with Cohen's d. Shapiro-Wilk test was used to assess sample normality, and statistical tests chosen accordingly. Differences in FID, SBR, CBR, PBR values and left-right striatum differences were assessed by the Student's *t*-test and p-values and 95% confidence intervals (95%CI) are shown. Values are presented as mean \pm standard deviation (SD). The area under the receiver operating characteristic (ROC) curve

(AUC), sensitivity, specificity, positive predictive value (PPV), and negative predictive value (NPV) were obtained to evaluate the performance of the classification DL model. Differences in CNR were assessed by Mann-Whitney U test. CNR are presented as mean \pm SD. Differences in VGAS were assessed by the Mann-Whitney U test. VGAS were presented as mean \pm SD.

Results

Fréchet Inception Distance

The FID between real PET and synthetic SPECT test sets (152.3 ± 0.58) was higher than the FID between real SPECT and synthetic SPECT (142.6 ± 0.70 ; $p < 0.001$; 95%CI [-9.78, -9.53]).

Deep-Learning Classification

The ROC curve of the DL classification model is presented in Figure 3.2. The model trained with synthetic SPECT achieved an AUC of 0.992, sensitivity of 97.2%, specificity of 90.0%, PPV of 98.1 %, and NPV of 85.7% for the classification of the real SPECT test set into NC vs. PD.

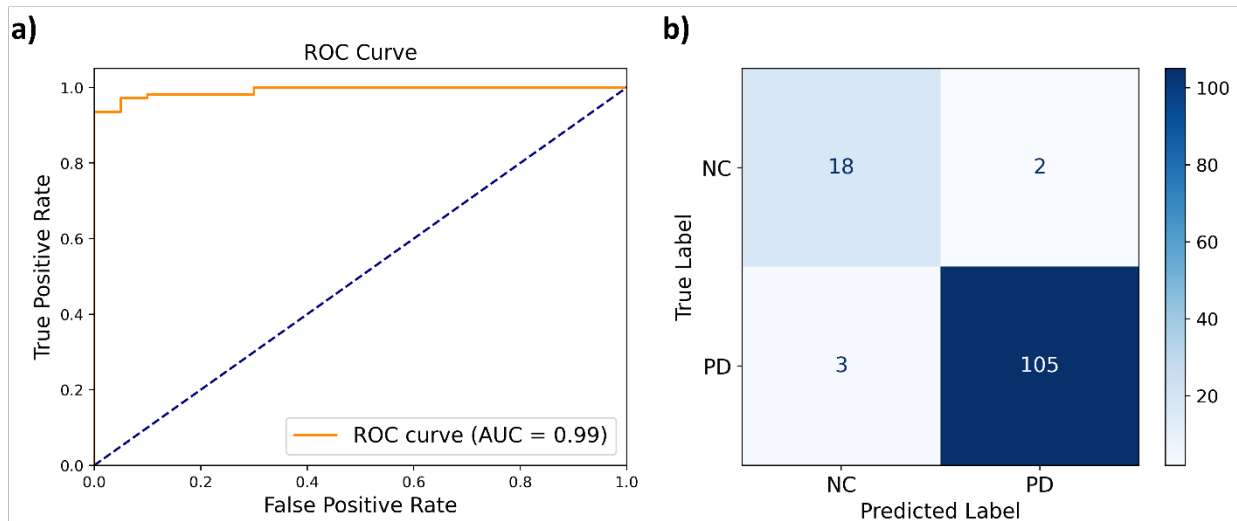


Figure 3.2. Performance of the DL classification model in NC vs PD classification in the real SPECT test set. (a) Receiver Operating Characteristics (ROC) Curve. (b) Confusion Matrix. NC: Normal controls; PD: Parkinson disease.

Semi-quantitative Analysis

As shown in Figure 3.3a, the SBR values of the NC synthetic SPECT dataset (1.83 ± 0.17) were not significantly different from the SBRs of the NC real SPECT (2.05 ± 0.42 ; $p = 0.05$, 95%CI [0.00, 0.45]). Similar results were found for the PD synthetic SPECT (1.13 ± 0.29) versus the real SPECT dataset (1.10 ± 0.33 ; $p = 0.31$, 95%CI [-0.05, 0.16]). However, differences were significant ($p < 0.001$) between synthetic SPECT and real PET (NC: 1.57 ± 0.20 ; 95%CI [0.12,

0.39]; PD: 0.92 ± 0.30 ; 95%CI [0.09, 0.33]), in both NC and PD. Similarly, to real PET and SPECT data, significant differences were found in striatal SBR in synthetic SPECT between NC and PD groups ($p < 0.001$; 95%CI [0.54, 0.84]).

In figure 3.3b, the caudate binding ratios (CBRs) of the NC synthetic SPECT dataset (1.74 ± 0.17) were significantly different from the CBRs of the NC real SPECT (2.02 ± 0.46 ; $p = 0.02$; 95%CI [0.05, 0.54]), with smaller differences than when comparing to NC real PET (1.17 ± 0.17 ; $p < 0.001$; 95%CI [0.44, 0.69]). In the PD cohort, the CBRs were not significantly different in the synthetic SPECT (1.12 ± 0.31) compared to the real SPECT (1.19 ± 0.38 ; $p = 0.26$; 95%CI [-0.19, 0.05]). Significant differences were found in CBRs in synthetic SPECT between NC and PD groups ($p < 0.001$; 95%CI [0.46, 0.77]).

In figure 3.3c, the putamen binding ratios (PBRs) differences are significant in the PD cohort between synthetic SPECT (1.14 ± 0.27) and real SPECT (0.96 ± 0.31 ; $p = 0.001$; 95%CI [0.07, 0.27]). PBR differences in the synthetic SPECT NC (1.93 ± 0.18) and PD cohorts are significant ($p < 0.001$; 95%CI [0.65, 0.93]).

As shown in figure 3.3d, absolute differences between right and left SBR are significant between PD synthetic SPECT (0.11 ± 0.09) and PD real SPECT (0.19 ± 0.15 ; $p = 0.001$; 95%CI [-0.12, -0.03]) and between NC synthetic SPET (0.11 ± 0.03) and NC real PET (0.07 ± 0.07 ; $p = 0.02$; 95%CI [0.01, 0.08]).

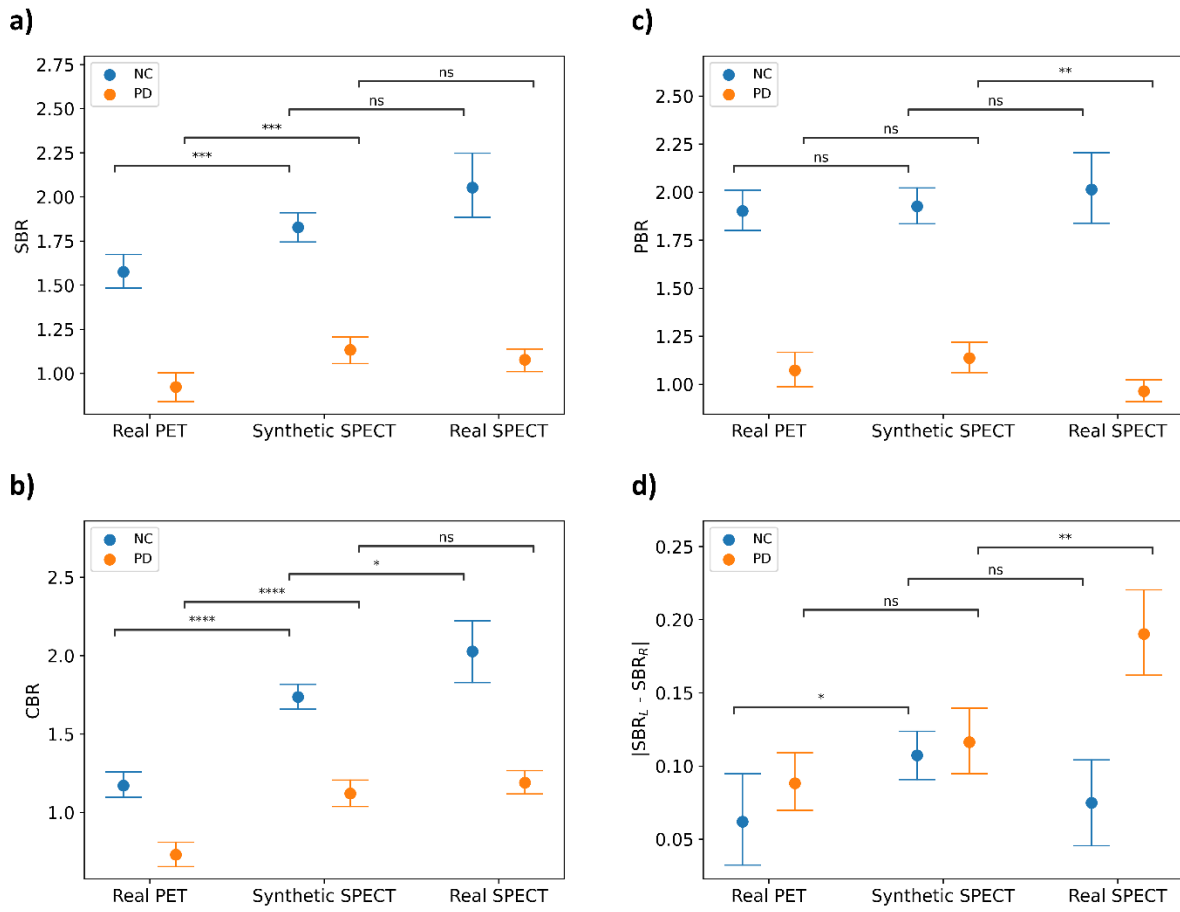


Figure 3.3. Average Specific Binding Ratios of the synthetic SPECT, real SPECT, and real PET test datasets, both in NC and PD, for striatum (a), caudate (b) and putamen (c) and left-right striatal differences (d). Error bars represent the standard deviation. ns: non-significant, $*p < 0.05$, $**p < 0.01$, $***p < 0.001$, $****p < 0.0001$ (Student's *t*-test). NC: Normal controls; PD: Parkinson disease.

Contrast-to-noise Ratio

The CNR was higher in real PET of both NC (18.85 ± 17.56) and PD (11.34 ± 9.74) compared to Synthetic SPECT of NC (9.66 ± 1.64 ; $p = 0.002$) and PD (6.31 ± 1.67 ; $p < 0.001$), respectively. The CNR was also higher in NC (14.48 ± 3.49) and PD (8.16 ± 3.62) of real SPECT compared to NC ($p < 0.001$) and PD ($p = 0.002$) of Synthetic SPECT. Results are presented in Figure 3.4.

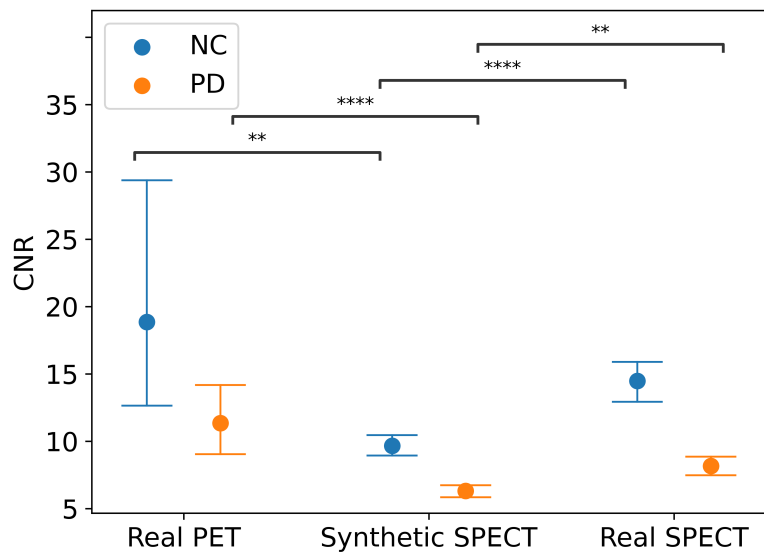


Figure 3.4. Average contrast-to-noise (CNR) of the synthetic SPECT, real SPECT, and real PET test datasets, both in NC and PD. Error bars represent the standard deviation. ** $p < 0.01$, *** $p < 0.0001$ (Mann-Whitney U test). NC: Normal controls; PD: Parkinson disease.

Blind Visual Assessment

As shown in Figure 3.5, Mann-Whitney U test showed no significant differences between real and synthetic SPECT in VGAS of all criteria analyzed (Synthetic Appearance: $p = 0.18$; Level of Noise: $p = 0.73$; Artifacts: $p = 0.86$; Confidence in diagnosis: $p = 0.11$). The results of individual readers are presented in the Supplementary Table 1.

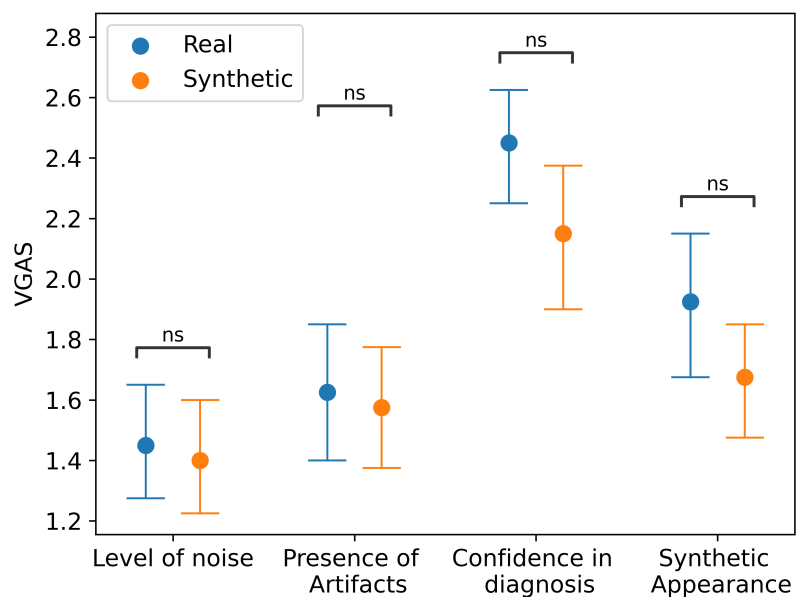


Figure 3.5. Differences in Visual Grading Analysis Score (VGAS) between real and synthetic SPECT images in all the categories analyzed – level of noise, presence of artifacts, confidence in diagnosis, and synthetic appearance. Error bars represent the standard deviation. ns: $p > 0.05$ (Mann-Whitney U test).

As displayed in Table 3.2, the NC vs PD diagnostic performance of the majority of the readers is lower in synthetic SPECT images than in the real ones.

Table 3.2. Diagnostic performance in terms of AUC, sensitivity, specificity, PPV, and NPV of individual readers on real and synthetic SPECT images. Diagnostic performance corresponds to the ability to differentiate NC vs PD cases.

Reader	Dataset	AUC	Sensitivity (%)	Specificity (%)	PPV (%)	NPV (%)
#1	Real	0.90	100	80	83.3	100
	Synthetic	0.90	100	80	83.3	100
#2	Real	0.90	100	80	83.3	100
	Synthetic	0.80	60	100	100	71.4
#3	Real	0.70	100	40	62.5	100
	Synthetic	0.50	80	20	50	50
#4	Real	0.90	100	80	83.3	100
	Synthetic	0.60	40	80	66.6	57.1

Examples of 2 cases of real and synthetic SPECT images from both NC and PD groups are shown in Figure 3.6. Mean images are shown on Supplementary Figure 1. An example of a synthetic SPECT with artifacts is shown in Supplementary Figure 3.

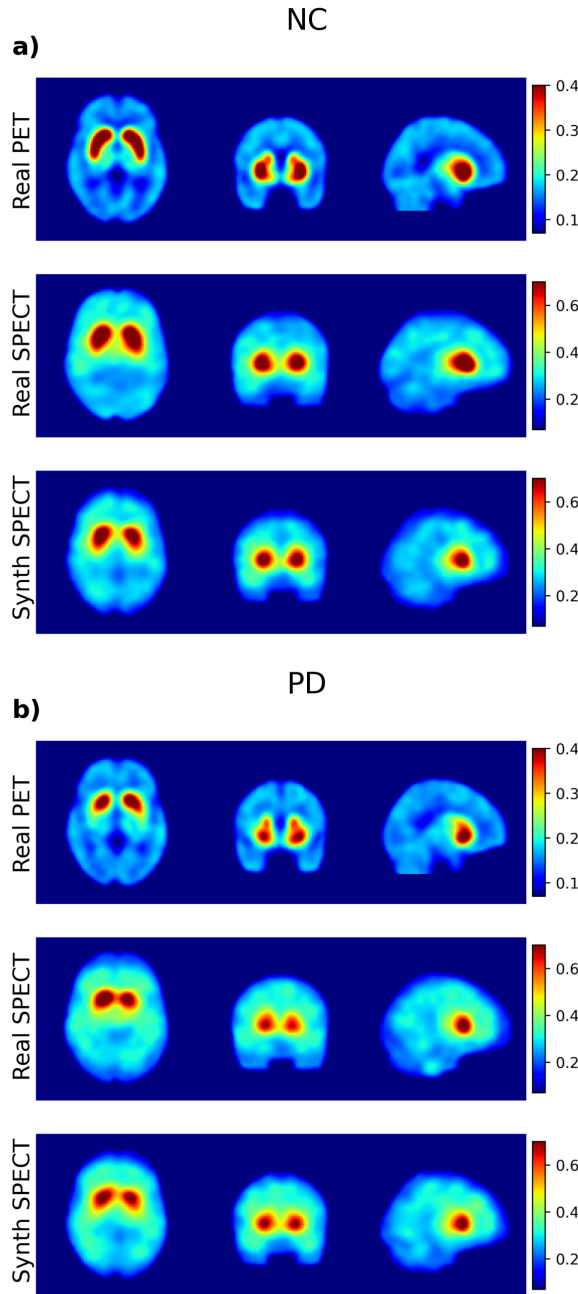


Figure 3.6. Example of images of (a) normal controls and (b) Parkinson's disease from real PET (upper row), real SPECT (middle row) and synthetic SPECT (bottom row).

Discussion

In this study, we explored for the first time the domain adaptation from DAT PET to DAT SPECT in the context of PD. Our results demonstrated the potential of Cycle GAN as a valuable tool for bridging the domain gap between these two modalities, improving AI-based diagnosis.

One of the key achievements of this study was the generation of visually indistinguishable synthetic DAT SPECT images from the DAT PET images. The FID of synthetic SPECT images compared to real SPECT was lower than that of synthetic SPECT compared to real PET. This suggests that the synthetic SPECT images closely resemble real SPECT not only in visual appearance but also in high-level statistical features. This finding highlights the effectiveness of our approach in preserving essential characteristics of the original SPECT images during the translation process.

Furthermore, the deep learning classification model trained on these synthetic images demonstrated strong performance in identifying PD in real SPECT data. This result highlights the potential of Cycle GAN in expanding the availability of training data for DL models, thereby reducing the dependency on large, expensive datasets. The synthetic images maintained the necessary functional information for DL classification, showing that our approach could be a valuable tool in data-scarce environments, particularly for multi-center studies involving different imaging modalities. As no real MSA or PSP SPECT data was available and, therefore, no tests could be performed on these data kinds, their synthetic counterparts were not generated.

At a semi-quantitative level, SBRs of synthetic DAT SPECT were not significantly different from the ones of the real DAT SPECT. Additionally, lower SBR values were found for the synthetic PD compared to synthetic NC images, confirming the preservation of disease-specific information in the image-to-image translation. SBR is a quantitative measure used in research and complements visual readings in clinical practice.^{133,264–266} However, the SBR values from different datasets are not consistent, due to subject-related physiological factors and different imaging systems, including different acquisition hardware and different image reconstruction software.^{135,267,268} Thus, it complicates comparisons in

multicenter/longitudinal studies. Other alternatives, such as phantom-based calibration and dedicated reconstruction algorithms attempted to mitigate this variability,²⁶⁸ but these approaches are not straightforward, as they involve addressing camera-specific factors. In our case, we have not just different subject populations, cameras, centers, but also different imaging modalities. As DAT SPECT is most used in European centers/studies^{60,246} and DAT PET is widely used in Asia, studies using both of these modalities can be of major importance, especially due to the limited APS data. Because Cycle GAN performed well in these different modality cases, we foresee that it can be used in simpler multi-system pipelines. However, there remain some areas for improvement. In the PD cohort, differences were noted in the putamen binding ratio and left-right striatal differences between synthetic and real SPECT, indicating that while the translation process preserves crucial diagnostic features, (such as decreased SBR, PBR and CBR in the PD cohort compared to NC) it is not yet perfect. Additionally, in terms of contrast-to-noise ratio, the synthetic SPECT have lower values than both real SPECT and synthetic SPECT, meaning a decrease in terms of contrast of striatum.

Blind visual assessment by the nuclear medicine physicians confirmed structural similarity between real and synthetic SPECT, with no differences in VGAS of analyzed categories (synthetic appearance, level of noise, presence of artifacts, and confidence in diagnosis). However, 3/4 physicians had reduced diagnostic accuracy in synthetic images compared to real ones, possibly due to the attenuation of certain discriminative features during translation, enough for DL network to identify, but not the physicians. This is also consistent with the differences in the putamen binding ratio and the left-right striatal differences, as well as with the low CNR.

When comparing Cycle GAN to other domain adaptation methods like AttentionGAN and diffusion models, several differences emerge. AttentionGAN²⁶⁹ leverages attention mechanisms to enhance feature preservation, potentially offering more precise image translations but at the cost of increased complexity and computational demand. Diffusion models^{231,253,270} are known for generating high-quality images through iterative noise reduction but require extensive computational resources and long training times. In contrast, Cycle GAN strikes a balance between image quality and computational efficiency, making it more practical for medical imaging applications. However, it may struggle with fine-grained

feature preservation, as indicated by the subtle discrepancies observed in our study. While Cycle GAN is effective for many tasks, integrating aspects of these advanced methods could further enhance translation quality in future research.

In terms of clinical relevance, our method could significantly enhance AI-assisted diagnostic tools by increasing the availability of training data, thereby making these tools more robust and generalizable. Several studies show that integrating deep learning-based data augmentation is an important strategy in this regard.²⁵⁴ It could also provide additional resources for educating new physicians. Furthermore, the ability to translate PET to SPECT could facilitate clinical comparisons of patient scans—where PET imaging was used—with existing standard databases of normal controls, which are predominantly SPECT-based in Europe.¹³⁵ However, for clinical adoption, it will be essential to address challenges such as meeting regulatory standards for synthetic images, integrating the method into existing clinical workflows, and ensuring the interpretability and reliability of AI-generated images.

It is important to acknowledge some other limitations. While our study focused on generating SPECT images from PET images due to current needs, generating PET images from SPECT could be a more advantageous approach given the higher spatial resolution of PET. However, translating from SPECT to PET presents additional challenges, especially with only limited and unpaired data available. Future studies should consider exploring this approach to leverage the higher detail in PET images.

Although Cycle GAN has shown promise in domain adaptation for medical imaging,^{271,272} challenges like data heterogeneity and the need for large-scale datasets for robust training still remain.^{234,273,274} A common issue in synthetic image generation is hallucination, where the model generates artifacts in the synthetic image.²⁷⁵ However, since our main goals is to enhance DL classification, minor structural abnormalities in synthetic images are less problematic. Additionally, tuning the parameters and the training approach proved to be challenging, as minor adjustments in the hyperparameters affect training stability.^{273,276} An external dataset for testing would be a valuable addition in future studies, to improve the robustness and generalizability of our results.

In the image quality quantitative metrics, CNR is low especially on the NC cohort, which can impair visual analysis. Nevertheless, SBR are similar in the synthetic and real SPECT and DL classification has high accuracy, meaning that even if not ideal for visual assessment, the synthetic images are helpful for semi-quantitative and DL-based diagnosis. It is also noteworthy that the SBR difference between real SPECT and synthetic SPECT is bigger in the NC than in the PD, even though not significantly. This can be due to the unbalanced training dataset, which holds much more PD (80%) than NC (20%). A more balanced training set could improve this disparity. Another limitation is the use of Normal DAT imaging scans and not just NC and the different PD/NC proportions for PET and SPECT datasets.

In the visual assessment, there are also important limitations. The interpretation and generalization of the results can be limited by the small sample size ($n=20$) and the Gaussian filters applied. As the spatial resolution of the PPMI SPECT images is already low, further reduction might have an impact on the diagnostic utility. Nonetheless, diagnostic performance of the four readers on real SPECT images was good ($AUC > 0.70$). Moreover, some studies show that domain adaptation might be achieved by simply smoothing images.²⁷⁷ Further studies should aim for larger samples and fewer preprocessing steps.

Lastly, the impact of domain adaptation on downstream tasks, such as disease classification, should be thoroughly investigated. Although quantitative metrics such as SBR and CNR offer some insight into the translation process and synthetic SPECT images appear realistic, they do not allow for direct evaluation of the synthetic images. We cannot know how comparable a real clinical SPECT image would be to the corresponding synthetic image, due to the absence of paired data. It is essential that next studies include paired datasets – as a more accurate and direct way to evaluate the synthetic images – and assess how well the synthetic data can improve the performance of existing AI models and clinical decision support systems in the context of DAT imaging.

Conclusion

Our study highlights the potential of Cycle GAN in DAT PET to DAT SPECT domain adaptation. This approach holds promise for more multicenter/longitudinal comparison studies and for expanding data availability needed to enhance the accuracy in diagnosing parkinsonian disorders. Future research is needed to address the remaining challenges and evaluate the clinical applicability of the proposed approach.

Declarations

Ethics approval and consent to participate

Study protocols were approved by the ethics committee of Huashan Hospital, and voluntary informed consent was obtained from each subject or their caregivers after an explanation of the procedures, according to the Declaration of Helsinki.

Consent for publication

Each subject or their caregivers offered written consent for publication and no personal information was presented in the current paper.

Availability of data and materials

The datasets generated and analyzed during the current study are available from the corresponding author upon reasonable request. Our code is available for download at <https://github.com/leonorlopes96/DAT-cycle-gan.git> for the Cycle GAN model and at <https://github.com/leonorlopes96/DAT-DL-classification.git> for the DL classification model.

3.2. Prediction of iRBD conversion using PET-based Deep Learning

This chapter is an original research article submitted to Annals of Neurology in March 2025.

Contributions:

I was responsible for the full development and implementation of the deep learning models used in this study, including the training and evaluation of the 3D convolutional neural networks for DAT and FDG PET scans. The code is available at <https://github.com/lopes-leonor/RBD-PET-prediction>. I designed and executed the computational pipeline to generate deep imaging risk scores (DIRS) for phenoconversion prediction in iRBD patients. I also developed the code for the assessment of the conventional methods features. In the context of this work I created a Python version of the Scale Subprofile Modelling, available at <https://github.com/lopes-leonor/Scaled-Subprofile-Model>. I conducted the data preprocessing, including spatial and intensity normalization, and performed statistical analyses to assess disease progression trajectories and prediction performance across multiple timepoints. I also produced the figures and tables, and was responsible for writing the manuscript, including the introduction, methods, results, discussion.

Deep Learning-Based Prediction of Isolated REM Sleep Behaviour Disorder Progression Using PET Imaging

Leonor Lopes^{1, 2†} Qian Xu, MD^{3,4†}, Jiaying Lu, MD PhD^{3,4†}, Carolin Schäfer, MD⁵, Jimin Hong, PhD^{1, 2}, Jingjie Ge, MD PhD^{3,4}, Cong Fu, MD^{4,6,7}, Jing Wang, MD^{3,4}, Jianjun Wu, MD^{4,6}, Jian Wang, MD^{4,6}, Claudio Bassetti, MD PhD⁸, Axel Rominger, MD PhD¹, Chuantao Zuo, MD PhD^{3,4*}, Ping Wu, MD PhD^{3,4*}, Huan Yu, MD PhD^{4,6,7*}, Kuangyu Shi, PhD^{1,9}

†These authors contributed equally to this work.

***Corresponding authors**

Author affiliations:

1 Department of Nuclear Medicine, Inselspital, University of Bern, Bern, Switzerland

2 Graduate School for Cellular and Biomedical Sciences, University of Bern, Bern, Switzerland

3 Department of Nuclear Medicine & PET Center, Huashan Hospital, Fudan University, Shanghai, China

4 National Center for Neurological Disorders & National Clinical Research Center for Aging and Medicine, Huashan Hospital, Fudan University, Shanghai, China

5 Sleep-Wake Epilepsy Center, Department of Neurology, Inselspital, University of Bern, Bern, Switzerland

6 Department of Neurology, Huashan Hospital, Fudan University, Shanghai, China

7 Sleep and Wake Disorders Center of Fudan University, Shanghai, China

8 Department of Neurology, Inselspital, University of Bern, Bern, Switzerland

9 Department of Informatics, Technische Universität München, Munich, Germany

Abstract

Objectives: Isolated REM sleep behavior disorder (iRBD) is a prodromal stage of neurodegenerative α -synucleinopathies, such as Parkinson's disease. At present, no biomarker is available for predicting phenoconversion. This study aimed to explore the use of deep learning in PET imaging to predict disease progression and phenoconversion of iRBD.

Methods: DAT and FDG PET scans of 38 iRBD patients (mean age 65.5 ± 6.3 , 30 male) with a mean follow-up of 7.1 ± 2.2 years were included. Two pre-trained deep learning classification models, one with DAT PET and the other with FDG PET, were used to calculate deep imaging risk scores - DIRS-DAT and DIRS-FDG - of conversion of iRBD. Performance in disease progression monitoring and predicting conversion were assessed and compared with conventional methods.

Results: Nineteen patients converted to Parkinson's Disease/Dementia with Lewy bodies (in 6.1 ± 2.4 years). DAT-DIRS and FDG-DIRS significantly increased with disease progression. DAT-DIRS model shows the best performance, with AUCs of 0.936, 0.947, 0.942, and 0.935 for predicting conversion within 2, 4, 6, and 8 years. FDG-DIRS model shows more moderate AUCs of 0.760, 0.727, 0.687, and 0.648, lower than the FDG conventional method. Of notice is the high negative predictive value for predicting conversion within 2 years of both FDG methods.

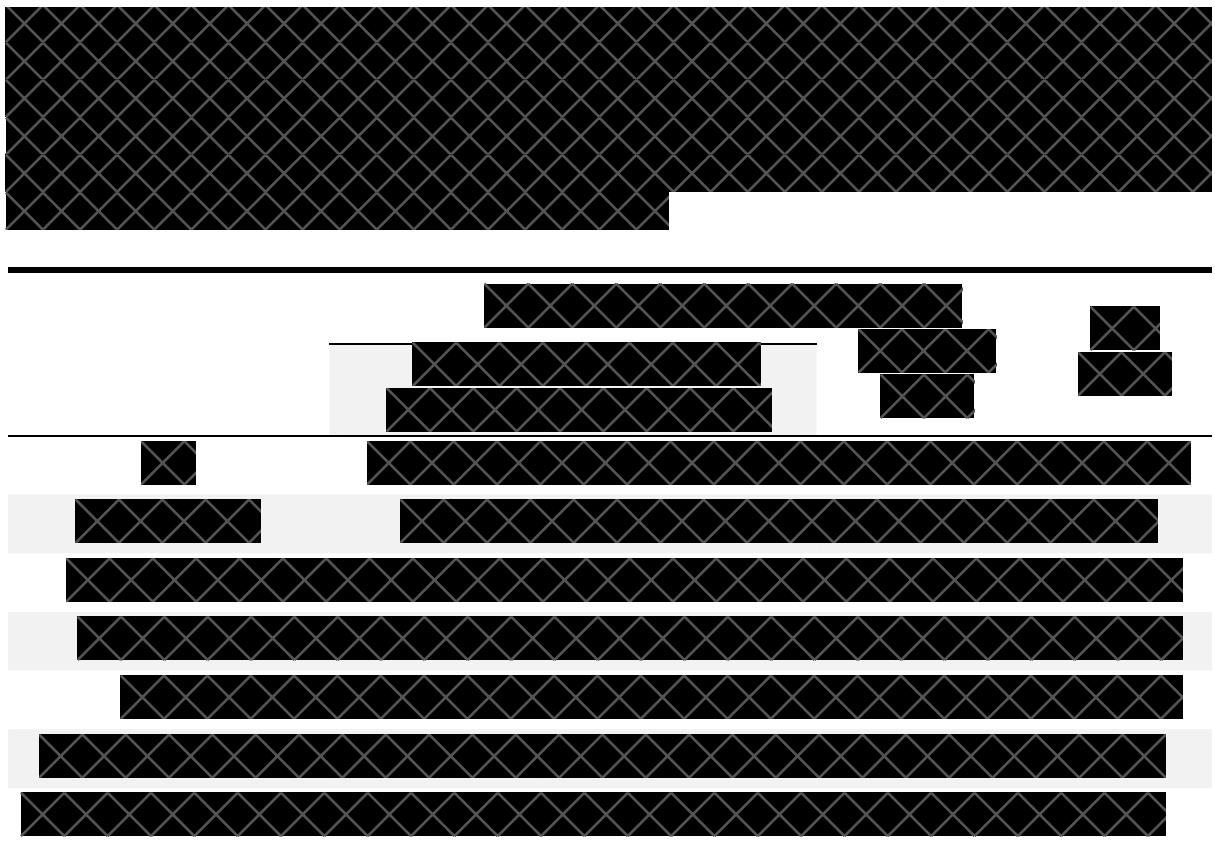
Interpretation: These findings confirmed the feasibility of PET imaging in predicting phenoconversion of iRBD. DL has the potential to improve performance of early diagnostic methods based on dopaminergic PET imaging for disease progression and phenoconversion of iRBD.

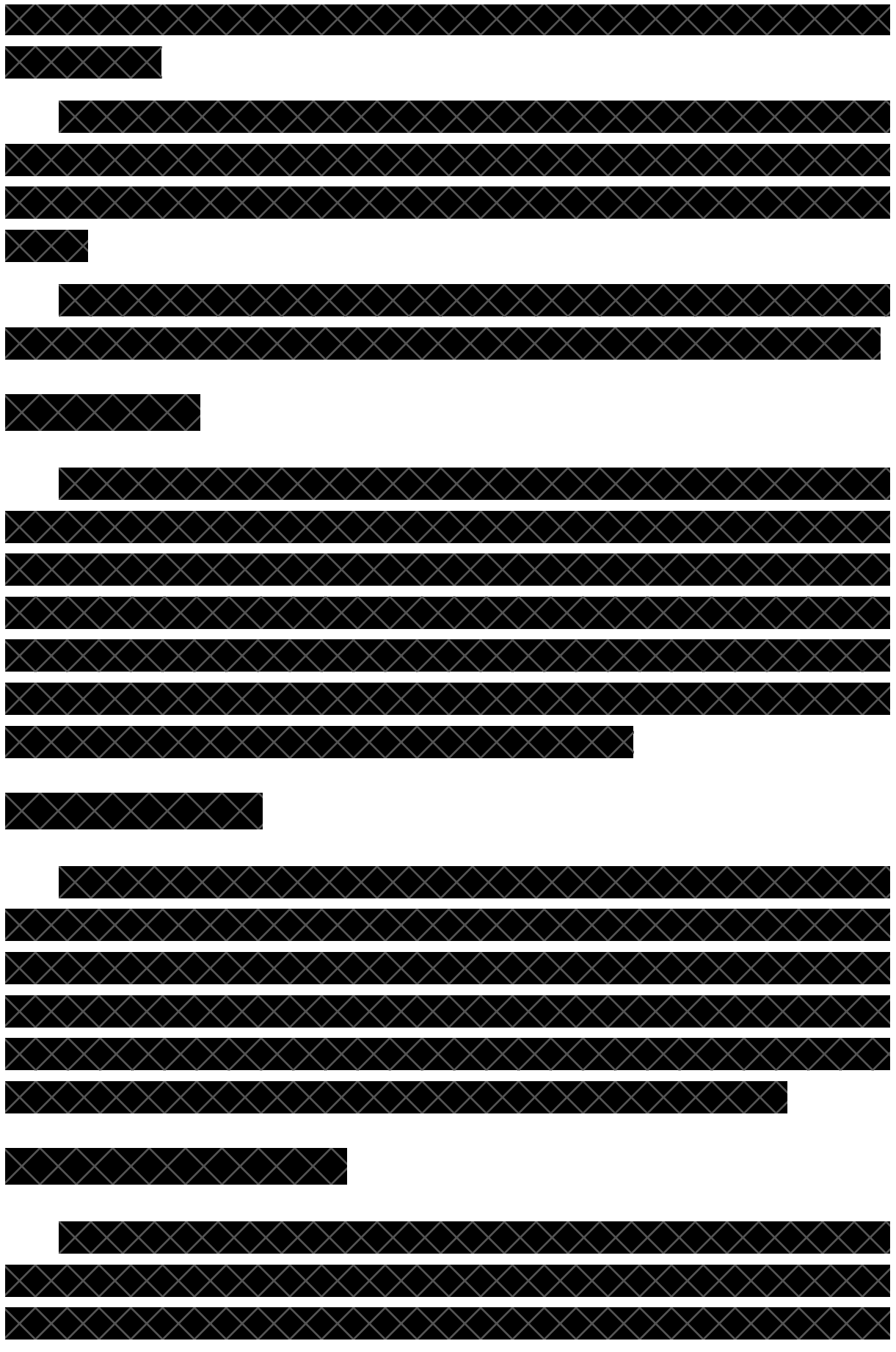
Keywords: iRBD; α -synucleinopathies; FDG PET; DAT PET; Deep Learning; phenoconversion.

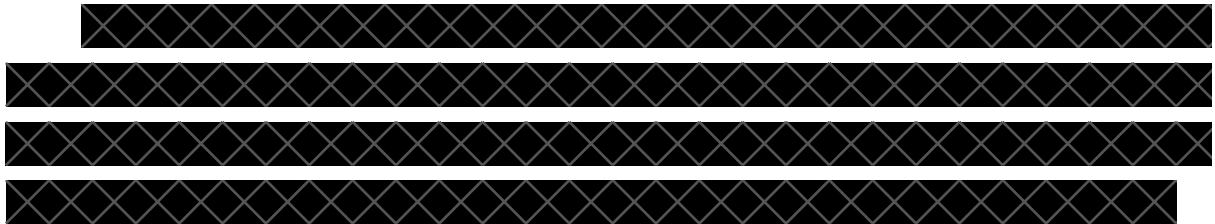
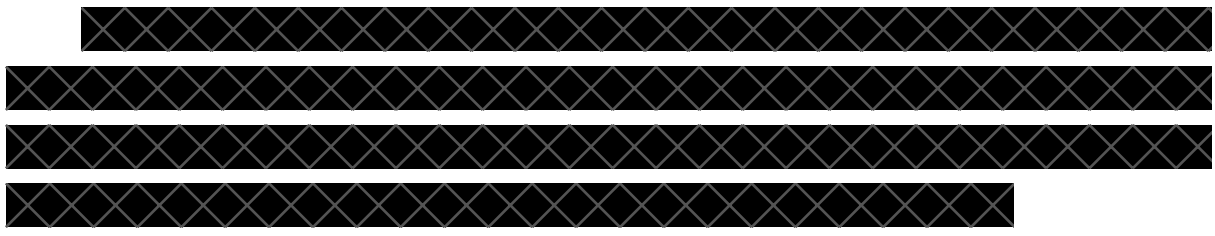
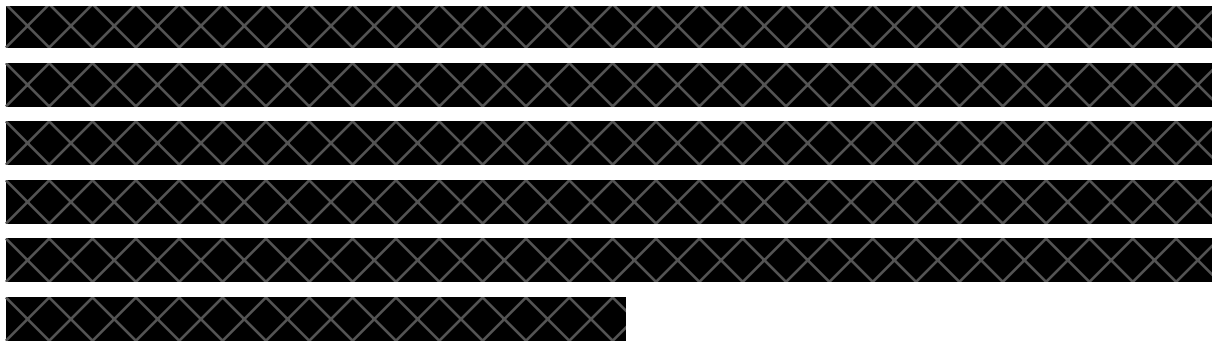


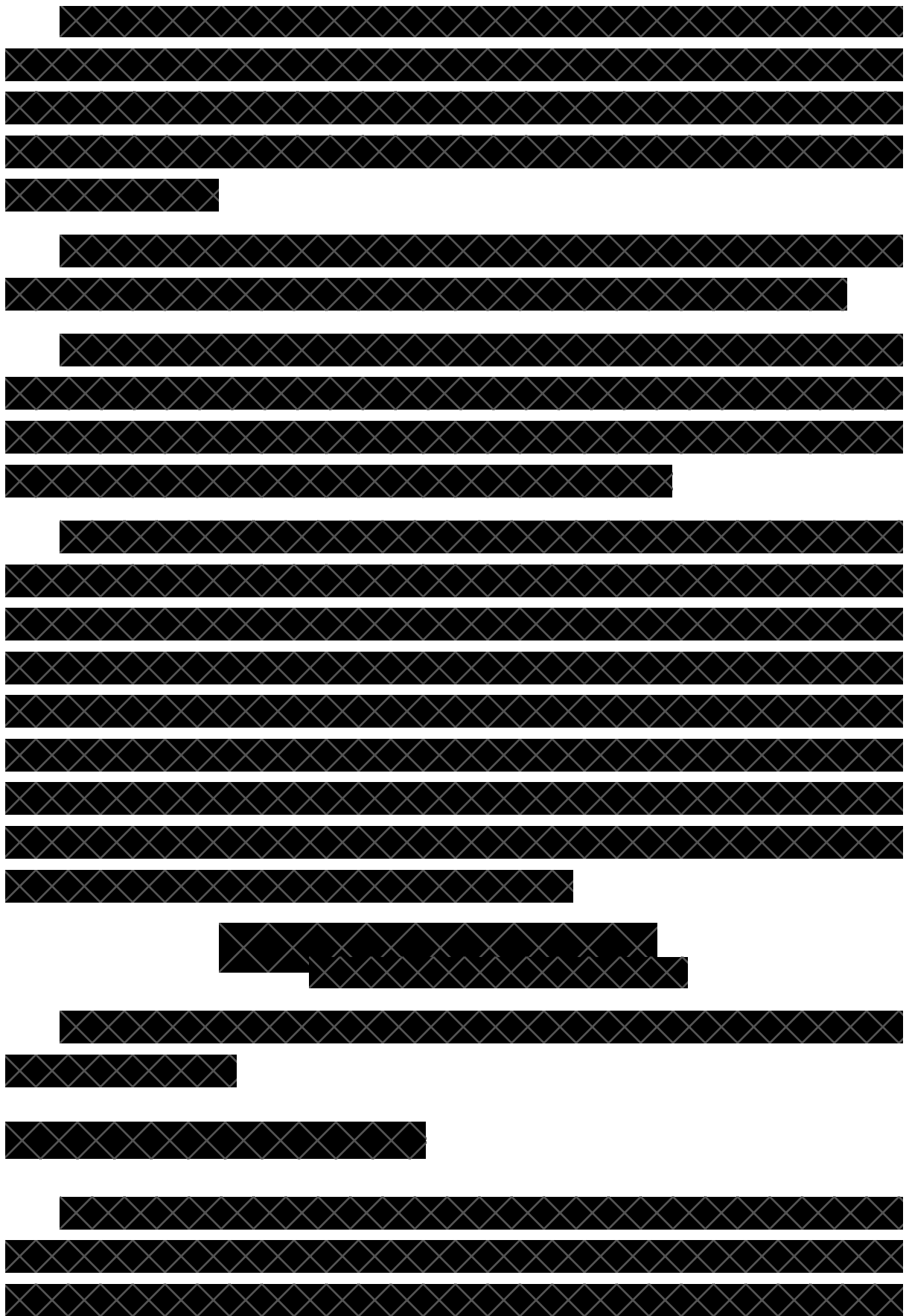




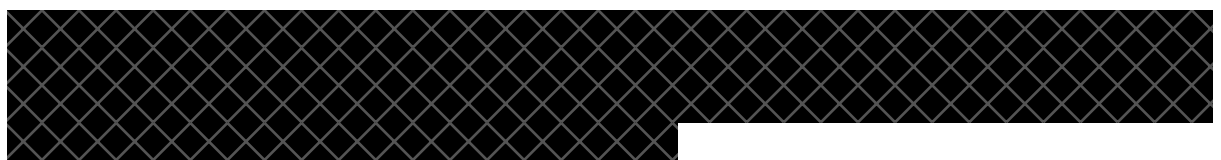
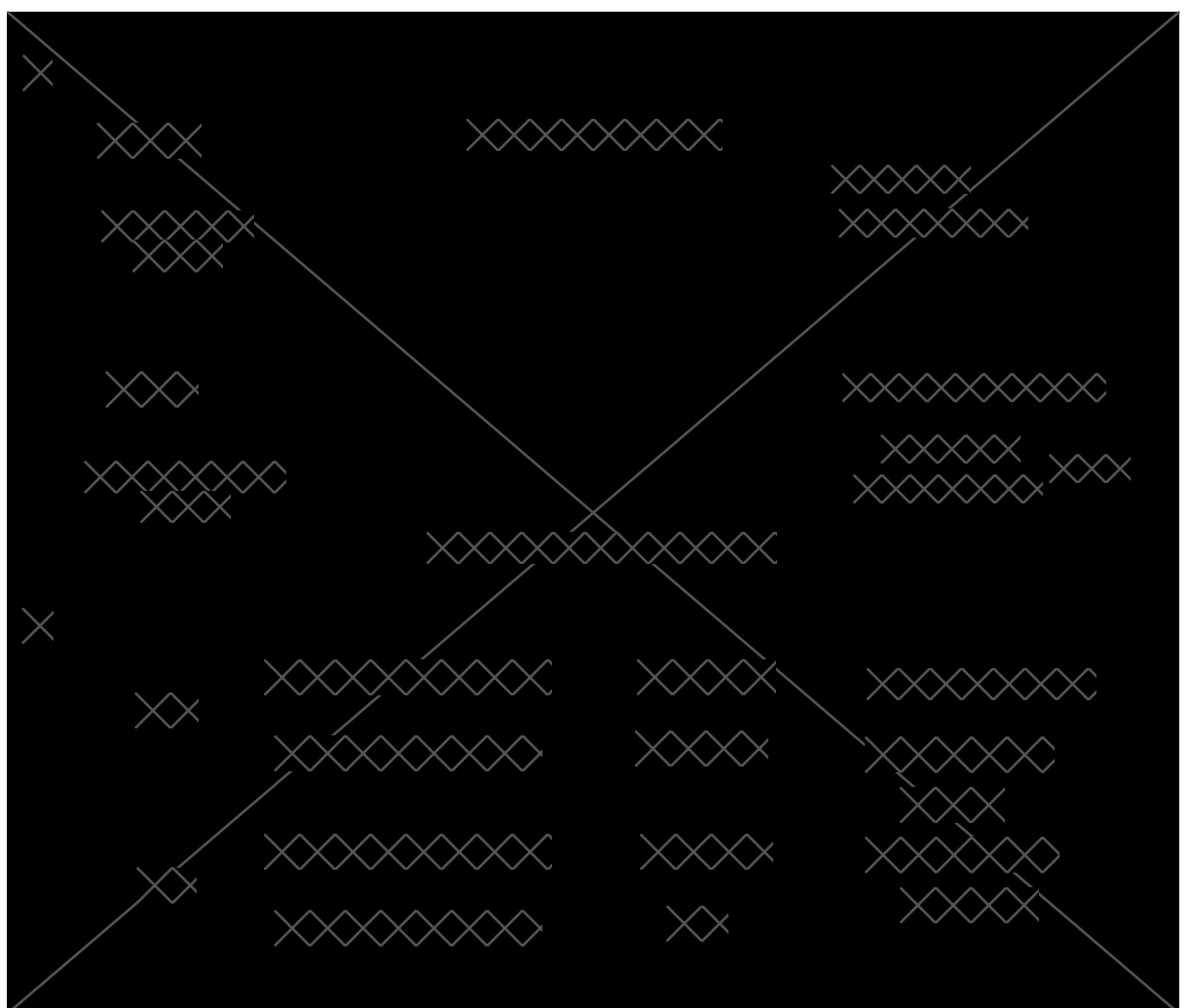
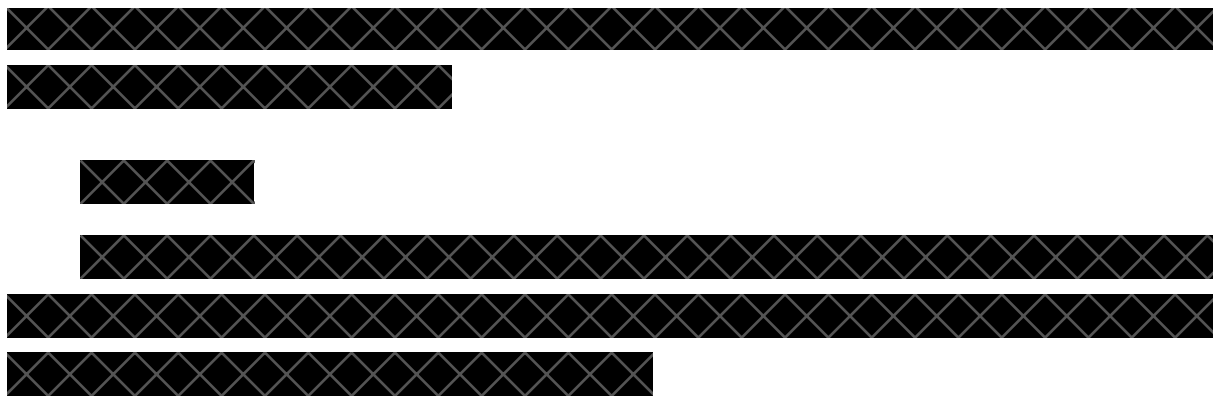


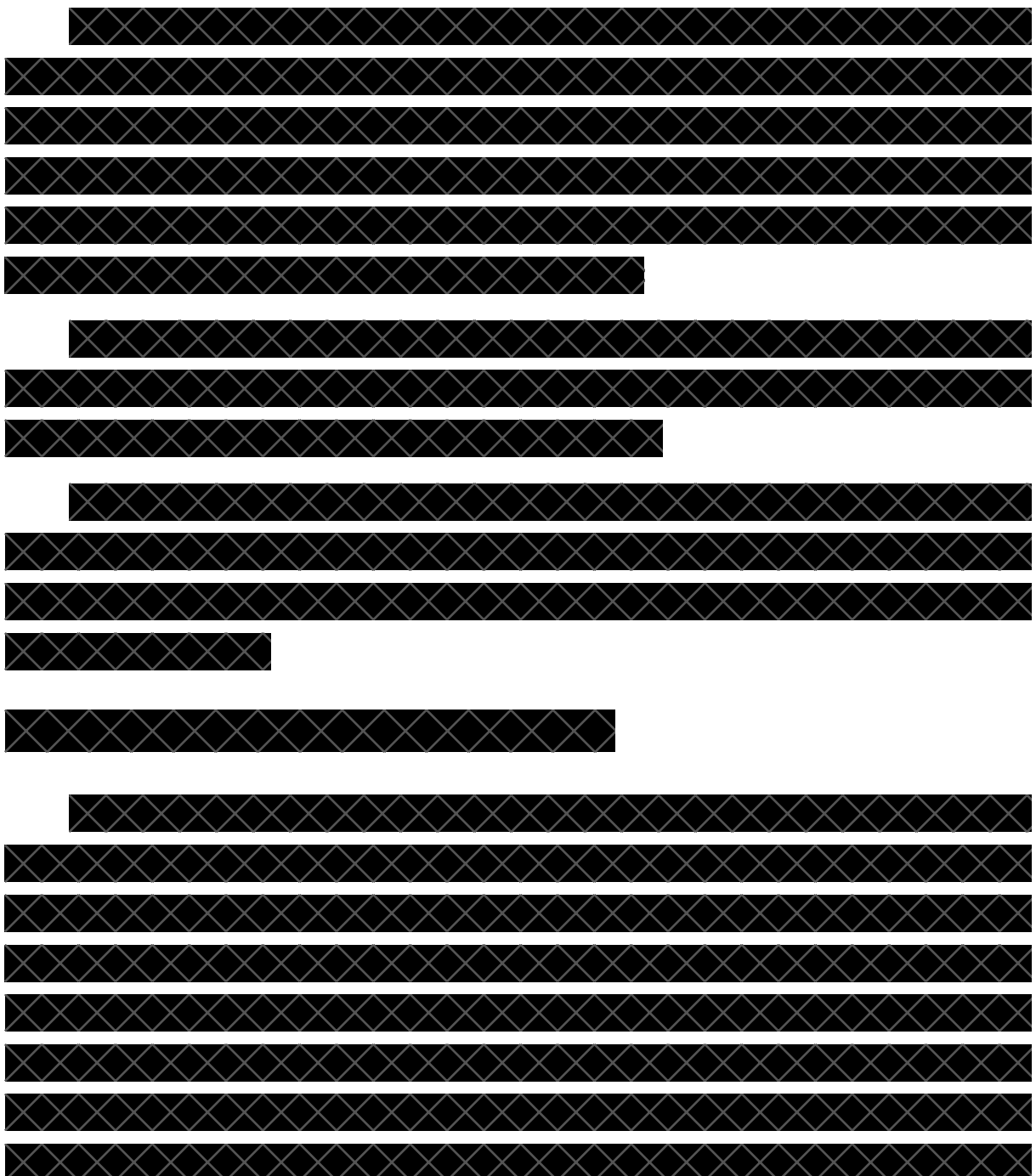


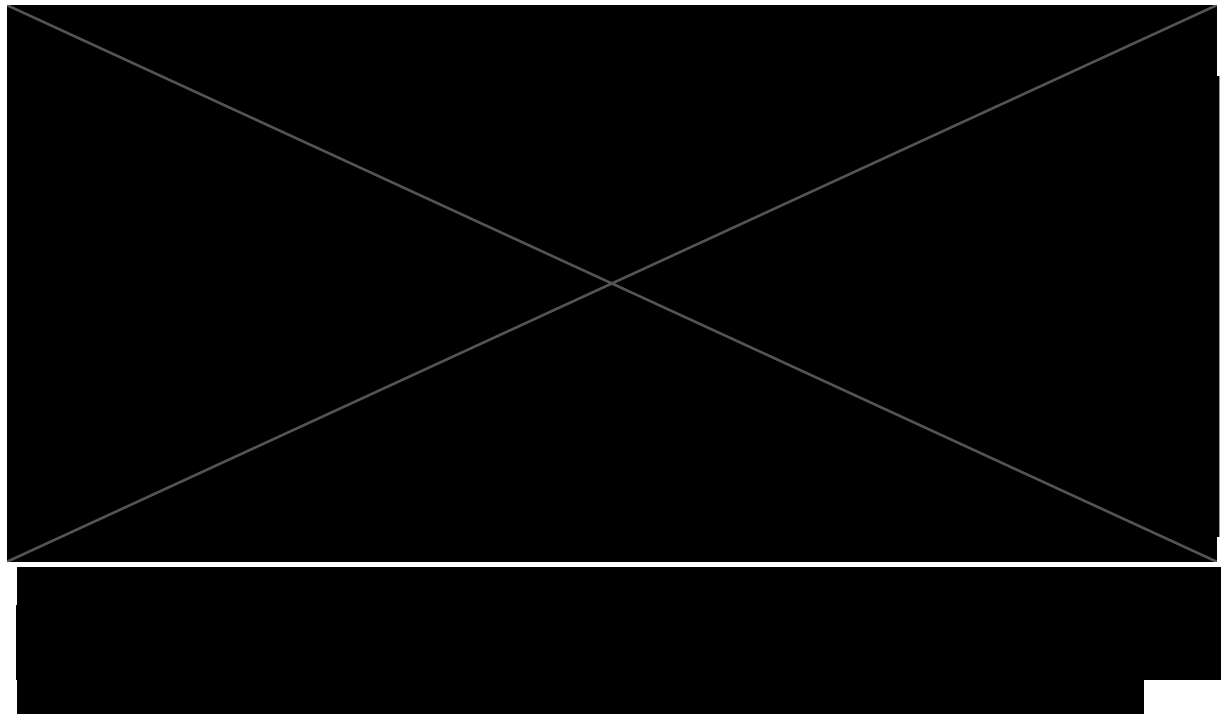
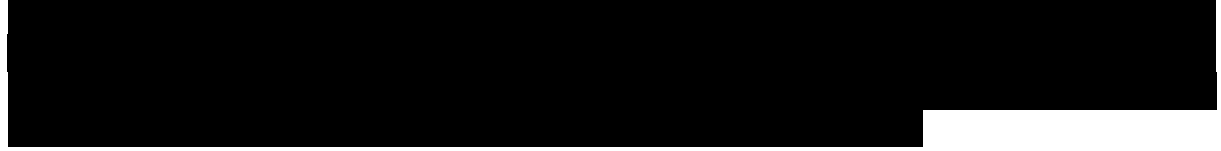
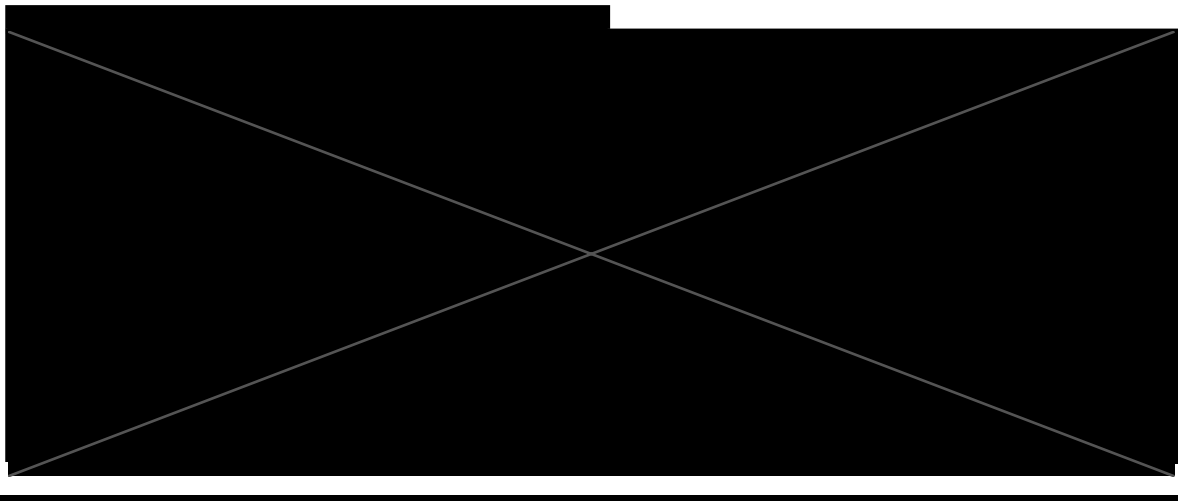


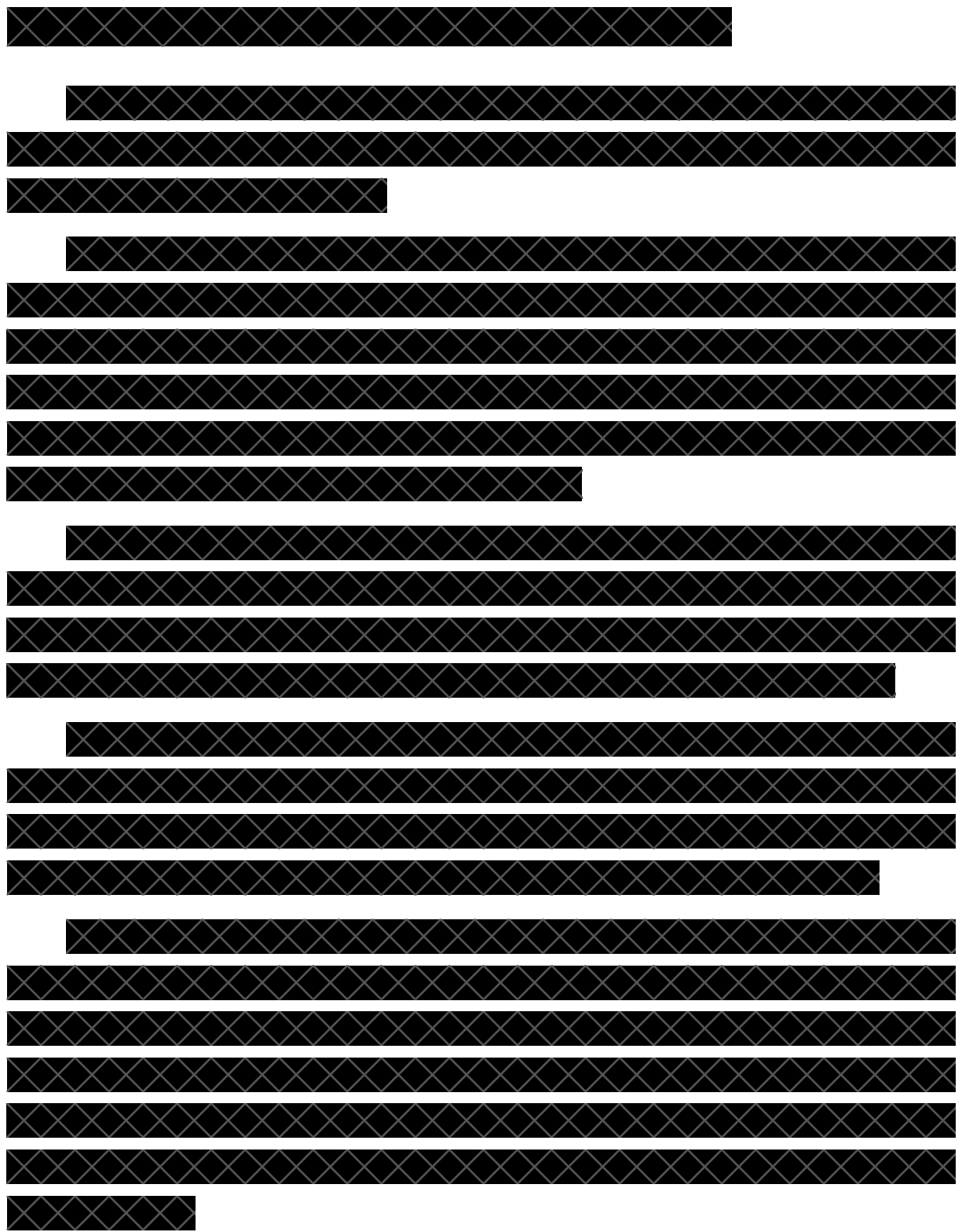




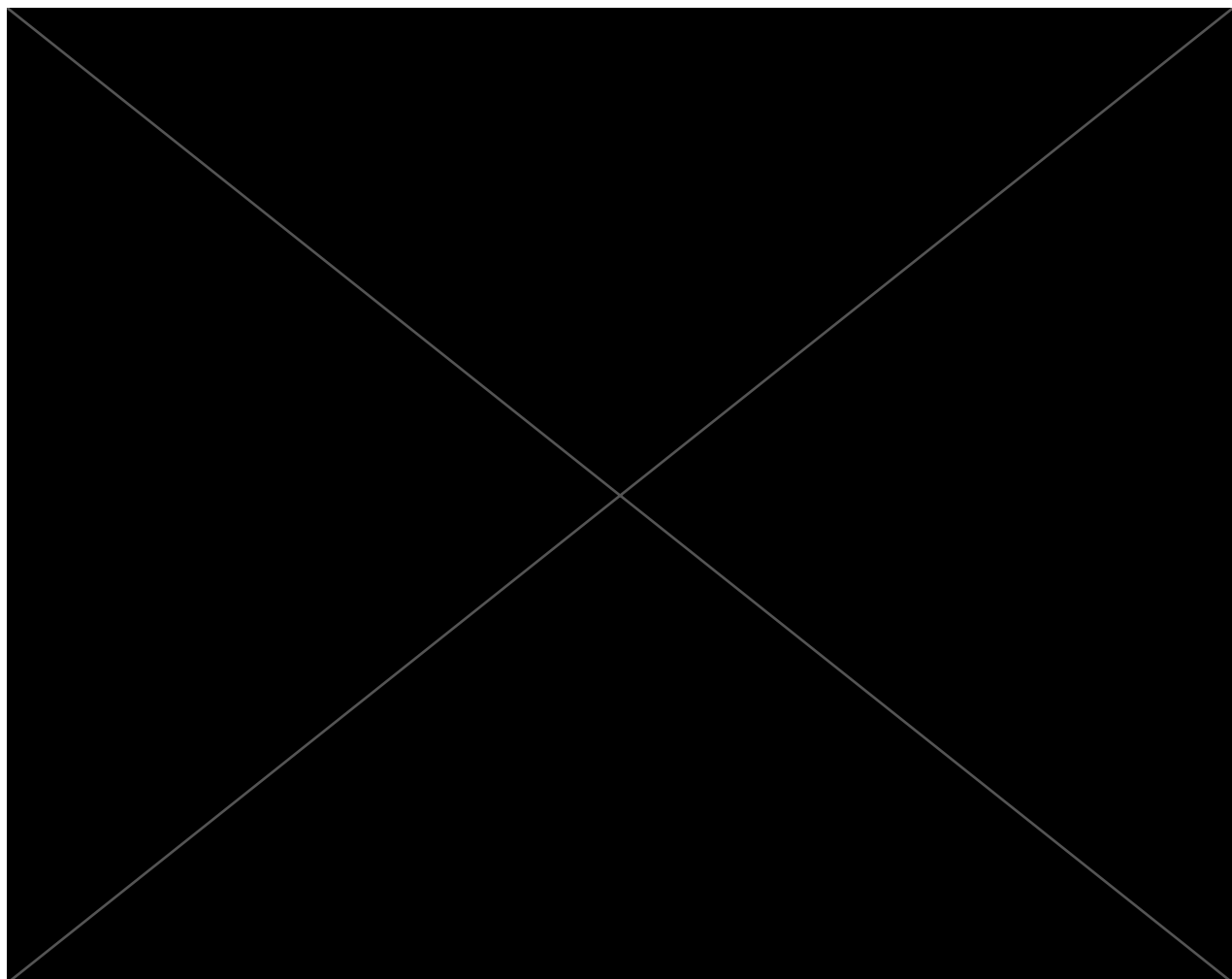




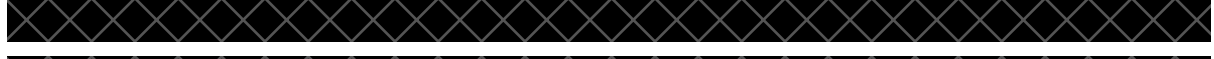


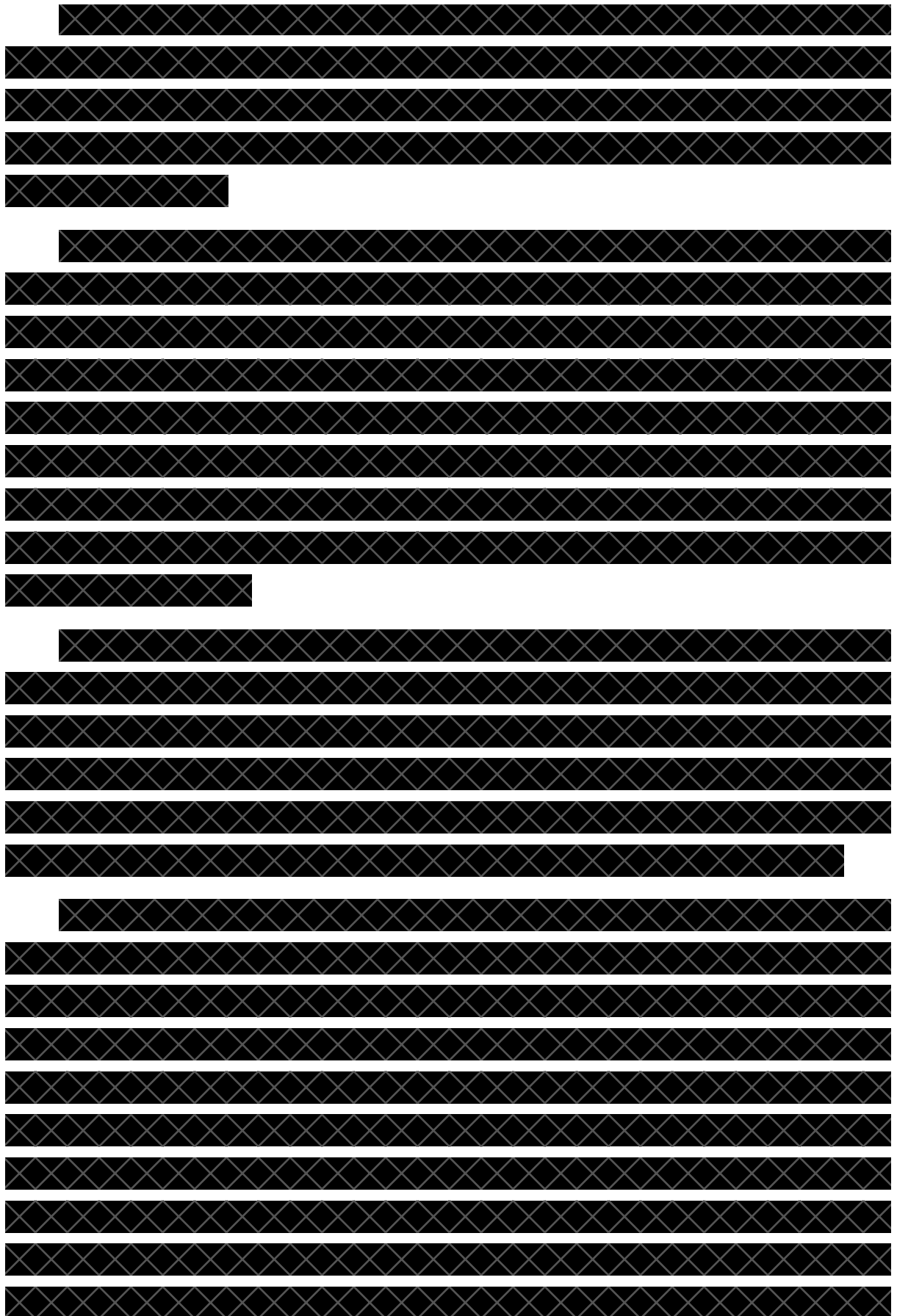


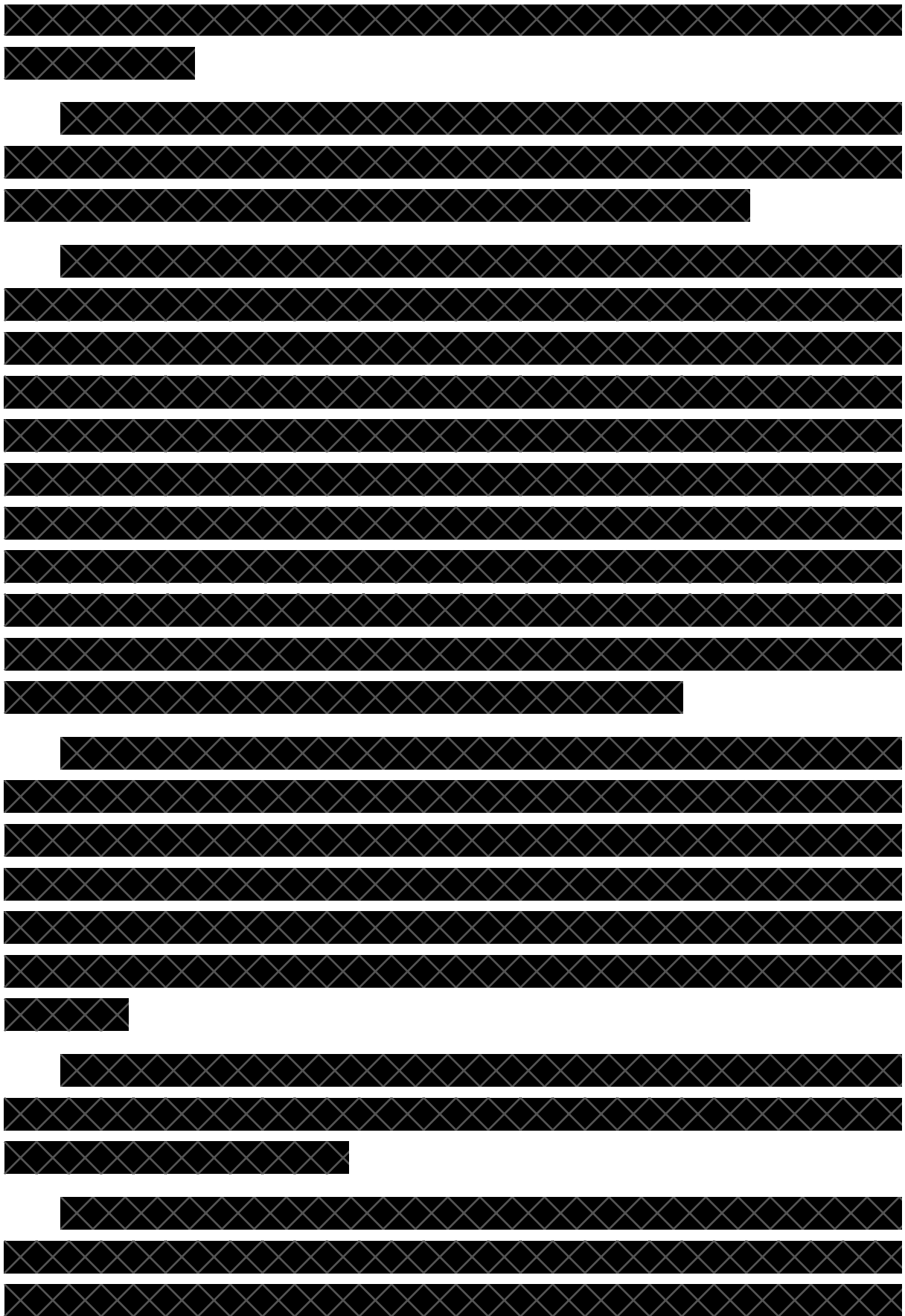


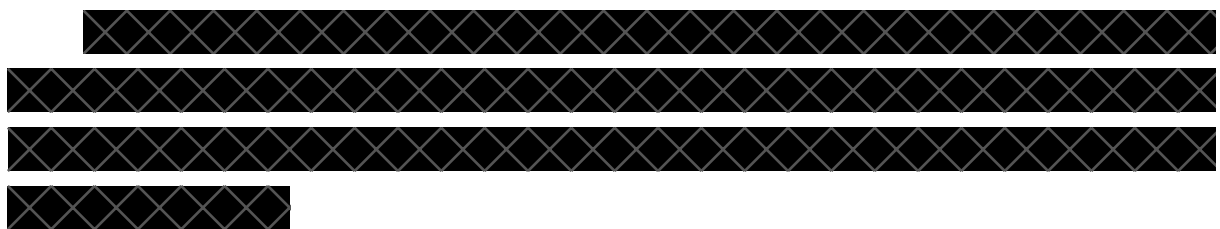












3.3. Diagnosis and Prediction of PD on Actigraphy

This chapter is an original research article to be submitted to Sleep.

Contributions:

I was responsible for the data collection and the design and implementation of the actigraphy analysis pipeline. This included feature engineering, development of traditional machine learning classifiers, and implementation of deep learning models—specifically a CNN and a pretrained transformer model—for classification of PD with and without RBD and controls. I handled all preprocessing of raw actigraphy data, defined the classification tasks, designed the model evaluation strategy, and performed feature importance analyses. I also prepared all figures and tables and was responsible for writing the manuscript.

Actigraphy meets AI: a Digital Biomarker for Isolated REM Sleep Behaviour Disorder's Progression to Parkinson's Disease

Leonor Lopes^{1,2,*}, Jan D. Warncke³, Irina Filchenko³, Kuangyu Shi¹, Claudio L. A. Bassetti³,
Carolin Schäfer³

***corresponding author**

Author affiliations:

1 - Department of Nuclear Medicine, Inselspital, Bern University Hospital, University of Bern,
Bern, Switzerland

2 - Graduate School for Cellular and Biomedical Sciences, University of Bern, Bern, Switzerland

3 - Schlaf-Wach-Epilepsie Zentrum, Department of Neurology, Inselspital, Bern University
Hospital, University of Bern, Bern, Switzerland

Abstract

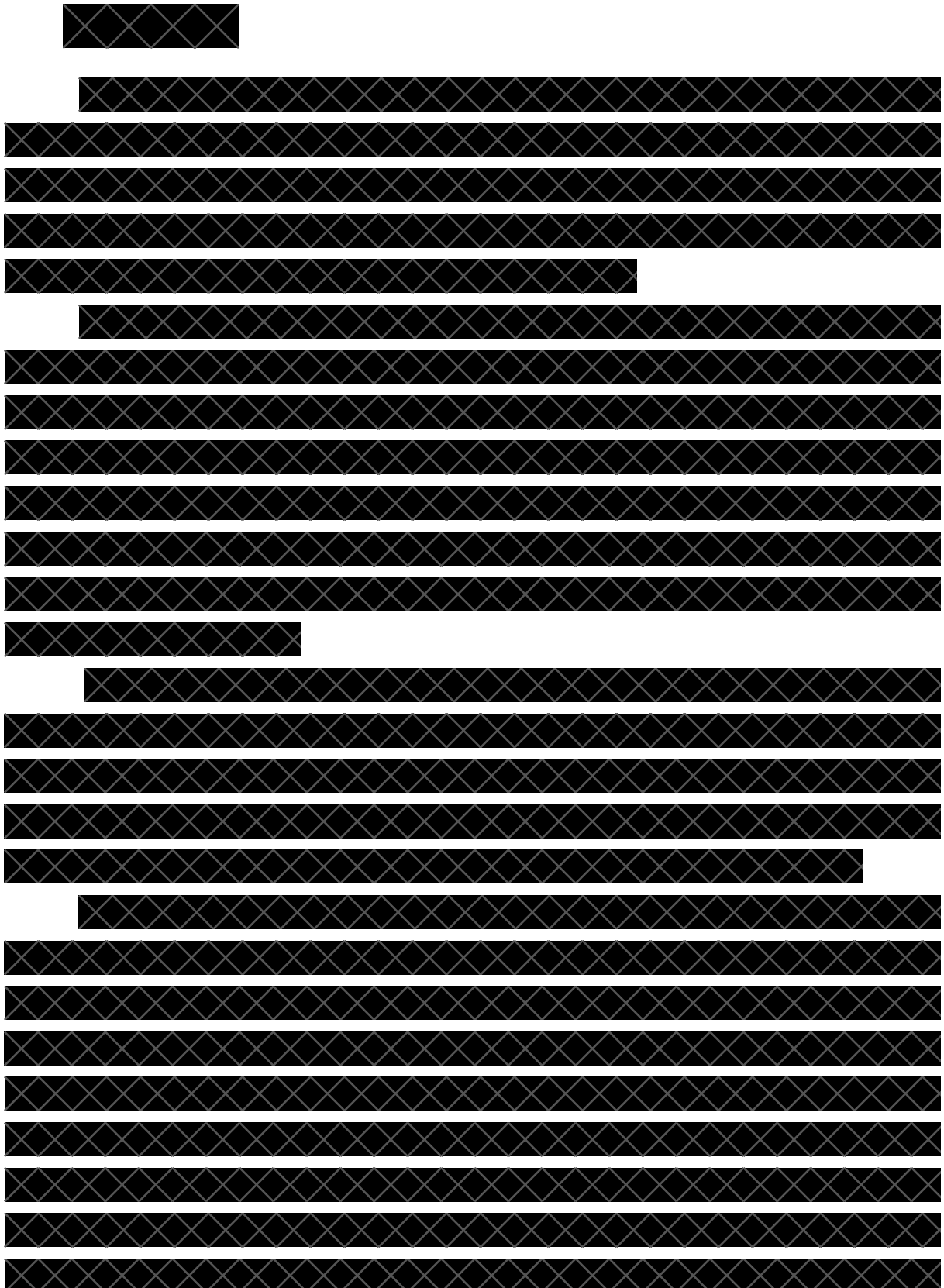
Study Objectives: Isolated REM sleep behavior disorder (iRBD) is a sleep disorder and early stage of alpha-synucleinopathies such as Parkinson's disease (PD). Actigraphy, a tool used to assess rest-activity patterns, is potentially valuable in monitoring the progression of iRBD to advanced stages of neurodegeneration. At present, however, only few studies demonstrated its diagnostic utility and predictive ability in the prodromal stages of α -synucleinopathies. This study evaluated artificial intelligence (AI) classification models based on actigraphy data in this regard.

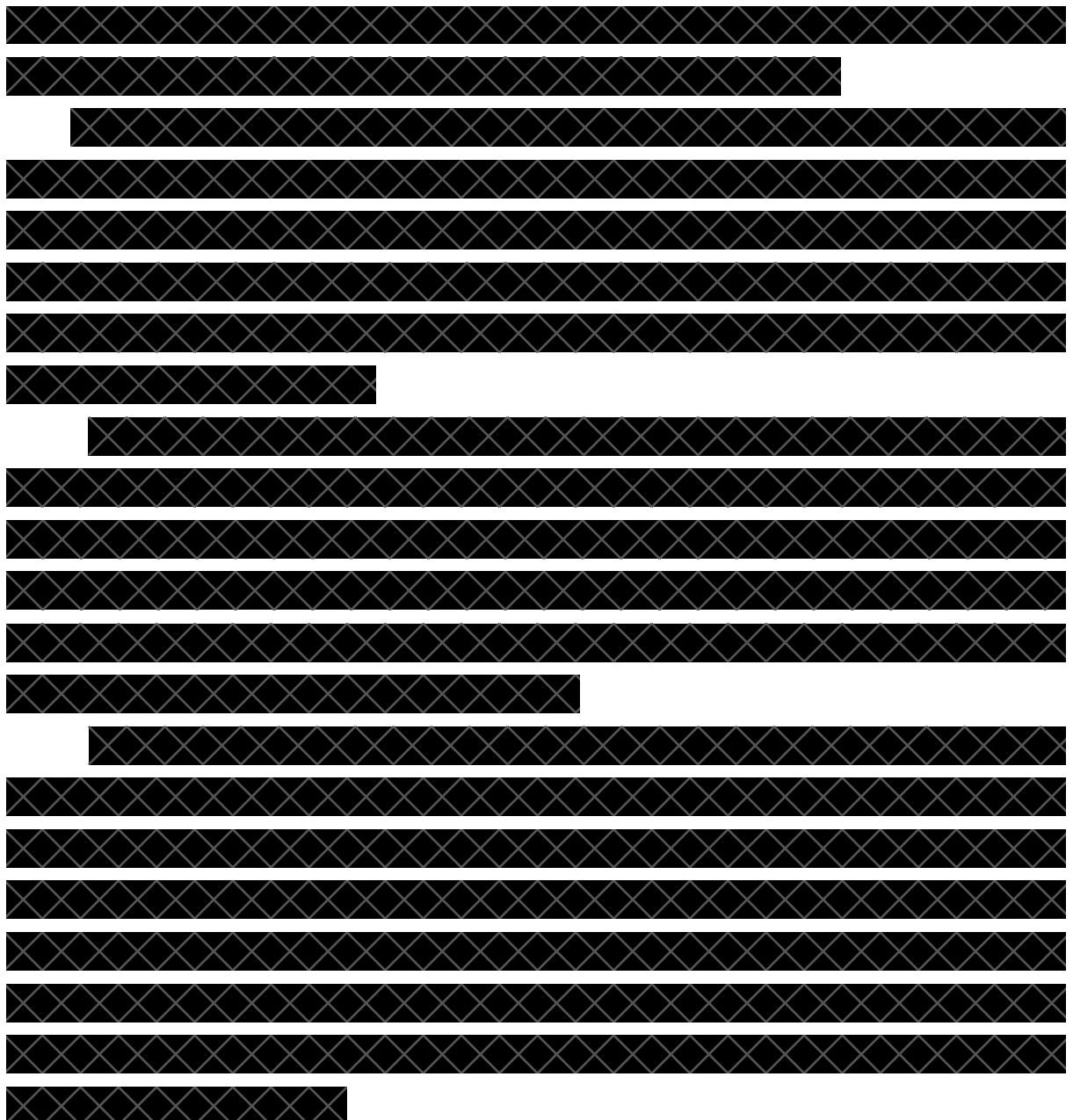
Methods: Two classification tasks were performed using machine learning (ML) models with extracted features, a convolutional neural network (CNN), and a pre-trained transformer model (PAT). The first task is to distinguish actigraphy data of patients with PD from data of controls with restless legs syndrome (RLS) and the second task is to distinguish PD patients with RBD (PD-RBD) from PD patients without RBD (PD-noRBD). The comparative analysis of the model performance was conducted. The model with the best performance was tested on iRBD patients.

Results: Patients with PD-RBD exhibited significantly altered actigraphy features compared to those with PD-noRBD and controls (such as total average daily activity, interdaily stability, intradaily variability and relative amplitude). In the classification of controls versus PD, the PAT model achieved the highest area under the curve (AUC) of 0.937, followed by convolutional neural network (CNN) (0.863) and machine learning (ML) (0.837). The sensitivity was 80.5%, and specificity was 95.7%. PAT model scores for iRBD patients fell between those of controls and PD patients. For the PD-RBD versus PD-noRBD classification, the PAT model again outperformed the other models (AUC = 0.956, sensitivity = 84.4%, and specificity = 92.9%), with the iRBD scores falling between the PD-RBD and PD-noRBD scores.

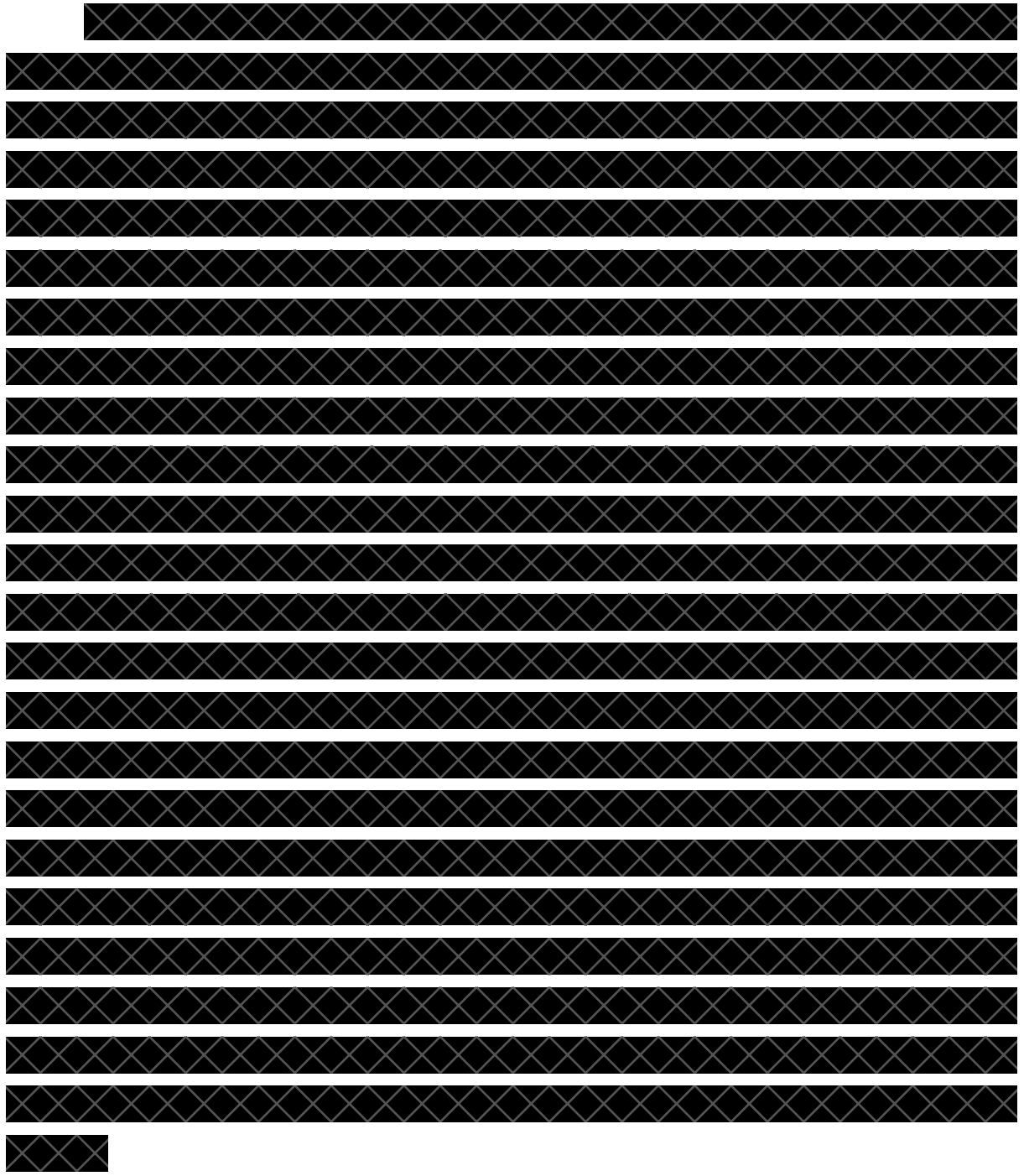
Conclusions: The developed actigraphy-based AI models can distinguish PD patients from healthy controls and identify PD subtypes. This supports the models' use as a non-invasive biomarker for diagnosis and disease stratification. Additionally, the classification scores of iRBD patients suggest the potential of this method for predicting conversion to overt PD.

Keywords: Parkinson's Disease; iRBD; Actigraphy; Artificial Intelligence.

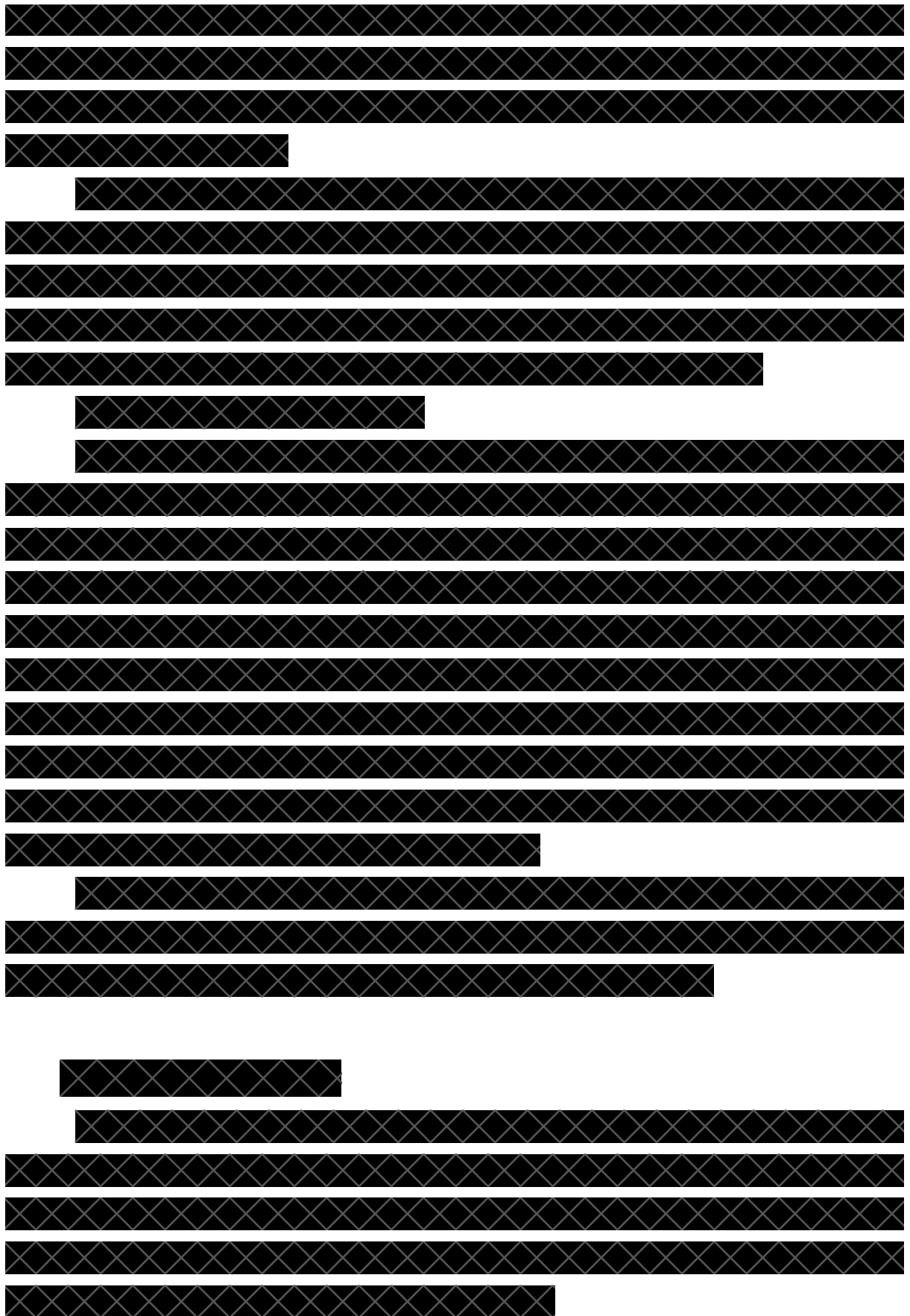


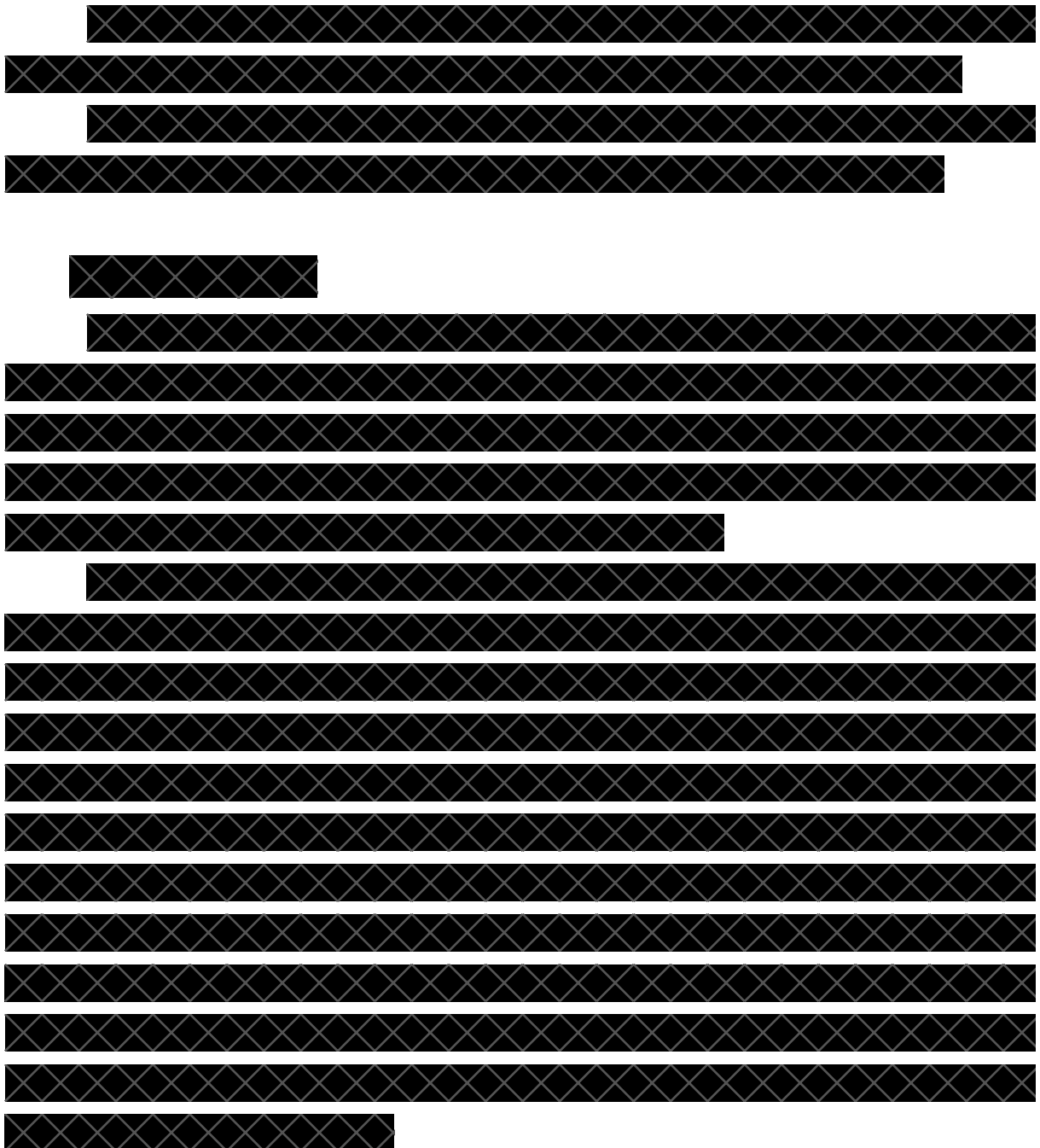


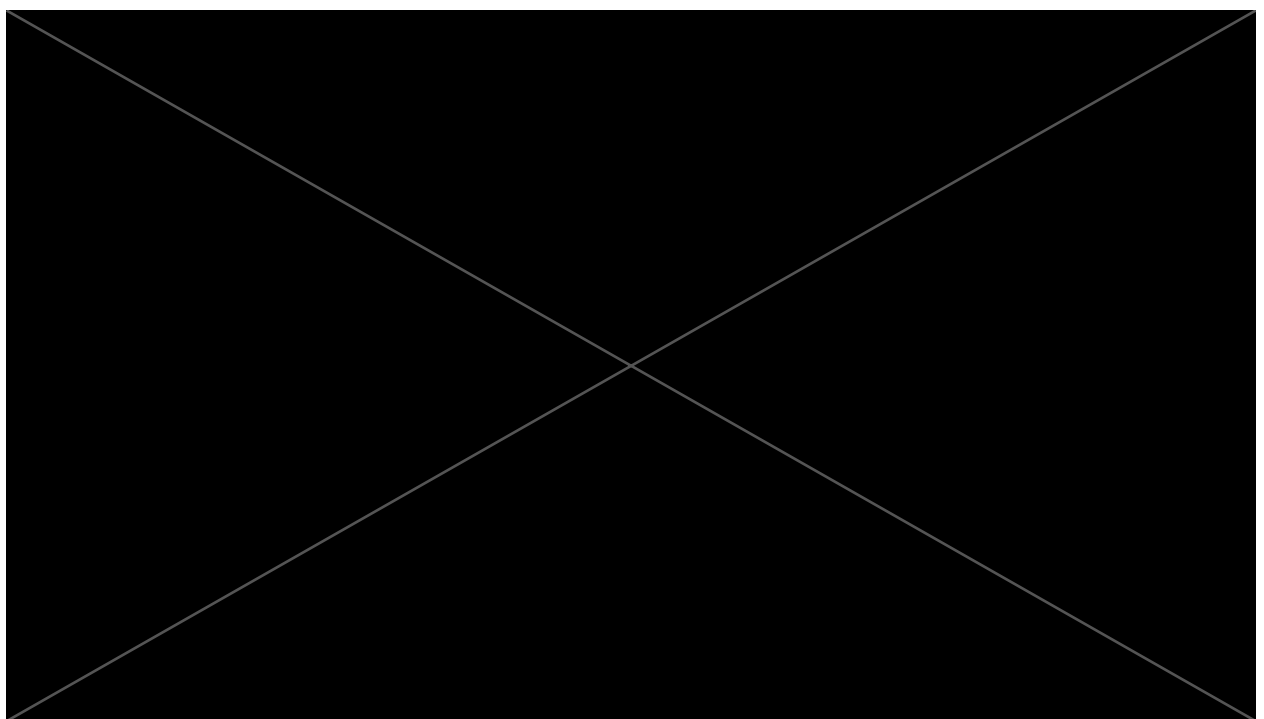
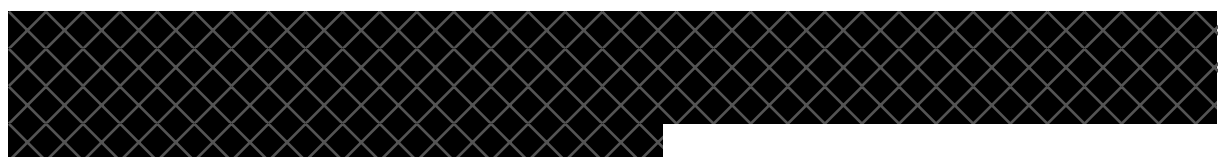










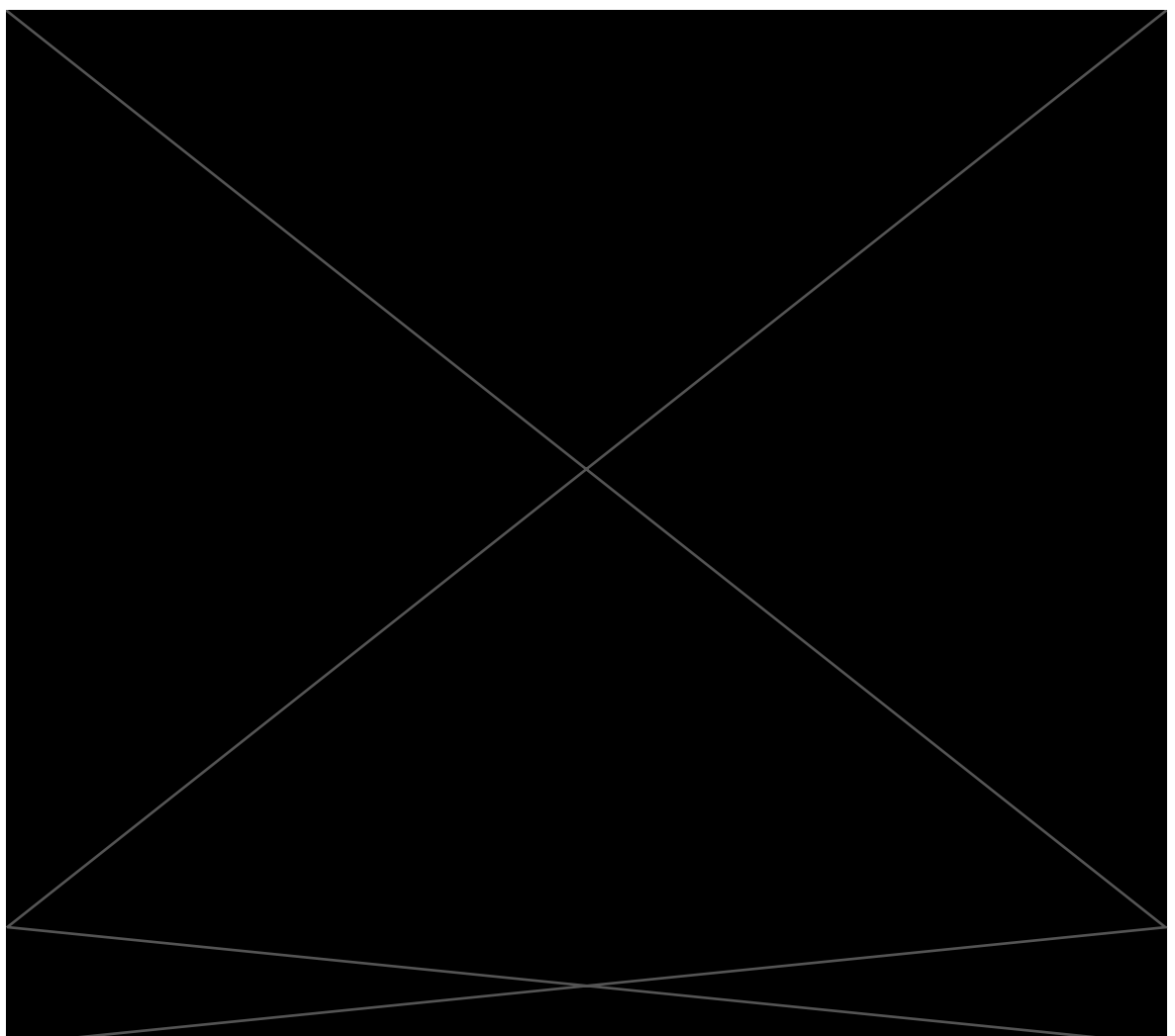


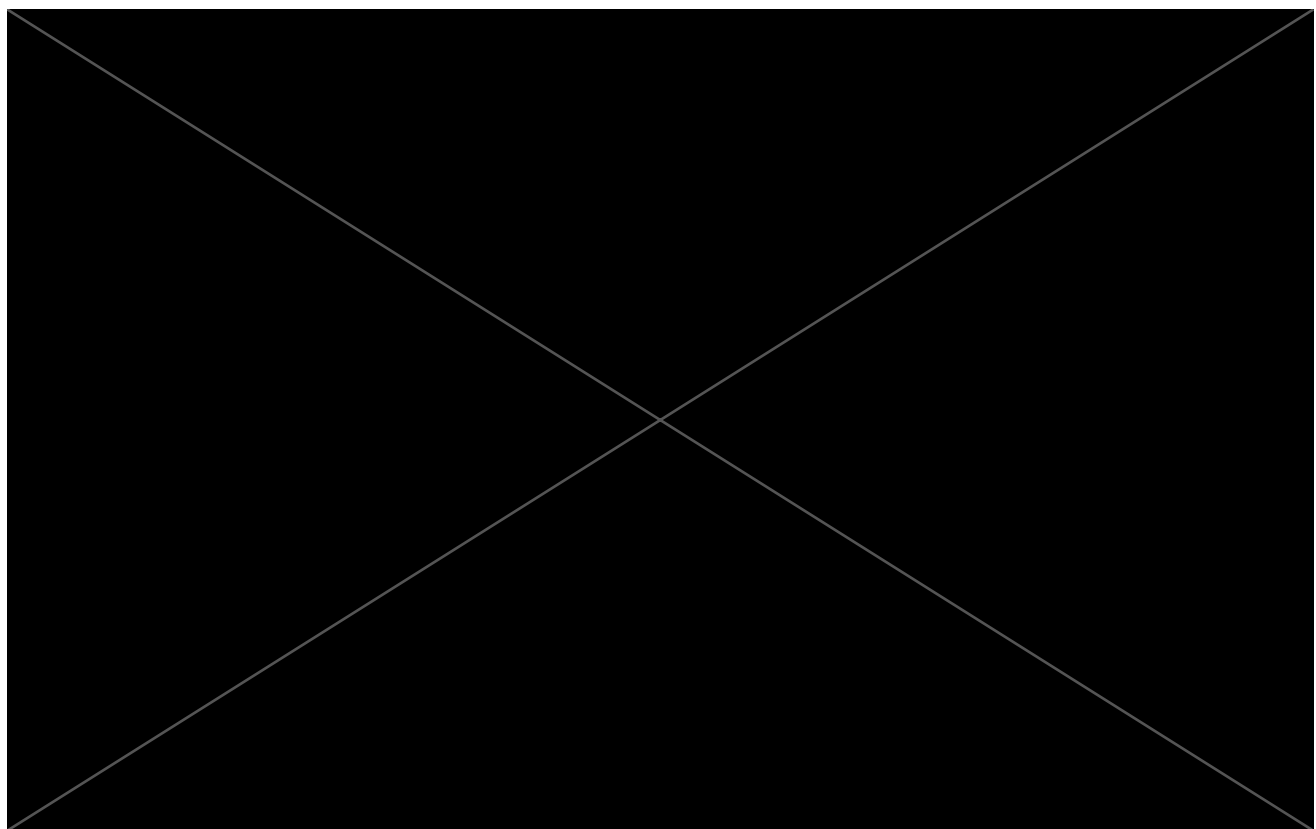
Comparison of Classical Actigraphy Features

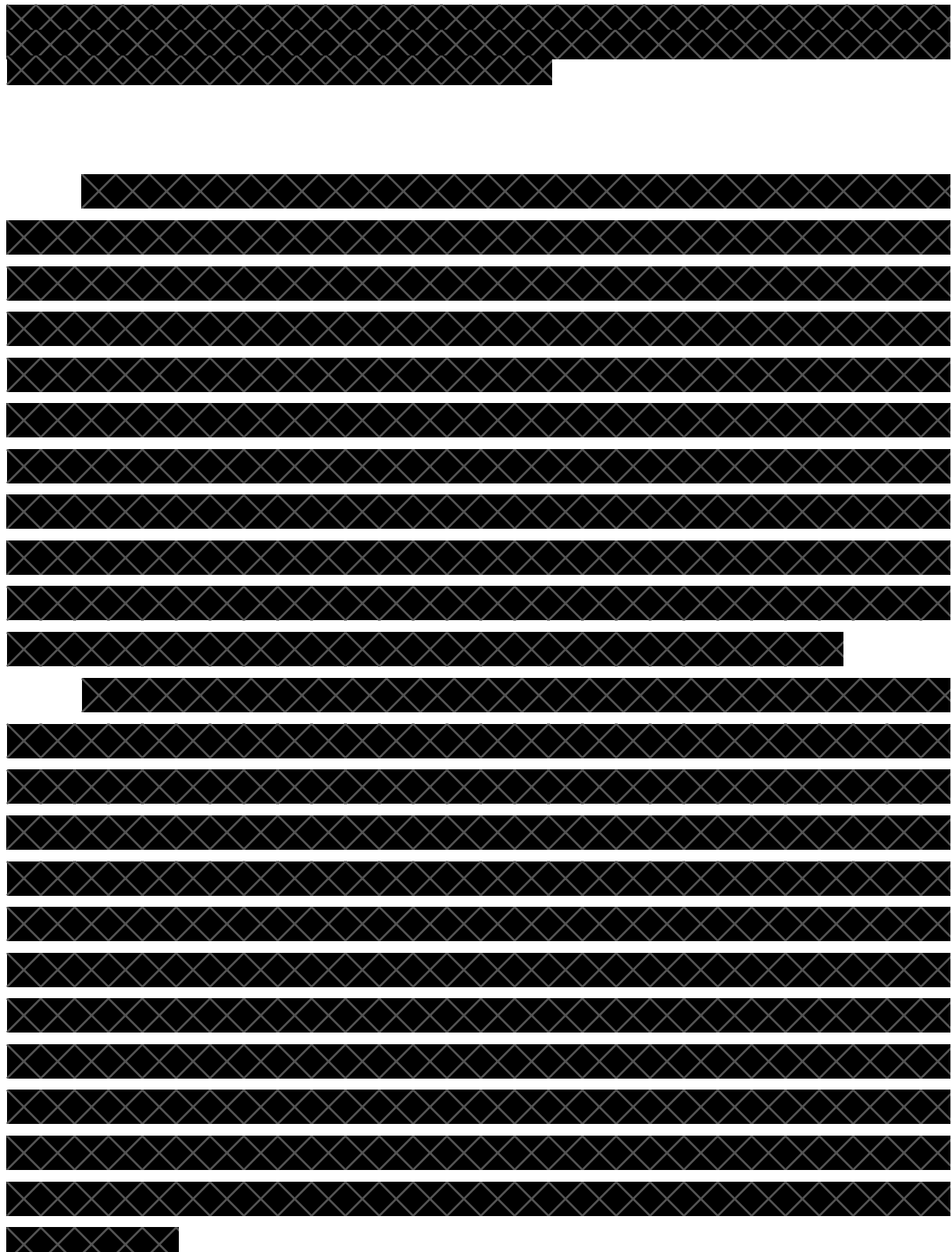
We started the analysis with the comparison of actigraphy features of PD-RBD, PD-noRBD, and controls with the aim of identifying distinct pattern differences in the respective groups. We investigated key actigraphy-derived rest-activity features in both PD patients with and without RBD and in controls. Those classical features are the mean activity level (activity counts/minute), the activity during the lowest 5 hours of activity during the day (L5), usually corresponding to the sleep period, activity during the 10 most active hours (M10), the interdaily stability (IS), being an indicator of the stability of the rest-activity pattern from day-to-day, the relative amplitude (RA), that measures the relationship between diurnal amplitude and night amplitude, the maximum value of 1 occurs when there is no movement during the night and the intradaily variability (IV) which quantifies the rhythm fragmentation of each day.

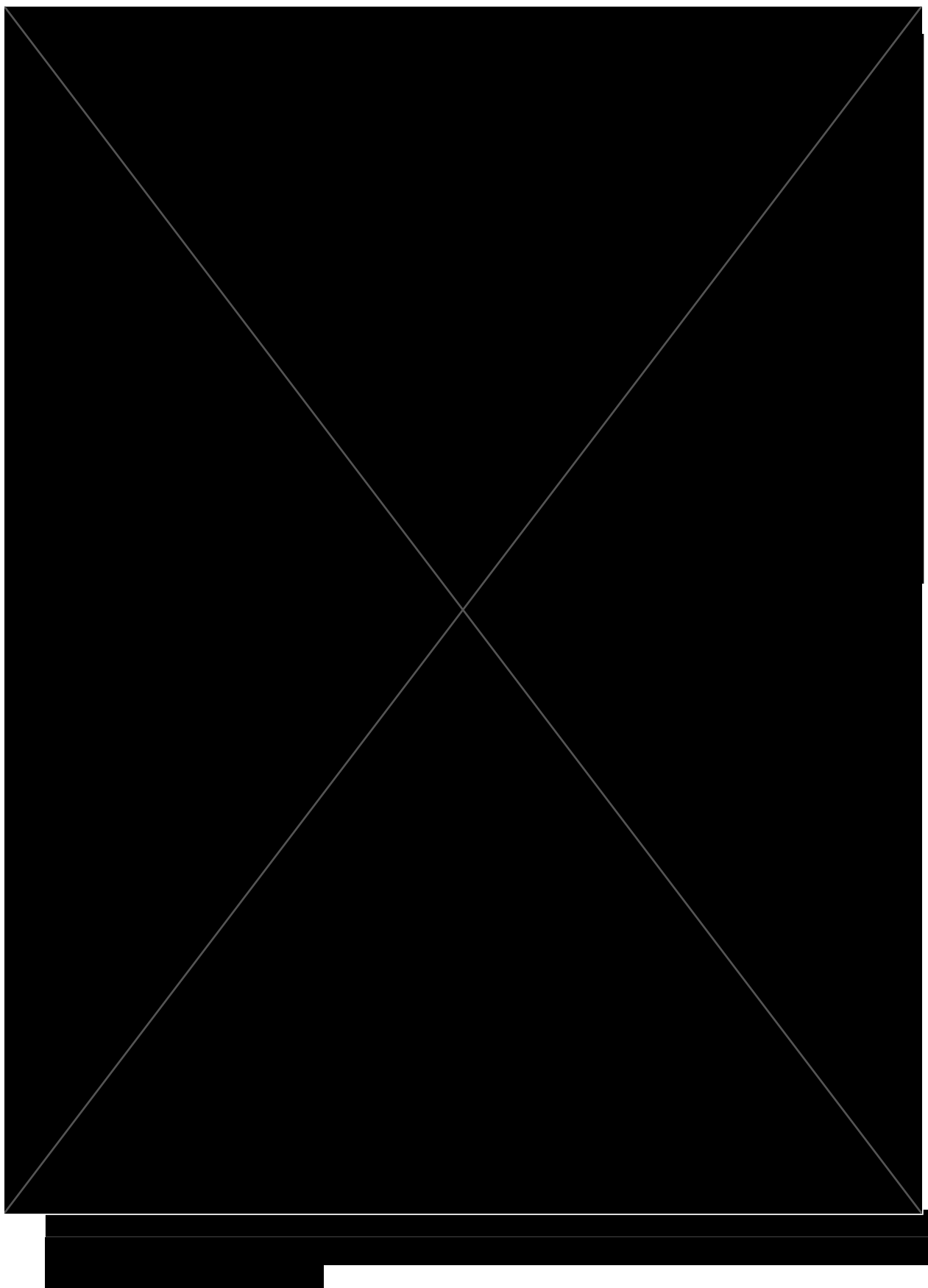
Figure 3.13a shows the mean activity levels for each group across the 24-hour period. Overall, the activity profiles are largely overlapping between groups, with no major differences during the daytime. However, during the night, individuals with PD-RBD exhibit higher activity levels compared to those with RLS and PD-noRBD.

A comparison of major rest-activity non-parametric features is displayed in figure 3.13b and c. Significant differences were observed for several features. Interdaily stability was significantly lower in PD-RBD compared to both PD-noRBD ($p < 0.001$) and RLS ($p < 0.001$), while no difference was found between PD-noRBD and RLS ($p = 0.679$). Intradaily variability was higher in PD-RBD compared to PD-noRBD ($p = 0.006$) and RLS ($p = 0.002$), whereas no difference was observed between PD-noRBD and RLS ($p = 0.718$). Relative amplitude was significantly reduced in PD-RBD compared to both PD-noRBD ($p < 0.001$) and RLS ($p < 0.001$), with no difference between PD-noRBD and RLS ($p = 0.695$). Mean activity during the least 5 active hours was significantly higher in PD-RBD compared to PD-noRBD ($p = 0.001$) and RLS ($p < 0.001$), while PD-noRBD and RLS showed no significant difference ($p = 0.093$). Mean activity during the 10 most active hours was significantly higher in PD-noRBD ($p=0.007$) and PD-RBD ($p=0.003$) than in RLS, with no differences between PD-noRBD and PD-RBD ($p=0.751$)

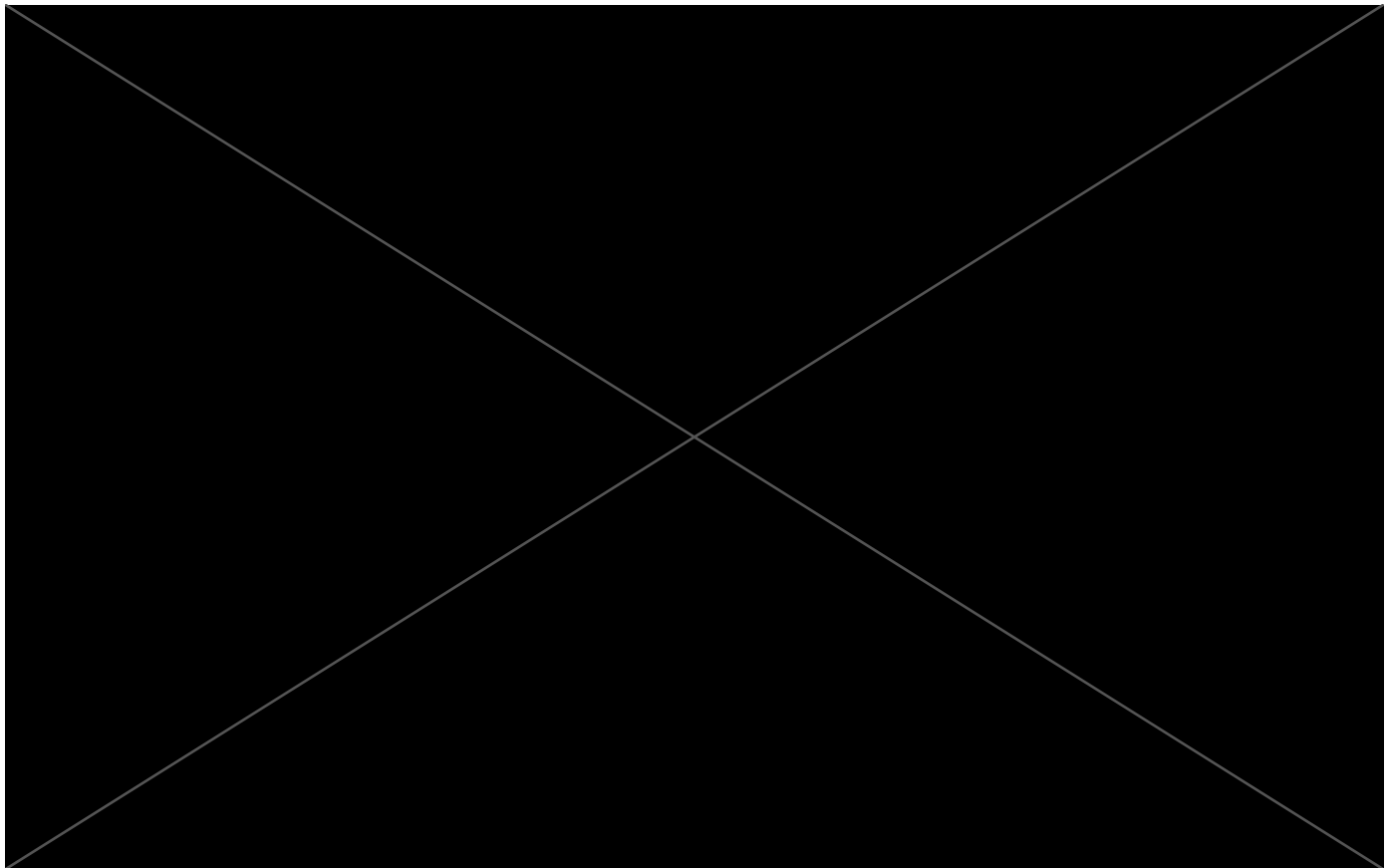




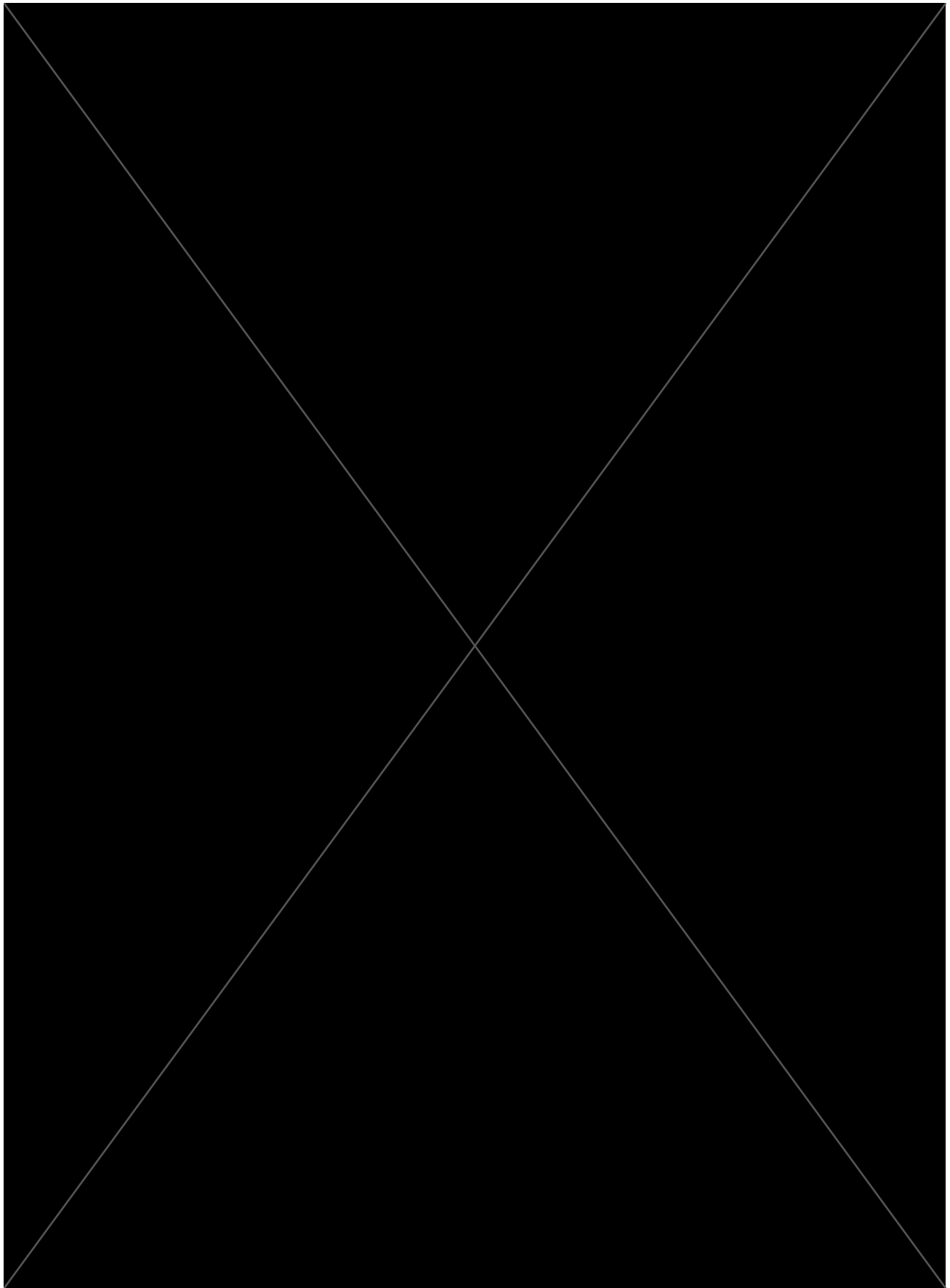


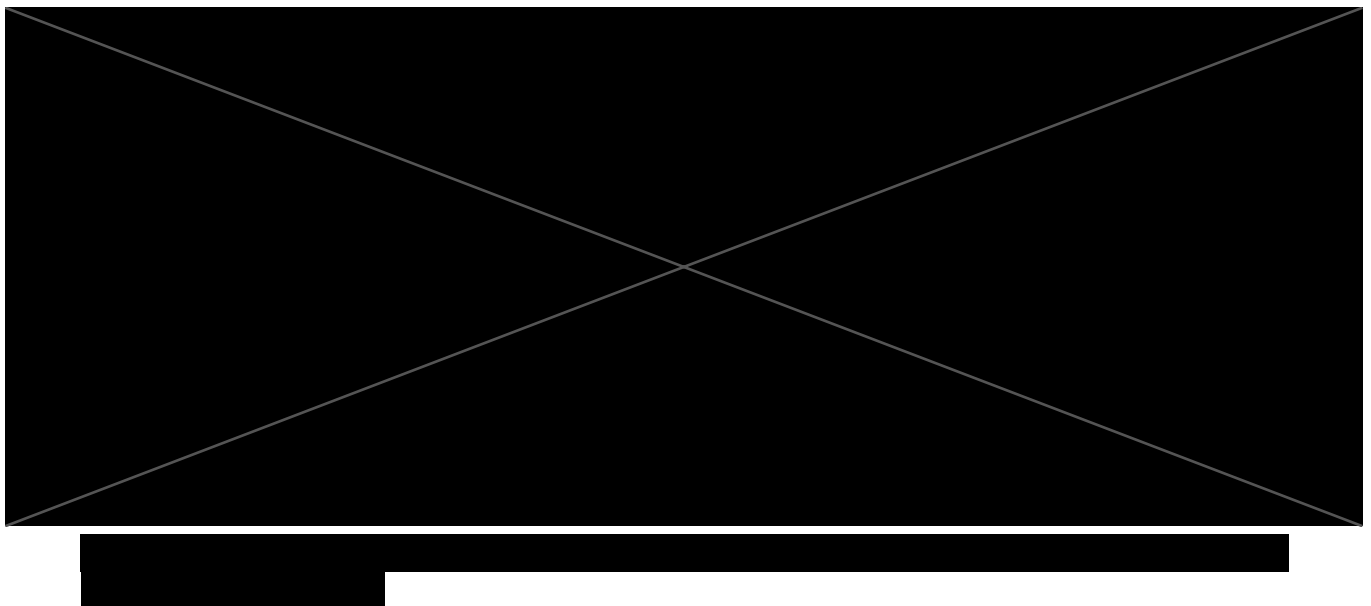
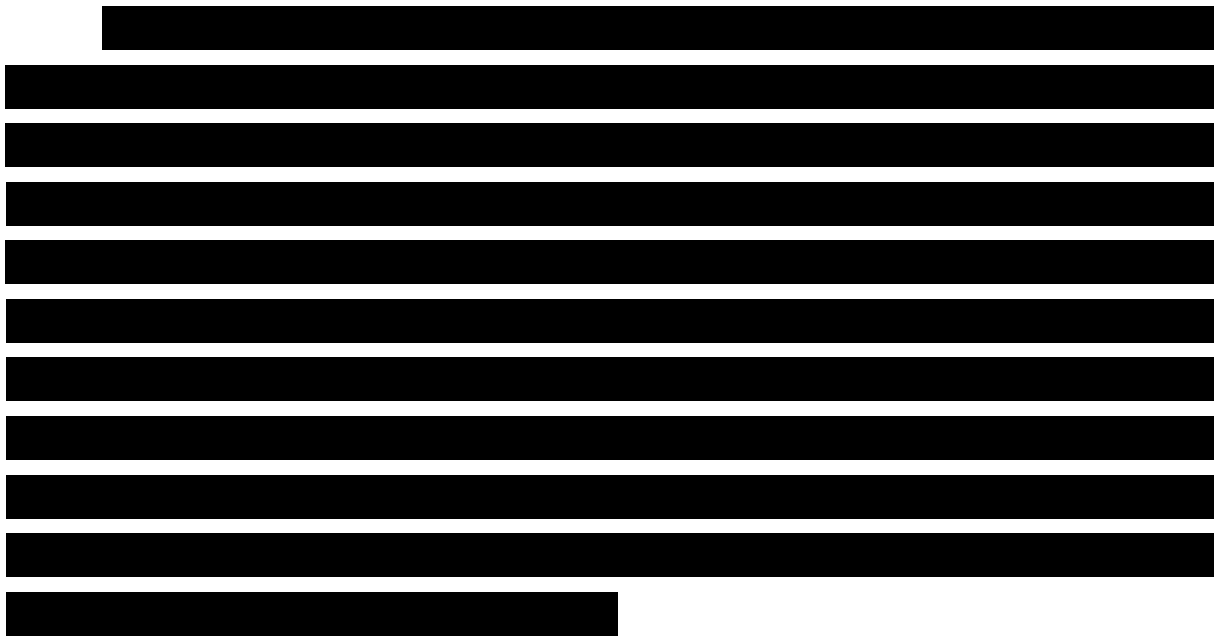




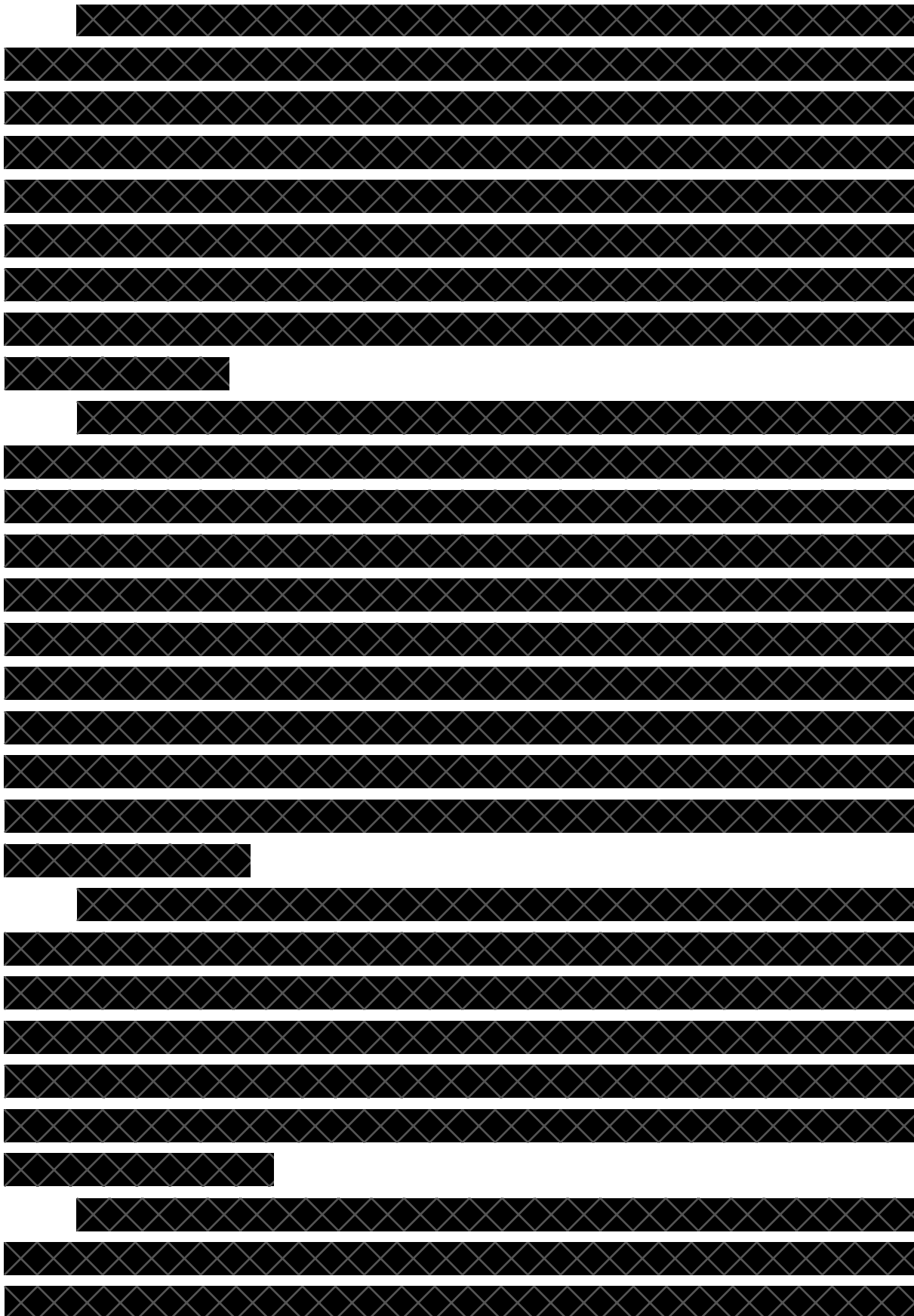


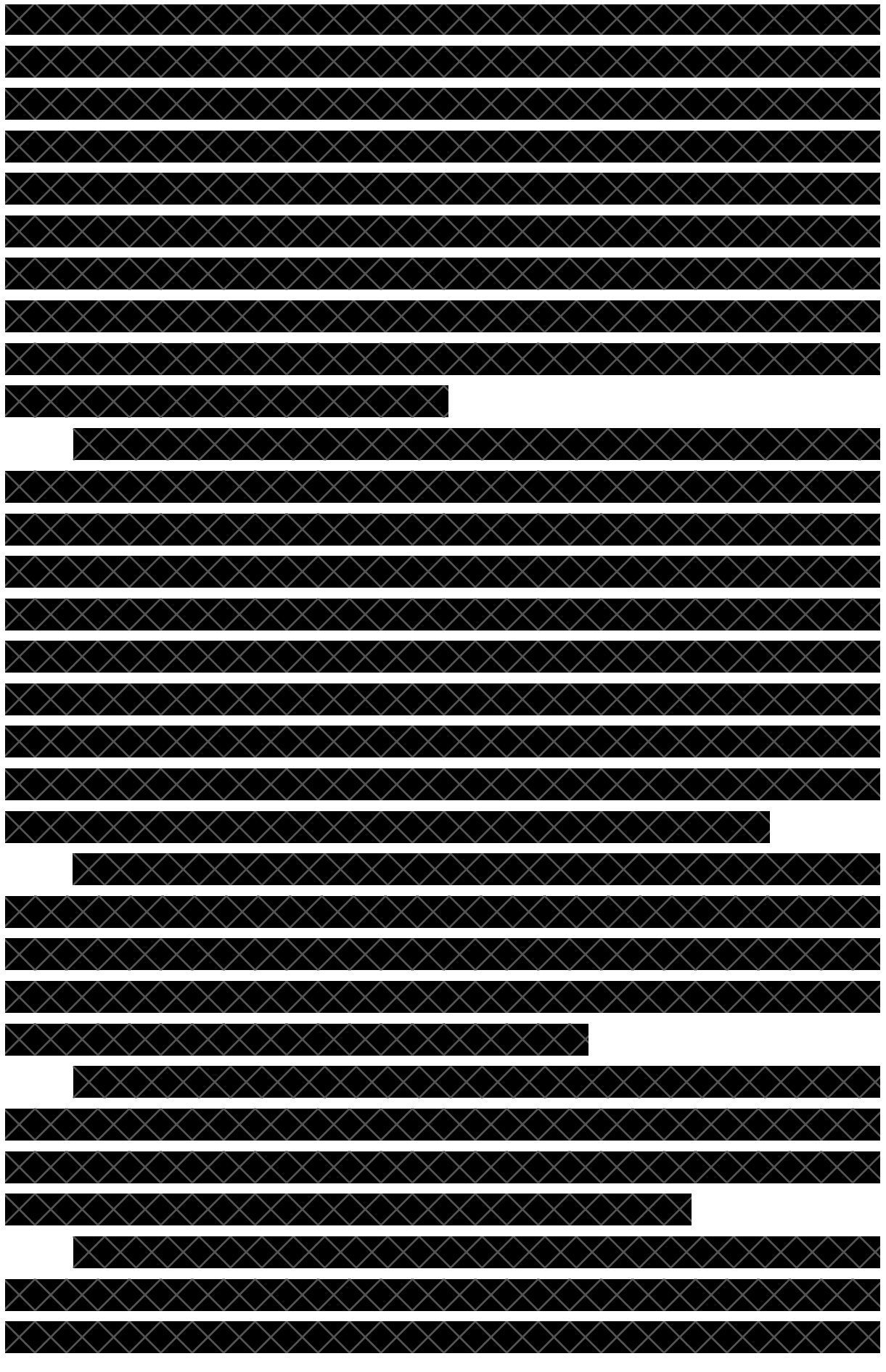
[REDACTED]













4. Discussion and Outlook

4.1. Discussion

Neurodegenerative disorders, particularly PD, are projected to rise dramatically in the coming decades. As the global population ages, the burden on healthcare systems will grow, with increasing numbers of individuals requiring long-term care.⁸ It is urgent that we act now to prepare for this challenge – by advancing early detection, improving disease monitoring, and ultimately developing preventive interventions. This aligns with the growing recognition of brain health as a public health priority, as emphasized by the WHO.⁴

Two strategies are essential. First, we must deepen our understanding of PD pathology so that we can find ways to not just treat but ultimately stop the disease progression. Critical intervention points should be identified ideally before irreversible neurodegeneration occurs. Second, we must develop accurate, accessible, and scalable tools for diagnosis and monitoring. Traditional clinical assessments and imaging methods, while effective, are often time-consuming, expensive, and dependent on specialized expertise—making them impractical for widespread screening. In contrast, AI-based tools offer rapid and automated solutions, and digital biomarkers such as actigraphy enable continuous, real-world data collection. Combined, these advances can support a shift toward preventive, personalized medicine.

This thesis contributes toward that future by developing AI-based biomarkers for PD and its prodromal stage, iRBD, using complementary data modalities. It explored two key perspectives: detailed in-vivo neuroimaging of functional alterations using PET and SPECT, and objective, non-invasive behavioral monitoring using actigraphy. Deep learning methods were used throughout to support automation, enhance sensitivity, and facilitate wide applicability. The work culminates in a prospective study enrolling iRBD patients for multimodal assessment with FDG PET, DAT SPECT, actigraphy, and standard clinical evaluations.

4.1.1. Key findings and implications

The first project developed a CycleGAN-based domain adaptation method to translate [¹¹C]CFT PET images into synthetic [¹²³I]FP-CIT SPECT images.²⁴¹ This work addressed a fundamental challenge in multicenter neuroimaging: the incompatibility of imaging modalities across clinical centers and datasets. The developed 3D CycleGAN generated synthetic SPECT images that were visually indistinguishable from real ones and retained disease-relevant features, as demonstrated by downstream classification performance. This cross-modality synthesis facilitates the use of large-scale PET datasets in SPECT-based environments, supporting broader AI model training and improving diagnostic workflows.

Importantly, synthetic data like this can help address one of the main barriers to AI development in medicine: data scarcity. AI models, particularly deep learning models, require large datasets. However, medical data is often limited and fragmented.³²⁴ By generating realistic synthetic SPECT images, we contribute not only to harmonization but also to data augmentation, enhancing downstream model performance and generalizability.³²⁵ This approach holds promise for future applications in longitudinal or multicenter studies, and as a foundation for automated diagnostic pipelines in movement disorder clinics.

The second study evaluated methods for predicting iRBD conversion to PD, using longitudinal FDG and DAT PET scans. The DAT-based models showed consistently higher predictive performance, confirming previous findings on the utility of dopaminergic imaging for early-stage diagnosis. Notably, the study included one of the first deep learning approaches to predict phenoconversion from FDG PET. Its performance was comparable to conventional imaging metrics, suggesting that AI can extract disease-relevant information from functional images in a manner that complements or enhances traditional approaches. Although multicenter and longitudinal studies are required for translation to clinical reality, this study provides the first step toward the use of DL in functional imaging for iRBD conversion prediction. Such methods will be particularly important once disease-modifying treatments become available. Already at present day, they can aid in the development of such treatments by helping to identify the most suitable patients for inclusion in clinical trials.^{75,95}

Furthermore, once validated, they can support clinicians in planning follow-up and clinical management, and in providing patient-centered information to guide future care decisions. However, these applications must still be carefully evaluated in terms of their risk-benefit balance.

Additionally, this study investigated two key processes of neurodegeneration: metabolic alterations, assessed using FDG PET, and dopaminergic neuronal dysfunction and loss, assessed using DAT imaging, in the same cohort. Analyzing both is of particular interest, as changes in glucose metabolism may reflect early neuronal and synaptic dysfunction, which can be influenced by various mechanisms including neuroinflammation, network disruption, and degenerative processes. In fact, neuroinflammation is thought to be one of the leading and triggering causes of PD and other neurodegenerative disorders,³⁴ while dopaminergic neuronal loss is more prominent in later stages, when cell death becomes apparent.^{11,326}

While metabolic alterations and neuroinflammation are often considered an early feature that could improve prognostication of disease progression, our analysis over an 8-year pre-conversion period suggests that dopaminergic dysfunction remains the more reliable marker. This could be due to the fact that FDG PET does not exclusively reflect neuroinflammation, as shown in previous studies,^{109,112} or that neuroinflammation alone is not a major driving factor of progression, being influenced by multiple other variables.

Nevertheless, FDG combined with deep learning still provides good prediction ability in our cohort, especially a high negative predictive value for prediction of conversion within 2 years. Consistently, a recent 4-year longitudinal study by Tang and colleagues showed an inverse correlation between baseline FDG PD-related pattern and times to phenoconversion.²⁹⁵ Other studies also showed increases in FDG derived patterns with iRBD disease progression, albeit conversion prediction was limited due to absence of enough converted patients.^{288,293} The strengths of our study compared to the previous ones are the relatively long follow-up period (mean of 7.1 ± 2.2 years), frequent imaging assessments, and a larger number of converted patients. Such design enabled us to assess phenoconversion risk more robustly and apply novel methodologies such as deep learning. Recent studies further highlight the prognostic value of FDG PET beyond conversion. Regional glucose metabolism has been shown to predict survival in PD and DLB, potentially even earlier than dementia

onset.³²⁷ Additionally, nigral hypometabolism on FDG PET may help identify PD patients without elevated cortical PD-related expression, improving early diagnosis.³²⁸

On the other hand, dopaminergic deficits appear to emerge very early – more than eight years before the onset of clinical symptoms – which highlights the need for intervention at the earliest stages of the disease. Previous studies had already pointed towards this conclusion.^{329–331} Iranzo and colleagues showed that DAT-SPECT had 75% sensitivity and 51% specificity to predict synucleinopathies development after 5 years.³³⁰ Another study reported that using machine learning methods, presynaptic dopaminergic imaging together with clinical data had a sensitivity of 77% and specificity of 85% in distinguishing synucleinopathy patients with RBD from non converted iRBD patients.³³¹ Our study confirms the previous results with a sensitivity and specificity above 80% for predicting conversion within 8 years.

All of the previously explored evidence further support and encourage the integration of nuclear medicine imaging into diagnostic and prognostic workflows, and, in the future, into treatment monitoring. Nuclear imaging modalities are the best way of visualizing pathological processes *in vivo* in humans, which is particularly important in the early stages of neurodegenerative diseases, when functional alterations precede anatomical changes, and subtle abnormalities may already be present.²⁸³ With ongoing advances in both hardware and software, radiation doses have decreased significantly and are now comparable to those of other imaging modalities, with further reductions expected. The emergence of total-body PET scanners with exceptionally high sensitivity and minimal radiation exposure may even pave the way for population-level screening.^{332,333} The use of AI-based automated diagnosis could help increase patient throughput and assist in interpretation, especially if these techniques become standard tools for screening in the future. However, the high cost of these technologies remains a major barrier.

Lastly, we explored the use of AI in actigraphy as a biomarker for diagnosing RBD in PD and for predicting conversion in individuals with iRBD. The state-of-the-art pretrained transformer model demonstrated strong performance in identifying RBD within PD patients and in distinguishing PD patients from healthy controls, using a larger sample than the only other AI-based study to perform a similar classification.¹⁴⁹ Importantly, the classification

scores for iRBD patients indicate the model's potential to predict conversion to overt PD – marking one of the first attempts to do so using actigraphy. These findings support the use of actigraphy as a non-invasive digital biomarker for disease classification and suggest that actigraphy-based models may help identify individuals at risk of developing PD at an early stage, paving the way for predictive applications. This approach aims to provide an accessible, community-based method for detecting neurodegenerative and sleep disorders using affordable, everyday wearable devices—an especially important goal given the growing prevalence of these conditions. Notably, this work aligns with one of the main priorities in neurodegenerative disease management: prevention.^{1,4} Emerging evidence highlights physical activity as a potential disease-modifying intervention,⁹⁶ and incorporating activity measurement into clinical workflows could serve a dual purpose—both as a monitoring tool and a therapeutic strategy.

At the same time, this project leveraged the potential of foundation models, which represent a promising future for AI in medicine. These models are typically trained in a self-supervised manner using vast amounts of uncurated data, eliminating the need for time-consuming manual labeling. By learning generalizable patterns from large datasets, they can be fine-tuned for specific tasks, such as classification, using relatively small, labeled datasets.³³⁴ This approach is particularly well-suited to medical applications, where curated data are often limited, but large volumes of unlabeled data are readily available. As AI becomes increasingly integrated into healthcare, the work presented here paves the way for innovative approaches to understand the link between physical activity and neurodegeneration.

4.1.2. Limitations

Despite the promising results, several limitations must be acknowledged. AI methods still face several challenges before they can be widely adopted in clinical practice. One of the main issues is generalizability. Many models perform well only within the specific data domain they were trained on, and tend to underperform when applied to external datasets.³³⁵ To ensure their broader utility, extensive external validation is essential.³³⁶

These data requirements, emphasizes the need for open-access medical data and increased data sharing across institutions and countries—while strictly maintaining patient privacy and data protection. A global collaborative effort is crucial, as patient characteristics can vary significantly across regions. Despite these challenges, significant progress has been made in recent years. Initiatives like the Parkinson's Progression Markers Initiative³³⁷ (used in the work described in section 3.1) and Alzheimer's Disease Neuroimaging Initiative³³⁸ are paving the way by providing large, high-quality datasets. These databases are also expanding to include more imaging modalities and data from prodromal patients, creating a solid foundation for future advancements.

The next critical step is the integration of AI methods into clinical trials, allowing researchers to assess their impact in real-world clinical contexts.^{339,340} In this regard, the European Artificial Intelligence Act (AI Act)³⁴¹ establishes an important regulatory framework for the responsible development and deployment of AI in healthcare. The Act categorizes AI-based software intended for medical use as high-risk, subjecting it to strict requirements such as robust risk-mitigation systems, high-quality datasets, transparency, and human oversight. These measures are essential for ensuring that AI applications in clinical trials not only meet high standards of safety and reliability but also align with ethical and legal expectations. Following clinical integration, ongoing monitoring of AI performance in real-world healthcare settings becomes essential to maintain safety, reliability, and continued effectiveness over time.^{339,340}

In terms of specific limitations related to the previously described projects, several challenges remain to be addressed. Below, some of the key issues identified across different approaches are outlined.

A key limitation of our domain transfer approach from dopaminergic PET to SPECT is the absence of paired data. Without corresponding PET-SPECT image pairs, it is difficult to verify whether the generated SPECT images accurately reflect what real ones would look like. The lack of ground truth hampers the clear evaluation of image fidelity. Furthermore, reliable generation of SPECT images may be affected by external effects on dopamine transporter binding. For example, recent evidence shows that treatment with venlafaxine or bupropion

can reduce striatal [¹²³I]FP-CIT binding to a degree similar to that seen in nigrostriatal degeneration. However, this drug-induced reduction is typically symmetric and lacks the rostro-caudal gradient characteristic of Parkinson's disease, allowing for its differentiation through visual analysis or clustering approaches.³⁴² In addition, while CycleGAN has been widely used for unpaired image-to-image translation, it presents practical challenges: it may lead to hallucinations, where features that did not exist previously in the image are created,²⁷⁵ it is computationally demanding, and requires careful tuning of hyperparameters, which can be time-consuming and non-trivial.^{234,273,274} To overcome these issues, we propose using diffusion models,^{231,253,270} which represent the current state-of-the-art in image generation. These models can be applied not only to the original task of DAT PET-to-SPECT translation, but also to extend their application to other imaging modalities, such as PSMA PET and SPECT.

A common challenge across many deep learning projects is the limited availability of data, particularly true in the case of rare disorders. In the project described in section 3.2 the main constraint is the small cohort size: only 38 iRBD patients with follow-up scans are available. Although this represents one of the largest follow-up imaging datasets for iRBD to date, it remains relatively small for training robust AI models. To mitigate this limitation, transfer learning from larger datasets of patients with overt parkinsonism is employed.³³⁵ The working hypothesis is that if a model can effectively distinguish between healthy controls and PD patients, it should also be able to capture intermediate disease stages—such as those seen in iRBD—along a continuous spectrum of neurodegeneration.

A persistent issue across all deep learning-based projects is the risk of overfitting to the training data, which limits the generalizability of the models to new, unseen data. To reduce this risk, robust cross-validation strategies during model development were employed.³⁴³ While this helps estimate model performance more reliably, it is not a substitute for external validation.

To truly assess the broader utility of these methods, testing on independent cohorts is essential. This is a key focus of the next phase of this work: a prospective study in which we plan to collect FDG PET, DAT SPECT, and actigraphy data from an iRBD cohort based in Switzerland. This dataset will provide an invaluable opportunity to validate our models in a external clinical setting.

Actigraphy is a valuable tool for non-invasive, long-term monitoring of sleep and activity patterns. However, it comes with inherent limitations. Due to primarily measuring movement, actigraphy can only provide indirect insights into physiological states and lacks information on other important aspects of sleep architecture and physiology. One common issue is its reduced sensitivity to wakefulness, which often leads to overestimation of total sleep time and underestimation of sleep onset latency—the time it takes to fall asleep.²¹⁰ As a result, certain overnight sleep quality metrics may be inaccurately estimated compared to PSG, the gold-standard sleep assessment tool.^{146,344} Although studies have shown strong correlations between actigraphy and PSG for parameters like total sleep time, sleep efficiency, and wake after sleep onset, the accuracy for detecting sleep onset latency remains more limited.¹⁴⁶ Another challenge lies in the influence of confounding variables, such as treatment with dopaminergic agents, which can alter movement patterns and confound actigraphy-based measurements.

Despite these limitations, AI methods may help bridge the gap between actigraphy and PSG by extracting complex, subtle patterns from actigraphy data that are not easily discernible to the human eye. Additionally, with next-generation wearable devices offering more comprehensive physiological measurements, the scope and accuracy of actigraphy-based assessments are expected to improve in the near future.

4.2. Outlook

The work presented in this thesis lays important groundwork for the integration of AI and multimodal biomarkers in the early detection and monitoring of PD and its prodromal stage, iRBD. Looking ahead, several promising directions emerge that could further expand the impact of this research and contribute to the future of neurodegenerative disease management.

First and foremost, the prospective study enrolling iRBD patients for longitudinal assessment with FDG PET, DAT SPECT, actigraphy, and clinical evaluation represents a pivotal next step. This unique dataset will enable the external validation of our current models in an

independent and real-world setting, providing essential evidence for clinical translation. Moreover, the collection of harmonized multimodal data across time points opens the door to developing integrated predictive models that can jointly capture metabolic, dopaminergic, and behavioral signatures of early neurodegeneration. Such multimodal fusion approaches, especially when paired with advanced AI architectures, could enhance prognostic accuracy and support personalized risk stratification.

One of the most anticipated developments in PET imaging for neurodegenerative diseases is the clinical implementation of reliable α -synuclein PET tracers, capable of directly visualizing the pathological aggregation of this hallmark protein *in vivo*.³⁴⁵ Such tracers would represent a transformative step in PD research and diagnosis, enabling the specific detection of synucleinopathy even at prodromal stages. In this regard, we are contributing to a collaborative project focused on validating the clinical utility of a newly developed α -synuclein tracer using dynamic PET imaging (Figure 4.1). Preliminary results from this ongoing work are highly promising and are expected to be published in the near future. If successful, this tracer could complement existing modalities such as DAT and FDG PET, offering a more comprehensive and mechanistic view of disease pathology and progression. The integration of α -synuclein imaging into clinical workflows and research trials would not only refine diagnostic precision but also facilitate the evaluation of disease-modifying therapies that target this pathological process.

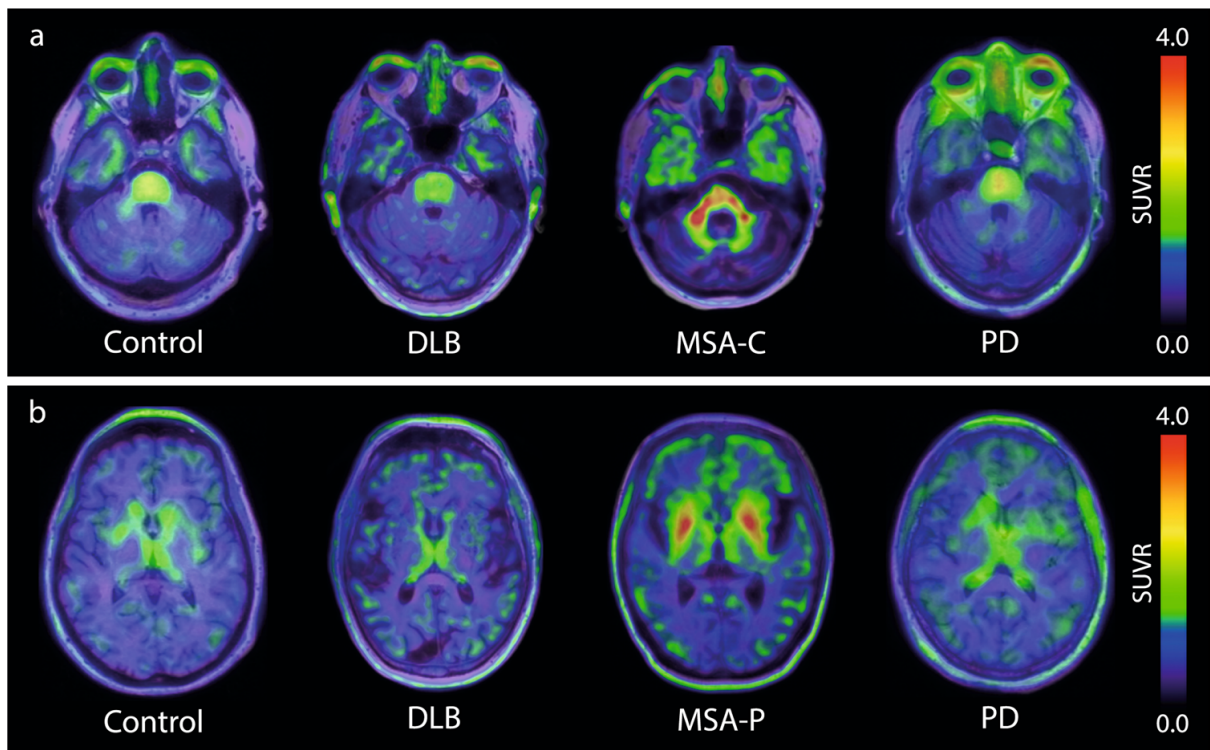


Figure 4.1. α -synuclein PET imaging with $[18\text{F}]\text{ACI-12589}$ tracer in participants with α -synucleinopathies. Adapted from Smith et al., Nature Communications, 2023.³⁴⁶

Methodologically, future efforts should prioritize the transition from conventional deep learning frameworks to newer paradigms such as foundation models and diffusion models. Foundation models offer scalability and flexibility by enabling fine-tuning on small, domain-specific datasets after pretraining on large, diverse corpora. This is especially advantageous in medicine, where annotated data is limited but unlabelled data is abundant. Similarly, the application of diffusion models in medical image synthesis could address current limitations in cross-modality translation, particularly in scenarios lacking paired data. By providing higher fidelity and more stable training compared to GANs,²⁷⁰ diffusion models may become the new standard for data harmonization and augmentation in neuroimaging.

Another important trajectory involves the integration of AI tools into clinical practice. AI models must be embedded within clinical workflows to assess their impact on decision-making, patient outcomes, and healthcare efficiency. This includes evaluating AI-assisted screening tools in primary care or community settings, where early signs of neurodegeneration may first be detectable through wearable technology. In parallel,

continued collaboration with clinicians and regulatory bodies will be critical to ensure safe, ethical, and transparent deployment of these tools in real-world settings. Future studies should explore the combination of actigraphy with additional wearable sensor data (e.g., heart rate variability, skin temperature, electrodermal activity) to create more comprehensive digital phenotypes. Multi-sensor integration may improve the specificity of behavioral biomarkers and enable the detection of subtle prodromal features across a broader spectrum of neurodegenerative and sleep disorders.

Finally, the increasing recognition of brain health as a public health priority highlights the need for scalable, equitable solutions. More accessible PET imaging, AI platforms, and widespread access to wearable technology could one day enable population-level screening for at-risk individuals. However, to realize this vision, it will be essential to address ongoing challenges related to cost, infrastructure, and digital health equity—ensuring that technological advances do not widen existing gaps in care access.

In sum, the convergence of neuroimaging, digital biomarkers, and AI is welcoming a new era of predictive, preventive, and personalized neurology. By continuing to build on the foundations laid in this thesis, future research can accelerate the transition from reactive to proactive care—offering patients earlier interventions, better outcomes, and more informed decisions about their brain health.

5. Bibliography

1. Bassetti CLA, Endres M, Sander A, et al. The European Academy of Neurology Brain Health Strategy: One brain, one life, one approach. *Eur J Neurol.* 2022;29(9):2559-2566. doi:<https://doi.org/10.1111/ene.15391>
2. Avan A, Hachinski V, Group the BHL and A. Brain health: Key to health, productivity, and well-being. *Alzheimer's & Dementia.* 2022;18(7):1396-1407. doi:<https://doi.org/10.1002/alz.12478>
3. World Health Organisation (WHO). Brain Health. 2025. Accessed April 1, 2025. https://www.who.int/health-topics/brain-health#tab=tab_1
4. World Health Organization (WHO). Optimizing brain health across the life course: WHO position paper. Published online 2022. Accessed April 1, 2025. Licence: CC BY-NC-SA 3.0 IGO; <https://creativecommons.org/licenses/by-nc-sa/3.0/igo/>.
5. Livingston G, Huntley J, Sommerlad A, et al. Dementia prevention, intervention, and care: 2020 report of the Lancet Commission. *The Lancet.* 2020;396(10248):413-446. doi:[10.1016/S0140-6736\(20\)30367-6](https://doi.org/10.1016/S0140-6736(20)30367-6)
6. The Lancet Neurology. A decisive year for the neurological community. *Lancet Neurol.* 2022;21(2):103. doi:[10.1016/S1474-4422\(22\)00001-1](https://doi.org/10.1016/S1474-4422(22)00001-1)
7. Wilson DM, Cookson MR, Van Den Bosch L, Zetterberg H, Holtzman DM, Dewachter I. Hallmarks of neurodegenerative diseases. *Cell.* 2023;186(4):693-714. doi:[10.1016/j.cell.2022.12.032](https://doi.org/10.1016/j.cell.2022.12.032)
8. Steinmetz JD, Seeher KM, Schiess N, et al. Global, regional, and national burden of disorders affecting the nervous system, 1990-2021: a systematic analysis for the Global Burden of Disease Study 2021. *Lancet Neurol.* 2024;23(4):344-381. doi:[10.1016/S1474-4422\(24\)00038-3](https://doi.org/10.1016/S1474-4422(24)00038-3)
9. Tay LX, Ong SC, Tay LJ, Ng T, Parumalivam T. Economic Burden of Alzheimer's Disease: A Systematic Review. *Value Health Reg Issues.* 2024;40:1-12. doi:[10.1016/j.vhri.2023.09.008](https://doi.org/10.1016/j.vhri.2023.09.008)
10. Wong YC, Krainc D. α -synuclein toxicity in neurodegeneration: mechanism and therapeutic strategies. *Nat Med.* 2017;23(2):1-13. doi:[10.1038/nm.4269](https://doi.org/10.1038/nm.4269)
11. Gadhave DG, Sugandhi V V, Jha SK, et al. Neurodegenerative disorders: Mechanisms of degeneration and therapeutic approaches with their clinical relevance. *Ageing Res Rev.* 2024;99:102357. doi:<https://doi.org/10.1016/j.arr.2024.102357>
12. Henstridge CM, Pickett E, Spires-Jones TL. Synaptic pathology: A shared mechanism in neurological disease. *Ageing Res Rev.* 2016;28:72-84. doi:<https://doi.org/10.1016/j.arr.2016.04.005>
13. Fricker M, Tolokovsky AM, Borutaite V, Coleman M, Brown GC. Neuronal Cell Death. *Physiol Rev.* 2018;98(2):813-880. doi:[10.1152/physrev.00011.2017](https://doi.org/10.1152/physrev.00011.2017)
14. Millecamp S, Julien JP. Axonal transport deficits and neurodegenerative diseases. *Nat Rev Neurosci.* 2013;14(3):161-176. doi:[10.1038/nrn3380](https://doi.org/10.1038/nrn3380)
15. Sheng ZH, Cai Q. Mitochondrial transport in neurons: impact on synaptic homeostasis and neurodegeneration. *Nat Rev Neurosci.* 2012;13(2):77-93. doi:[10.1038/nrn3156](https://doi.org/10.1038/nrn3156)
16. Nussbacher JK, Tabet R, Yeo GW, Lagier-Tourenne C. Disruption of RNA Metabolism in Neurological Diseases and Emerging Therapeutic Interventions. *Neuron.* 2019;102(2):294-320. doi:[10.1016/j.neuron.2019.03.014](https://doi.org/10.1016/j.neuron.2019.03.014)
17. Madabhushi R, Pan L, Tsai LH. DNA Damage and Its Links to Neurodegeneration. *Neuron.* 2014;83(2):266-282. doi:[10.1016/j.neuron.2014.06.034](https://doi.org/10.1016/j.neuron.2014.06.034)
18. Parkinson J. An Essay on the Shaking Palsy. *J Neuropsychiatry Clin Neurosci.* 2002;14(2):223-236. doi:[10.1176/jnp.14.2.223](https://doi.org/10.1176/jnp.14.2.223)
19. Dauer W, Przedborski S. Parkinson's Disease: Mechanisms and Models. *Neuron.* 2003;39(6):889-909. doi:[10.1016/S0896-6273\(03\)00568-3](https://doi.org/10.1016/S0896-6273(03)00568-3)

20. Przedborski S. The two-century journey of Parkinson disease research. *Nat Rev Neurosci*. 2017;18(4):251-259. doi:10.1038/nrn.2017.25
21. Jacobs BM, Belete D, Bestwick J, et al. Parkinson's disease determinants, prediction and gene-environment interactions in the UK Biobank. *J Neurol Neurosurg Psychiatry*. 2020;91(10):1046-1054. doi:10.1136/jnnp-2020-323646
22. de Rijk MC, Tzourio C, Breteler MM, et al. Prevalence of parkinsonism and Parkinson's disease in Europe: the EUROPARKINSON Collaborative Study. European Community Concerted Action on the Epidemiology of Parkinson's disease. *J Neurol Neurosurg Psychiatry*. 1997;62(1):10-15. doi:10.1136/jnnp.62.1.10
23. Wooten GF. Are men at greater risk for Parkinson's disease than women? *J Neurol Neurosurg Psychiatry*. 2004;75(4):637-639. doi:10.1136/jnnp.2003.020982
24. Ben-Shlomo Y, Darweesh S, Llibre-Guerra J, Marras C, San Luciano M, Tanner C. The epidemiology of Parkinson's disease. *The Lancet*. 2024;403(10423):283-292. doi:10.1016/S0140-6736(23)01419-8
25. Morris HR, Spillantini MG, Sue CM, Williams-Gray CH. The pathogenesis of Parkinson's disease. *The Lancet*. 2024;403(10423):293-304. doi:10.1016/S0140-6736(23)01478-2
26. Golbe LI, Di Iorio G, Bonavita V, Miller DC, Duvoisin RC. A large kindred with autosomal dominant Parkinson's disease. *Ann Neurol*. 1990;27(3):276-282. doi:10.1002/ana.410270309
27. Singleton A, Hardy J. A generalizable hypothesis for the genetic architecture of disease: pleomorphic risk loci. *Hum Mol Genet*. 2011;20(R2):R158-R162. doi:10.1093/hmg/ddr358
28. Kluss JH, Mamais A, Cookson MR. LRRK2 links genetic and sporadic Parkinson's disease. *Biochem Soc Trans*. 2019;47(2):651-661. doi:<https://doi.org/10.1042/BST20180462>
29. Clausen L, Okarmus J, Voutsinos V, Meyer M, Lindorff-Larsen K, Hartmann-Petersen R. PRKN-linked familial Parkinson's disease: cellular and molecular mechanisms of disease-linked variants. *Cellular and Molecular Life Sciences*. 2024;81(1):223. doi:10.1007/s00018-024-05262-8
30. Funayama M, Nishioka K, Li Y, Hattori N. Molecular genetics of Parkinson's disease: Contributions and global trends. *J Hum Genet*. 2023;68(3):125-130. doi:10.1038/s10038-022-01058-5
31. Schweighauser M, Shi Y, Tarutani A, et al. Structures of α -synuclein filaments from multiple system atrophy. *Nature*. 2020;585(7825):464-469. doi:10.1038/s41586-020-2317-6
32. Bi M, Du X, Jiao Q, Chen X, Jiang H. Expanding the role of proteasome homeostasis in Parkinson's disease: beyond protein breakdown. *Cell Death Dis*. 2021;12(2):154. doi:10.1038/s41419-021-03441-0
33. Picca A, Guerra F, Calvani R, et al. Mitochondrial Dysfunction, Protein Misfolding and Neuroinflammation in Parkinson's Disease: Roads to Biomarker Discovery. *Biomolecules*. 2021;11(10):1508. doi:10.3390/biom11101508
34. Calabresi P, Mechelli A, Natale G, Volpicelli-Daley L, Di Lazzaro G, Ghiglieri V. Alpha-synuclein in Parkinson's disease and other synucleinopathies: from overt neurodegeneration back to early synaptic dysfunction. *Cell Death Dis*. 2023;14(3):176. doi:10.1038/s41419-023-05672-9
35. Arotarena ML, Dovero S, Prigent A, et al. Bidirectional gut-to-brain and brain-to-gut propagation of synucleinopathy in non-human primates. *Brain*. 2020;143(5):1462-1475. doi:10.1093/brain/awaa096
36. Recasens A, Ulusoy A, Kahle PJ, Di Monte DA, Dehay B. In vivo models of alpha-synuclein transmission and propagation. *Cell Tissue Res*. 2018;373(1):183-193. doi:10.1007/s00441-017-2730-9
37. Hodge GK, Butcher LL. Pars compacta of the substantia nigra modulates motor activity but is not involved importantly in regulating food and water intake. *Naunyn Schmiedebergs Arch Pharmacol*. 1980;313(1):51-67. doi:10.1007/BF00505805
38. Jin X, Tecuapetla F, Costa RM. Basal ganglia subcircuits distinctively encode the parsing and concatenation of action sequences. *Nat Neurosci*. 2014;17(3):423-430. doi:10.1038/nn.3632

39. Braak H, Tredici K Del, Rüb U, de Vos RAI, Jansen Steur ENH, Braak E. Staging of brain pathology related to sporadic Parkinson's disease. *Neurobiol Aging*. 2003;24(2):197-211. doi:[https://doi.org/10.1016/S0197-4580\(02\)00065-9](https://doi.org/10.1016/S0197-4580(02)00065-9)
40. Beach TG, Adler CH, Lue L, et al. Unified staging system for Lewy body disorders: correlation with nigrostriatal degeneration, cognitive impairment and motor dysfunction. *Acta Neuropathol*. 2009;117(6):613-634. doi:10.1007/s00401-009-0538-8
41. Horsager J, Knudsen K, Sommerauer M. Clinical and imaging evidence of brain-first and body-first Parkinson's disease. *Neurobiol Dis*. 2022;164:105626. doi:<https://doi.org/10.1016/j.nbd.2022.105626>
42. Borghammer P, Horsager J, Andersen K, et al. Neuropathological evidence of body-first vs. brain-first Lewy body disease. *Neurobiol Dis*. 2021;161:105557. doi:<https://doi.org/10.1016/j.nbd.2021.105557>
43. Xu Z, Hu T, Xu C, et al. Disease progression in proposed brain-first and body-first Parkinson's disease subtypes. *NPJ Parkinsons Dis*. 2024;10(1):111. doi:10.1038/s41531-024-00730-1
44. Postuma RB, Berg D, Stern M, et al. MDS clinical diagnostic criteria for Parkinson's disease. *Movement Disorders*. 2015;30(12):1591-1601. doi:<https://doi.org/10.1002/mds.26424>
45. Berardelli A, Rothwell JC, Thompson PD, Hallett M. Pathophysiology of bradykinesia in Parkinson's disease. *Brain*. 2001;124(11):2131-2146. doi:10.1093/brain/124.11.2131
46. Jankovic J. Parkinson's disease: clinical features and diagnosis. *Journal of Neurology, Neurosurgery & Psychiatry*. 2008;79(4):368. doi:10.1136/jnnp.2007.131045
47. Asci F, Falletti M, Zampogna A, et al. Rigidity in Parkinson's disease: evidence from biomechanical and neurophysiological measures. *Brain*. 2023;146(9):3705-3718. doi:10.1093/brain/awad114
48. Tolosa E, Gaig C, Santamaría J, Compta Y. Diagnosis and the premotor phase of Parkinson disease. *Neurology*. 2009;72(7_supplement_2). doi:10.1212/WNL.0b013e318198db11
49. Williams-Gray CH, Mason SL, Evans JR, et al. The CamPaIGN study of Parkinson's disease: 10-year outlook in an incident population-based cohort. *J Neurol Neurosurg Psychiatry*. 2013;84(11):1258-1264. doi:10.1136/jnnp-2013-305277
50. Fahn S, Elton R, Members of the UPDRS Development Committee. Unified Parkinson's Disease Rating Scale. In: *Recent Developments in Parkinson's Disease*. Vol 2. Macmillan Healthcare Information, Florham Park; 1987:153-164.
51. Goetz CG, Fahn S, Martinez-Martin P, et al. Movement Disorder Society-sponsored revision of the Unified Parkinson's Disease Rating Scale (MDS-UPDRS): Process, format, and clinimetric testing plan. *Movement Disorders*. 2007;22(1):41-47. doi:10.1002/mds.21198
52. Goetz CG, Tilley BC, Shaftman SR, et al. Movement Disorder Society-sponsored revision of the Unified Parkinson's Disease Rating Scale (MDS-UPDRS): Scale presentation and clinimetric testing results. *Movement Disorders*. 2008;23(15):2129-2170. doi:10.1002/mds.22340
53. Hoehn MM, Yahr MD. Parkinsonism: Onset, progression and mortality. *Neurology*. 1967;17(5):427-427. doi:10.1212/WNL.17.5.427
54. Martínez-Martín P, Rodríguez-Blázquez C, Forjaz MJ, de Pedro J. The clinical impression of severity index for Parkinson's disease: International validation study. *Movement Disorders*. 2009;24(2):211-217. doi:10.1002/mds.22320
55. Marinus J, Visser M, Stiggelbout AM, et al. A short scale for the assessment of motor impairments and disabilities in Parkinson's disease: The SPES/SCOPA. *J Neurol Neurosurg Psychiatry*. 2004;75(3):388-395. doi:10.1136/jnnp.2003.017509
56. Brown RG, Gotham AM, Der GJ, Marsden CD. Depression and disability in Parkinson's disease: A follow-up of 132 cases. *Psychol Med*. 1988;18(1):49-55. doi:10.1017/S0033291700001872
57. Bhidayasiri R, Martinez-Martin P. Clinical Assessments in Parkinson's Disease. In: ; 2017:129-182. doi:10.1016/bs.irn.2017.01.001

58. Samson E, Noseworthy MD. A review of diagnostic imaging approaches to assessing Parkinson's disease. *Brain Disord.* 2022;6:100037. doi:<https://doi.org/10.1016/j.dscb.2022.100037>
59. Walter U, Loewenbrück KF, Dodel R, et al. Systematic review-based guideline "Parkinson's disease" of the German Society of Neurology: diagnostic use of transcranial sonography. *J Neurol.* 2024;271(12):7387-7401. doi:10.1007/s00415-024-12502-1
60. Morbelli S, Esposito G, Arbizu J, et al. EANM practice guideline/SNMMI procedure standard for dopaminergic imaging in Parkinsonian syndromes 1.0. *Eur J Nucl Med Mol Imaging.* 2020;47(8):1885-1912. doi:10.1007/s00259-020-04817-8
61. Nobili F, Arbizu J, Bouwman F, et al. European Association of Nuclear Medicine and European Academy of Neurology recommendations for the use of brain 18F-fluorodeoxyglucose positron emission tomography in neurodegenerative cognitive impairment and dementia: Delphi consensus. *Eur J Neurol.* 2018;25(10):1201-1217. doi:<https://doi.org/10.1111/ene.13728>
62. Walker Z, Gandolfo F, Orini S, et al. Clinical utility of FDG PET in Parkinson's disease and atypical parkinsonism associated with dementia. *Eur J Nucl Med Mol Imaging.* 2018;45(9):1534-1545. doi:10.1007/s00259-018-4031-2
63. McKeith IG, Boeve BF, Dickson DW, et al. Diagnosis and management of dementia with Lewy bodies. *Neurology.* 2017;89(1):88-100. doi:10.1212/WNL.0000000000004058
64. Sekiya H, Tipton PW, Kawazoe M, et al. Current Landscape of Clinical Diagnosis in Multiple System Atrophy. *Neurology.* 2024;103(11). doi:10.1212/WNL.00000000000210021
65. Ling H. Clinical Approach to Progressive Supranuclear Palsy. *J Mov Disord.* 2016;9(1):3-13. doi:10.14802/jmd.15060
66. Armstrong MJ, Litvan I, Lang AE, et al. Criteria for the diagnosis of corticobasal degeneration. *Neurology.* 2013;80(5):496-503. doi:10.1212/WNL.0b013e31827f0fd1
67. Shin HW, Chung SJ. Drug-Induced Parkinsonism. *Journal of Clinical Neurology.* 2012;8(1):15. doi:10.3988/jcn.2012.8.1.15
68. Glass PG, Lees AJ, Bacellar A, Zijlmans J, Katzenbach R, Silveira-Moriyama L. The clinical features of pathologically confirmed vascular Parkinsonism. *J Neurol Neurosurg Psychiatry.* 2012;83(10):1027-1029. doi:10.1136/jnnp-2012-302828
69. Bhatia KP, Bain P, Bajaj N, et al. Consensus Statement on the classification of tremors. from the task force on tremor of the International Parkinson and Movement Disorder Society. *Movement Disorders.* 2018;33(1):75-87. doi:10.1002/mds.27121
70. Höglinder G, Bähr M, Becktepe J, et al. Diagnosis and treatment of Parkinson's disease (guideline of the German Society for Neurology). *Neurol Res Pract.* 2024;6(1):30. doi:10.1186/s42466-024-00325-4
71. Seppi K, Ray Chaudhuri K, Coelho M, et al. Update on treatments for nonmotor symptoms of Parkinson's disease—an evidence-based medicine review. *Movement Disorders.* 2019;34(2):180-198. doi:10.1002/mds.27602
72. Hartmann CJ, Fliegen S, Groiss SJ, Wojtecki L, Schnitzler A. An update on best practice of deep brain stimulation in Parkinson's disease. *Ther Adv Neurol Disord.* 2019;12. doi:10.1177/1756286419838096
73. Mahlknecht P, Seppi K, Poewe W. The Concept of Prodromal Parkinson's Disease. *J Parkinsons Dis.* 2015;5(4):681-697. doi:10.3233/JPD-150685
74. Berg D, Postuma RB, Adler CH, et al. MDS research criteria for prodromal Parkinson's disease. *Movement Disorders.* 2015;30(12):1600-1611. doi:10.1002/mds.26431
75. Berg D, Marek K, Ross GW, Poewe W. Defining at-risk populations for Parkinson's disease: Lessons from ongoing studies. *Movement Disorders.* 2012;27(5):656-665. doi:10.1002/mds.24985

76. Ross GW, Abbott RD, Petrovitch H, Tanner CM, White LR. Pre-motor features of Parkinson's disease: the Honolulu-Asia Aging Study experience. *Parkinsonism Relat Disord.* 2012;18:S199-S202. doi:10.1016/S1353-8020(11)70062-1
77. Rota L, Pellegrini C, Benvenuti L, et al. Constipation, deficit in colon contractions and alpha-synuclein inclusions within the colon precede motor abnormalities and neurodegeneration in the central nervous system in a mouse model of alpha-synucleinopathy. *Transl Neurodegener.* 2019;8(1):5. doi:10.1186/s40035-019-0146-z
78. Bassetti CL, Bargiolas P. REM sleep behavior disorder. *Front Neurol Neurosci.* 2017;41:104-116.
79. Iranzo A, Santamaria J, Tolosa E. Idiopathic rapid eye movement sleep behaviour disorder: diagnosis, management, and the need for neuroprotective interventions. *Lancet Neurol.* 2016;15(4):405-419. doi:10.1016/S1474-4422(16)00057-0
80. Haba-Rubio J, Frauscher B, Marques-Vidal P, et al. Prevalence and determinants of rapid eye movement sleep behavior disorder in the general population. *Sleep.* 2018;41(2). doi:10.1093/sleep/zsx197
81. Lee WJ, Baek SH, Im HJ, et al. REM Sleep Behavior Disorder and Its Possible Prodromes in General Population. *Neurology.* 2023;101(23). doi:10.1212/WNL.00000000000207947
82. Ju YE, Larson-Prior L, Duntley S. Changing demographics in REM sleep behavior disorder: Possible effect of autoimmunity and antidepressants. *Sleep Med.* 2011;12(3):278-283. doi:10.1016/j.sleep.2010.07.022
83. Hu MT. REM sleep behavior disorder (RBD). *Neurobiol Dis.* 2020;143:104996. doi:<https://doi.org/10.1016/j.nbd.2020.104996>
84. Wang H, Zhang T, Fan W. Prevalence and impact of rapid eye movement sleep behavior disorder in multiple system atrophy: a systematic review and meta-analysis. *Front Neurol.* 2024;15. doi:10.3389/fneur.2024.1453944
85. Zhang J, Xu CY, Liu J. Meta-analysis on the prevalence of REM sleep behavior disorder symptoms in Parkinson's disease. *BMC Neurol.* 2017;17(1):23. doi:10.1186/s12883-017-0795-4
86. Sateia MJ. International Classification of Sleep Disorders-Third Edition. *Chest.* 2014;146(5):1387-1394. doi:10.1378/chest.14-0970
87. Postuma RB, Lang AE, Gagnon JF, Pelletier A, Montplaisir JY. How does parkinsonism start? Prodromal parkinsonism motor changes in idiopathic REM sleep behaviour disorder. *Brain.* 2012;135(6):1860-1870. doi:10.1093/brain/aws093
88. Bramich S, King A, Kuruvilla M, Naismith SL, Noyce A, Alty J. Isolated REM sleep behaviour disorder: current diagnostic procedures and emerging new technologies. *J Neurol.* 2022;269(9):4684-4695. doi:10.1007/s00415-022-11213-9
89. Nomura T, Inoue Y, Kagimura T, Nakashima K. Clinical significance of REM sleep behavior disorder in Parkinson's disease. *Sleep Med.* 2013;14(2):131-135. doi:10.1016/j.sleep.2012.10.011
90. Liu Y, Lawton MA, Lo C, et al. Longitudinal Changes in Parkinson's Disease Symptoms with and Without Rapid Eye Movement Sleep Behavior Disorder: The Oxford Discovery Cohort Study. *Movement Disorders.* 2021;36(12):2821-2832. doi:10.1002/mds.28763
91. Iranzo A. The REM sleep circuit and how its impairment leads to REM sleep behavior disorder. *Cell Tissue Res.* 2018;373(1):245-266. doi:10.1007/s00441-018-2852-8
92. Stefani A, Antelmi E, Arnaldi D, et al. From mechanisms to future therapy: a synopsis of isolated REM sleep behavior disorder as early synuclein-related disease. *Mol Neurodegener.* 2025;20(1):19. doi:10.1186/s13024-025-00809-0
93. Postuma RB, Iranzo A, Hu M, et al. Risk and predictors of dementia and parkinsonism in idiopathic REM sleep behaviour disorder: a multicentre study. *Brain.* 2019;142(3):744-759. doi:10.1093/brain/awz030
94. Rees RN, Noyce AJ, Schrag AE. Identification of Prodromal Parkinson Disease. *Neurology.* 2024;102(11). doi:10.1212/WNL.00000000000209394

95. Berg D, Crotty GF, Keavney JL, Schwarzschild MA, Simuni T, Tanner C. Path to Parkinson Disease Prevention. *Neurology*. 2022;99(7_Supplement_1):76-83. doi:10.1212/WNL.00000000000200793
96. de Vries NM, Darweesh SKL, Bloem BR. Citius, Fortius, Altius—Understanding Which Components Drive Exercise Benefits in Parkinson Disease. *JAMA Neurol*. 2021;78(12):1443-1445. doi:10.1001/jamaneurol.2021.3744
97. Davis KM, Ryan JL, Aaron VD, Sims JB. PET and SPECT Imaging of the Brain: History, Technical Considerations, Applications, and Radiotracers. *Seminars in Ultrasound, CT and MRI*. 2020;41(6):521-529. doi:<https://doi.org/10.1053/j.sult.2020.08.006>
98. Crișan G, Moldovean-Cioroianu NS, Timaru DG, Andrieș G, Căinap C, Chiș V. Radiopharmaceuticals for PET and SPECT Imaging: A Literature Review over the Last Decade. *Int J Mol Sci*. 2022;23(9):5023. doi:10.3390/ijms23095023
99. Cherry SR. In vivo molecular and genomic imaging: new challenges for imaging physics. *Phys Med Biol*. 2004;49(3):R13-R48. doi:10.1088/0031-9155/49/3/R01
100. Rong J, Haider A, Jeppesen TE, Josephson L, Liang SH. Radiochemistry for positron emission tomography. *Nat Commun*. 2023;14(1):3257. doi:10.1038/s41467-023-36377-4
101. Phelps ME. PET: the merging of biology and imaging into molecular imaging. *J Nucl Med*. 2000;41(4):661-681.
102. Jansen FP, Vanderheyden JL. The future of SPECT in a time of PET. *Nucl Med Biol*. 2007;34(7):733-735. doi:10.1016/j.nucmedbio.2007.06.013
103. Rahmim A, Zaidi H. PET versus SPECT: strengths, limitations and challenges. *Nucl Med Commun*. 2008;29(3):193-207. doi:10.1097/MNM.0b013e3282f3a515
104. SEIDLIN SM. RADIOACTIVE IODINE THERAPY. *J Am Med Assoc*. 1946;132(14):838. doi:10.1001/jama.1946.02870490016004
105. Burkett BJ, Bartlett DJ, McGarrah PW, et al. A Review of Theranostics: Perspectives on Emerging Approaches and Clinical Advancements. *Radiol Imaging Cancer*. 2023;5(4). doi:10.1148/rycan.220157
106. Eberlein U, Cremonesi M, Lassmann M. Individualized Dosimetry for Theranostics: Necessary, Nice to Have, or Counterproductive? *Journal of Nuclear Medicine*. 2017;58(Supplement 2):97S-103S. doi:10.2967/jnumed.116.186841
107. Minoshima S, Cross D, Thientunyakit T, Foster NL, Drzezga A. 18F-FDG PET Imaging in Neurodegenerative Dementing Disorders: Insights into Subtype Classification, Emerging Disease Categories, and Mixed Dementia with Copathologies. *Journal of Nuclear Medicine*. 2022;63(Supplement 1):2S-12S. doi:10.2967/jnumed.121.263194
108. Watts ME, Pocock R, Claudianos C. Brain Energy and Oxygen Metabolism: Emerging Role in Normal Function and Disease. *Front Mol Neurosci*. 2018;11. doi:10.3389/fnmol.2018.00216
109. Sokoloff L. Function-related Changes in Energy Metabolism in the Nervous System: Localization and Mechanisms. *Keio J Med*. 1993;42(3):95-103. doi:10.2302/kjm.42.95
110. Magistretti PJ, Pellerin L. Cellular Bases of Brain Energy Metabolism and Their Relevance to Functional Brain Imaging: Evidence for a Prominent Role of Astrocytes. *Cerebral Cortex*. 1996;6(1):50-61. doi:10.1093/cercor/6.1.50
111. Zimmer ER, Parent MJ, Souza DG, et al. [18F]FDG PET signal is driven by astroglial glutamate transport. *Nat Neurosci*. 2017;20(3):393-395. doi:10.1038/nn.4492
112. Xiang X, Wind K, Wiedemann T, et al. Microglial activation states drive glucose uptake and FDG-PET alterations in neurodegenerative diseases. *Sci Transl Med*. 2021;13(615). doi:10.1126/scitranslmed.abe5640

113. Maldjian JA, Whitlow CT. Whither the Hippocampus? FDG-PET Hippocampal Hypometabolism in Alzheimer Disease Revisited. *American Journal of Neuroradiology*. 2012;33(10):1975-1982. doi:10.3174/ajnr.A3113
114. Frings L, Blazhenets G, Brumberg J, Rau A, Urbach H, Meyer PT. Deformation-based morphometry applied to FDG PET data reveals hippocampal atrophy in Alzheimer's disease. *Sci Rep*. 2024;14(1):20030. doi:10.1038/s41598-024-70380-z
115. Guedj E, Varrone A, Boellaard R, et al. EANM procedure guidelines for brain PET imaging using [18F]FDG, version 3. *Eur J Nucl Med Mol Imaging*. 2022;49(2):632-651. doi:10.1007/s00259-021-05603-w
116. Arbizu J, Morbelli S, Minoshima S, et al. SNMMI Procedure Standard/EANM Practice Guideline for Brain [¹⁸F]FDG PET Imaging, Version 2.0. *Journal of Nuclear Medicine*. Published online October 17, 2024:jnumed.124.268754. doi:10.2967/jnumed.124.268754
117. Thie JA. Understanding the Standardized Uptake Value, Its Methods, and Implications for Usage. *Journal of Nuclear Medicine*. 2004;45(9):1431. <http://jnm.snmjournals.org/content/45/9/1431.abstract>
118. López-González FJ, Silva-Rodríguez J, Paredes-Pacheco J, et al. Intensity normalization methods in brain FDG-PET quantification. *Neuroimage*. 2020;222:117229. doi:10.1016/j.neuroimage.2020.117229
119. Nobili F, Festari C, Altomare D, et al. Automated assessment of FDG-PET for differential diagnosis in patients with neurodegenerative disorders. *Eur J Nucl Med Mol Imaging*. 2018;45(9):1557-1566. doi:10.1007/s00259-018-4030-3
120. Caminiti SP, Sala A, Presotto L, et al. Validation of FDG-PET datasets of normal controls for the extraction of SPM-based brain metabolism maps. *Eur J Nucl Med Mol Imaging*. 2021;48(8):2486-2499. doi:10.1007/s00259-020-05175-1
121. Alexander GE, Moeller JR. Application of the scaled subprofile model to functional imaging in neuropsychiatric disorders: A principal component approach to modeling brain function in disease. *Hum Brain Mapp*. 1994;2(1-2):79-94. doi:<https://doi.org/10.1002/hbm.460020108>
122. Moeller J. R, Strother S. C. A Regional Covariance Approach to the Analysis of Functional Patterns in Positron Emission Tomographic Data. *Journal of Cerebral Blood Flow & Metabolism*. 1991;11(1_suppl):A121-A135. doi:10.1038/jcbfm.1991.47
123. Spetsieris PG, Eidelberg D. Scaled subprofile modeling of resting state imaging data in Parkinson's disease: Methodological issues. *Neuroimage*. 2011;54(4):2899-2914. doi:<https://doi.org/10.1016/j.neuroimage.2010.10.025>
124. Eidelberg D. Metabolic brain networks in neurodegenerative disorders: a functional imaging approach. *Trends Neurosci*. 2009;32(10):548-557. doi:10.1016/j.tins.2009.06.003
125. Matthews DC, Lerman H, Lukic A, et al. FDG PET Parkinson's disease-related pattern as a biomarker for clinical trials in early stage disease. *Neuroimage Clin*. 2018;20:572-579. doi:<https://doi.org/10.1016/j.nicl.2018.08.006>
126. Wu P, Wang J, Peng S, et al. Metabolic brain network in the Chinese patients with Parkinson's disease based on ¹⁸F-FDG PET imaging. *Parkinsonism Relat Disord*. 2013;19(6):622-627. doi:10.1016/j.parkreldis.2013.02.013
127. Meles SK, Pagani M, Arnaldi D, et al. The Alzheimer's disease metabolic brain pattern in mild cognitive impairment. *Journal of Cerebral Blood Flow & Metabolism*. 2017;37(12):3643-3648. doi:10.1177/0271678X17732508
128. Buchert R, Wegner F, Huppertz H, et al. Automatic covariance pattern analysis outperforms visual reading of ¹⁸F-fluorodeoxyglucose-positron emission tomography (<sc>FDG-PET</sc>) in variant progressive supranuclear palsy. *Movement Disorders*. 2023;38(10):1901-1913. doi:10.1002/mds.29581
129. Thobois S, Jahanshahi M, Pinto S, Frackowiak R, Limousin-Dowsey P. PET and SPECT functional imaging studies in Parkinsonian syndromes: from the lesion to its consequences. *Neuroimage*. 2004;23(1):1-16. doi:<https://doi.org/10.1016/j.neuroimage.2004.04.039>

130. Xu H, Yang F. The interplay of dopamine metabolism abnormalities and mitochondrial defects in the pathogenesis of schizophrenia. *Transl Psychiatry*. 2022;12(1):464. doi:10.1038/s41398-022-02233-0
131. Booij J, van Wieringen JP, van de Giessen E, Knol RJJ, Finnema SJ. PET and SPECT Imaging of the Central Dopamine System in Humans. In: Dierckx RAJO, Otte A, de Vries EFJ, van Waarde A, Lammertsma AA, eds. *PET and SPECT of Neurobiological Systems*. Springer International Publishing; 2021:295-318. doi:10.1007/978-3-030-53176-8_11
132. Tian M, Zuo C, Cahid Civelek A, et al. International consensus on clinical use of presynaptic dopaminergic positron emission tomography imaging in parkinsonism. *Eur J Nucl Med Mol Imaging*. 2024;51(2):434-442. doi:10.1007/s00259-023-06403-0
133. Booij J, Dubroff J, Pryma D, et al. Diagnostic Performance of the Visual Reading of [123I]-Ioflupane SPECT Images With or Without Quantification in Patients With Movement Disorders or Dementia. *Journal of Nuclear Medicine*. 2017;58(11):1821. doi:10.2967/jnumed.116.189266
134. Tossici-Bolt L, Dickson JC, Sera T, et al. [(123)I]FP-CIT ENC-DAT normal database: the impact of the reconstruction and quantification methods. *EJNMMI Phys*. 2017;4(1):8. doi:10.1186/s40658-017-0175-6
135. Varrone A, Dickson JC, Tossici-Bolt L, et al. European multicentre database of healthy controls for [123I]FP-CIT SPECT (ENC-DAT): age-related effects, gender differences and evaluation of different methods of analysis. *Eur J Nucl Med Mol Imaging*. 2013;40(2):213-227. doi:10.1007/s00259-012-2276-8
136. Pan W, Song Y, Kwak S, Yoshida S, Yamamoto Y. Quantitative Evaluation of the Use of Actigraphy for Neurological and Psychiatric Disorders. *Behavioural Neurology*. 2014;2014:1-6. doi:10.1155/2014/897282
137. Liguori C, Mombelli S, Fernandes M, et al. The evolving role of quantitative actigraphy in clinical sleep medicine. *Sleep Med Rev*. 2023;68:101762. doi:<https://doi.org/10.1016/j.smrv.2023.101762>
138. Benson K, Friedman L, Noda A, Wicks D, Wakabayashi E, Yesavage J. The Measurement of Sleep by Actigraphy: Direct Comparison of 2 Commercially Available Actigraphs in a Nonclinical Population. *Sleep*. 2004;27(5):986-989. doi:10.1093/sleep/27.5.986
139. Rupp TL, Balkin TJ. Comparison of Motionlogger Watch and Actiwatch actigraphs to polysomnography for sleep/wake estimation in healthy young adults. *Behav Res Methods*. 2011;43(4):1152-1160. doi:10.3758/s13428-011-0098-4
140. Cole RJ, Kripke DF, Gruen W, Mullaney DJ, Gillin JC. Automatic Sleep/Wake Identification From Wrist Activity. *Sleep*. 1992;15(5):461-469. doi:10.1093/sleep/15.5.461
141. Sadeh A, Sharkey M, Carskadon MA. Activity-Based Sleep-Wake Identification: An Empirical Test of Methodological Issues. *Sleep*. 1994;17(3):201-207. doi:10.1093/sleep/17.3.201
142. Patterson MR, Nunes AAS, Gerstel D, et al. 40 years of actigraphy in sleep medicine and current state of the art algorithms. *NPJ Digit Med*. 2023;6(1):51. doi:10.1038/s41746-023-00802-1
143. Walia HK, Mehra R. Chapter 24 - Practical aspects of actigraphy and approaches in clinical and research domains. In: Levin KH, Chauvel P, eds. *Handbook of Clinical Neurology*. Vol 160. Elsevier; 2019:371-379. doi:<https://doi.org/10.1016/B978-0-444-64032-1.00024-2>
144. TSM, S MC, Joseph C, et al. Use of Actigraphy for the Evaluation of Sleep Disorders and Circadian Rhythm Sleep-Wake Disorders: An American Academy of Sleep Medicine Systematic Review, Meta-Analysis, and GRADE Assessment. *Journal of Clinical Sleep Medicine*. 2025;14(07):1209-1230. doi:10.5664/jcsm.7228
145. Marino M, Li Y, Rueschman MN, et al. Measuring Sleep: Accuracy, Sensitivity, and Specificity of Wrist Actigraphy Compared to Polysomnography. *Sleep*. 2013;36(11):1747-1755. doi:10.5665/sleep.3142
146. Montserrat SOM, D EJ, K MM, Daniel A. Home Is Where Sleep Is: An Ecological Approach to Test the Validity of Actigraphy for the Assessment of Insomnia. *Journal of Clinical Sleep Medicine*. 2010;06(01):21-29. doi:10.5664/jcsm.27706

147. Madrid-Navarro CJ, Puertas Cuesta FJ, Escamilla-Sevilla F, et al. Validation of a Device for the Ambulatory Monitoring of Sleep Patterns: A Pilot Study on Parkinson's Disease. *Front Neurol.* 2019;10. doi:10.3389/fneur.2019.00356
148. Ancoli-Israel S, Cole R, Alessi C, Chambers M, Moorcroft W, Pollak CP. The Role of Actigraphy in the Study of Sleep and Circadian Rhythms. *Sleep.* 2003;26(3):342-392. doi:10.1093/sleep/26.3.342
149. Raschellà F, Scafà S, Puiatti A, Martin Moraud E, Ratti PL. Actigraphy Enables Home Screening of Rapid Eye Movement Behavior Disorder in Parkinson's Disease. *Ann Neurol.* 2023;93(2):317-329. doi:<https://doi.org/10.1002/ana.26517>
150. Diem SJ, Blackwell TL, Stone KL, et al. Measures of Sleep–Wake Patterns and Risk of Mild Cognitive Impairment or Dementia in Older Women. *The American Journal of Geriatric Psychiatry.* 2016;24(3):248-258. doi:<https://doi.org/10.1016/j.jagp.2015.12.002>
151. Pan W, Kwak S, Li F, et al. Actigraphy monitoring of symptoms in patients with Parkinson's disease. *Physiol Behav.* 2013;119:156-160. doi:10.1016/j.physbeh.2013.05.044
152. Obayashi K, Saeki K, Yamagami Y, Kurumatani N, Sugie K, Kataoka H. Circadian activity rhythm in Parkinson's disease: findings from the PHASE study. *Sleep Med.* 2021;85:8-14. doi:<https://doi.org/10.1016/j.sleep.2021.06.023>
153. Leng Y, Blackwell T, Cawthon PM, Ancoli-Israel S, Stone KL, Yaffe K. Association of Circadian Abnormalities in Older Adults With an Increased Risk of Developing Parkinson Disease. *JAMA Neurol.* 2020;77(10):1270. doi:10.1001/jamaneurol.2020.1623
154. Baumann-Vogel H, Imbach LL, Sürkü O, et al. The Impact of Subthalamic Deep Brain Stimulation on Sleep–Wake Behavior: A Prospective Electrophysiological Study in 50 Parkinson Patients. *Sleep.* 2017;40(5):zsx033. doi:10.1093/sleep/zsx033
155. Dowling GA, Mastick J, Colling E, Carter JH, Singer CM, Aminoff MJ. Melatonin for sleep disturbances in Parkinson's disease. *Sleep Med.* 2005;6(5):459-466. doi:<https://doi.org/10.1016/j.sleep.2005.04.004>
156. Santiago PL, Malco R, Daniel P. C, and Merello M. Activity—Rest Rhythm Abnormalities in Parkinson's Disease Patients are Related to Dopaminergic Therapy. *International Journal of Neuroscience.* 2010;120(1):11-16. doi:10.3109/00207450903326179
157. Brink-Kjaer A, Gupta N, Marin E, et al. Ambulatory Detection of Isolated Rapid-Eye-Movement Sleep Behavior Disorder Combining Actigraphy and Questionnaire. *Movement Disorders.* 2023;38(1):82-91. doi:10.1002/mds.29249
158. Filardi M, Stefanini A, Holzknecht E, Pizza F, Plazzi G, Högl B. Objective rest–activity cycle analysis by actigraphy identifies isolated rapid eye movement sleep behavior disorder. *Eur J Neurol.* 2020;27(10):1848-1855. doi:10.1111/ene.14386
159. Louter M, Arends JB, Bloem BR, Overeem S. Actigraphy as a diagnostic aid for REM sleep behavior disorder in Parkinson's disease. *BMC Neurol.* 2014;14(1):76. doi:10.1186/1471-2377-14-76
160. Feng H, Chen L, Liu Y, et al. Rest-Activity Pattern Alterations in Idiopathic <scp>REM</scp> Sleep Behavior Disorder. *Ann Neurol.* 2020;88(4):817-829. doi:10.1002/ana.25853
161. Lopes L, Lopez-Montes A, Chen Y, et al. The Evolution of Artificial Intelligence in Nuclear Medicine. *Semin Nucl Med.* Published online 2025. doi:<https://doi.org/10.1053/j.semnuclmed.2025.01.006>
162. Kline R. Cybernetics, Automata Studies, and the Dartmouth Conference on Artificial Intelligence. *IEEE Annals of the History of Computing.* 2011;33(4):5-16. doi:10.1109/MAHC.2010.44
163. Kippenhan JS, Barker WW, Pascal S, Nagel J, Duara R. Evaluation of a neural-network classifier for PET scans of normal and Alzheimer's disease subjects. *J Nucl Med.* 1992;33(8):1459-1467.
164. Silver DL, Hurwitz GA. The predictive and explanatory power of inductive decision trees: a comparison with artificial neural network learning as applied to the noninvasive diagnosis of coronary artery disease. *J Investig Med.* 1997;45(2):99-108.

165. Jayasurya K, Fung G, Yu S, et al. Comparison of Bayesian network and support vector machine models for two-year survival prediction in lung cancer patients treated with radiotherapy. *Med Phys*. 2010;37(4):1401-1407. doi:10.1118/1.3352709
166. Sampedro F, Escalera S, Domenech A, Carrio I. A computational framework for cancer response assessment based on oncological PET-CT scans. *Comput Biol Med*. 2014;55:92-99. doi:10.1016/j.combiomed.2014.10.014
167. Arsanjani R, Dey D, Khachatrian T, et al. Prediction of revascularization after myocardial perfusion SPECT by machine learning in a large population. *Journal of Nuclear Cardiology*. 2015;22(5):877-884. doi:10.1007/s12350-014-0027-x
168. Cabral C, Morgado PM, Campos Costa D, Silveira M. Predicting conversion from MCI to AD with FDG-PET brain images at different prodromal stages. *Comput Biol Med*. 2015;58:101-109. doi:10.1016/j.combiomed.2015.01.003
169. Šajn L, Kukar M, Kononenko I, Milčinski M. Automatic Segmentation of Whole-Body Bone Scintigrams as a Preprocessing Step for Computer Assisted Diagnostics. In: ; 2005:363-372. doi:10.1007/11527770_49
170. Sharif MS, Abbad M, Amira A, Zaidi H. Artificial Neural Network-Based System for PET Volume Segmentation. *Int J Biomed Imaging*. 2010;2010(1). doi:10.1155/2010/105610
171. Ronneberger O, Fischer P, Brox T. U-Net: Convolutional Networks for Biomedical Image Segmentation. Published online May 18, 2015.
172. Isensee F, Jaeger PF, Kohl SAA, Petersen J, Maier-Hein KH. nnU-Net: a self-configuring method for deep learning-based biomedical image segmentation. *Nat Methods*. 2021;18(2):203-211. doi:10.1038/s41592-020-01008-z
173. Wang G, Qi J. PET Image Reconstruction Using Kernel Method. *IEEE Trans Med Imaging*. 2015;34(1):61-71. doi:10.1109/TMI.2014.2343916
174. Hofmann M, Bezrukov I, Mantlik F, et al. MRI-Based Attenuation Correction for Whole-Body PET/MRI: Quantitative Evaluation of Segmentation- and Atlas-Based Methods. *Journal of Nuclear Medicine*. 2011;52(9):1392-1399. doi:10.2967/jnumed.110.078949
175. Han X. MR-based synthetic CT generation using a deep convolutional neural network method. *Med Phys*. 2017;44(4):1408-1419. doi:10.1002/mp.12155
176. Kaplan S, Zhu YM. Full-Dose PET Image Estimation from Low-Dose PET Image Using Deep Learning: a Pilot Study. *J Digit Imaging*. 2019;32(5):773-778. doi:10.1007/s10278-018-0150-3
177. Xue S, Gafita A, Zhao Y, et al. First Voxel-wise Prediction of Post-therapy Dosimetry for 177 Lu-PSMA I&T Therapy. In: ; 2020. doi:10.1055/s-0040-1708141
178. Vaswani A, Shazeer N, Parmar N, et al. Attention Is All You Need. Published online June 12, 2017.
179. Dosovitskiy A, Beyer L, Kolesnikov A, et al. An Image is Worth 16x16 Words: Transformers for Image Recognition at Scale. Published online October 22, 2020.
180. Petit O, Thome N, Rambour C, Soler L. U-Net Transformer: Self and Cross Attention for Medical Image Segmentation. Published online March 10, 2021.
181. Kippenhan JS, Barker WW, Pascal S, Nagel J, Duara R. Evaluation of a Neural-Network Classifier for PET Scans of Normal and Alzheimer's Disease Subjects. *Journal of Nuclear Medicine*. 1992;33(8):1459-1467. Accessed December 12, 2024. <https://jnm.snmjournals.org/content/33/8/1459>
182. Hinrichs C, Singh V, Mukherjee L, Xu G, Chung MK, Johnson SC. Spatially augmented LPboosting for AD classification with evaluations on the ADNI dataset. *Neuroimage*. 2009;48(1):138-149. doi:10.1016/j.neuroimage.2009.05.056
183. Kohannim O, Hua X, Hibar DP, et al. Boosting power for clinical trials using classifiers based on multiple biomarkers. *Neurobiol Aging*. 2010;31(8):1429-1442. doi:10.1016/j.neurobiolaging.2010.04.022

184. Gray KR, Wolz R, Heckemann RA, Aljabar P, Hammers A, Rueckert D. Multi-region analysis of longitudinal FDG-PET for the classification of Alzheimer's disease. *Neuroimage*. 2012;60(1):221-229. doi:10.1016/j.neuroimage.2011.12.071
185. Padilla P, Lopez M, Gorri JM, Ramirez J, Salas-Gonzalez D, Alvarez I. NMF-SVM Based CAD Tool Applied to Functional Brain Images for the Diagnosis of Alzheimer's Disease. *IEEE Trans Med Imaging*. 2012;31(2):207-216. doi:10.1109/TMI.2011.2167628
186. Vandenbergh R, Nelissen N, Salmon E, et al. Binary classification of 18F-flutemetamol PET using machine learning: Comparison with visual reads and structural MRI. *Neuroimage*. 2013;64:517-525. doi:10.1016/j.neuroimage.2012.09.015
187. Segovia F, Bastin C, Salmon E, Górriz JM, Ramírez J, Phillips C. Combining PET Images and Neuropsychological Test Data for Automatic Diagnosis of Alzheimer's Disease. *PLoS One*. 2014;9(2):e88687. doi:10.1371/journal.pone.0088687
188. Suk HI, Shen D. Deep Learning-Based Feature Representation for AD/MCI Classification. Published online 2013:583-590. doi:10.1007/978-3-642-40763-5_72
189. Huertas-Fernández I, García-Gómez FJ, García-Solís D, et al. Machine learning models for the differential diagnosis of vascular parkinsonism and Parkinson's disease using [123I]FP-CIT SPECT. *Eur J Nucl Med Mol Imaging*. 2015;42(1):112-119. doi:10.1007/s00259-014-2882-8
190. Oliveira FPM, Faria DB, Costa DC, Castelo-Branco M, Tavares JMRS. Extraction, selection and comparison of features for an effective automated computer-aided diagnosis of Parkinson's disease based on [123I]FP-CIT SPECT images. *Eur J Nucl Med Mol Imaging*. 2018;45(6):1052-1062. doi:10.1007/s00259-017-3918-7
191. Comte V, Schmutz H, Chardin D, Orlhac F, Darcourt J, Humbert O. Development and validation of a radiomic model for the diagnosis of dopaminergic denervation on [18F]FDOPA PET/CT. *Eur J Nucl Med Mol Imaging*. 2022;49(11):3787-3796. doi:10.1007/s00259-022-05816-7
192. Wenzel M, Milletari F, Krüger J, et al. Automatic classification of dopamine transporter SPECT: deep convolutional neural networks can be trained to be robust with respect to variable image characteristics. *Eur J Nucl Med Mol Imaging*. 2019;46(13):2800-2811. doi:10.1007/s00259-019-04502-5
193. Choi H, Kim YK, Yoon EJ, Lee JY, Lee DS. Cognitive signature of brain FDG PET based on deep learning: domain transfer from Alzheimer's disease to Parkinson's disease. *Eur J Nucl Med Mol Imaging*. 2020;47(2):403-412. doi:10.1007/s00259-019-04538-7
194. Wu P, Zhao Y, Wu J, et al. Differential diagnosis of parkinsonism based on deep metabolic imaging indices. *Journal of Nuclear Medicine*. Published online March 3, 2022:jnmed.121.263029. doi:10.2967/jnmed.121.263029
195. Zhao Y, Wu P, Wu J, et al. Decoding the dopamine transporter imaging for the differential diagnosis of parkinsonism using deep learning. *Eur J Nucl Med Mol Imaging*. 2022;49(8):2798-2811. doi:10.1007/s00259-022-05804-x
196. Etminani K, Soliman A, Davidsson A, et al. A 3D deep learning model to predict the diagnosis of dementia with Lewy bodies, Alzheimer's disease, and mild cognitive impairment using brain 18F-FDG PET. *Eur J Nucl Med Mol Imaging*. 2022;49(2):563-584. doi:10.1007/s00259-021-05483-0
197. Kaur A, Mittal M, Bhatti JS, Thareja S, Singh S. A systematic literature review on the significance of deep learning and machine learning in predicting Alzheimer's disease. *Artif Intell Med*. 2024;154:102928. doi:10.1016/j.artmed.2024.102928
198. Dzialas V, Doering E, Eich H, et al. Houston, We Have <scp>AI</scp> Problem! Quality Issues with Neuroimaging-Based Artificial Intelligence in Parkinson's Disease: A Systematic Review. *Movement Disorders*. Published online September 5, 2024. doi:10.1002/mds.30002
199. Hong J, Lu J, Liu F, et al. Uncovering distinct progression patterns of tau deposition in progressive supranuclear palsy using [18F]Florozolotau PET imaging and subtype/stage inference algorithm. *EBioMedicine*. 2023;97:104835. doi:10.1016/j.ebiom.2023.104835

200. Lu J, Clement C, Hong J, et al. Improved interpretation of 18F-florzolotau PET in progressive supranuclear palsy using a normalization-free deep-learning classifier. *iScience*. 2023;26(8):107426. doi:10.1016/j.isci.2023.107426
201. Matsubara K, Ibaraki M, Shinohara Y, Takahashi N, Toyoshima H, Kinoshita T. Prediction of an oxygen extraction fraction map by convolutional neural network: validation of input data among MR and PET images. *Int J Comput Assist Radiol Surg*. 2021;16(11):1865-1874. doi:10.1007/s11548-021-02356-7
202. Kerr WT, Nguyen ST, Cho AY, et al. Computer-Aided Diagnosis and Localization of Lateralized Temporal Lobe Epilepsy Using Interictal FDG-PET. *Front Neurol*. 2013;4. doi:10.3389/fneur.2013.00031
203. Shih YC, Lee TH, Yu HY, et al. Machine Learning Quantitative Analysis of FDG PET Images of Medial Temporal Lobe Epilepsy Patients. *Clin Nucl Med*. 2022;47(4):287-293. doi:10.1097/RNU.00000000000004072
204. Liao K, Wu H, Jiang Y, et al. Machine learning techniques based on 18F-FDG PET radiomics features of temporal regions for the classification of temporal lobe epilepsy patients from healthy controls. *Front Neurol*. 2024;15. doi:10.3389/fneur.2024.1377538
205. Vedaei F, Mashhadi N, Alizadeh M, et al. Deep learning-based multimodality classification of chronic mild traumatic brain injury using resting-state functional MRI and PET imaging. *Front Neurosci*. 2024;17. doi:10.3389/fnins.2023.1333725
206. Kim JY, Oh D, Sung K, et al. Visual interpretation of [18F]Florbetaben PET supported by deep learning-based estimation of amyloid burden. *Eur J Nucl Med Mol Imaging*. 2021;48(4):1116-1123. doi:10.1007/s00259-020-05044-x
207. Trevenen ML, Turlach BA, Eastwood PR, Straker LM, Murray K. Using hidden Markov models with raw, triaxial wrist accelerometry data to determine sleep stages. *Aust N Z J Stat*. 2019;61(3):273-298. doi:<https://doi.org/10.1111/anzs.12270>
208. Sundararajan K, Georgievska S, te Lindert BHW, et al. Sleep classification from wrist-worn accelerometer data using random forests. *Sci Rep*. 2021;11(1):24. doi:10.1038/s41598-020-79217-x
209. Walch O, Huang Y, Forger D, Goldstein C. Sleep stage prediction with raw acceleration and photoplethysmography heart rate data derived from a consumer wearable device. *Sleep*. 2019;42(12). doi:10.1093/sleep/zsz180
210. Boe AJ, McGee Koch LL, O'Brien MK, et al. Automating sleep stage classification using wireless, wearable sensors. *NPJ Digit Med*. 2019;2(1):131. doi:10.1038/s41746-019-0210-1
211. Song TA, Chowdhury SR, Malekzadeh M, et al. AI-Driven sleep staging from actigraphy and heart rate. *PLoS One*. 2023;18(5):e0285703. doi:10.1371/journal.pone.0285703
212. Yuan H, Plekhanova T, Walmsley R, et al. Self-supervised learning of accelerometer data provides new insights for sleep and its association with mortality. *NPJ Digit Med*. 2024;7(1):86. doi:10.1038/s41746-024-01065-0
213. Kusmakar S, Karmakar C, Zhu Y, et al. A machine learning model for multi-night actigraphic detection of chronic insomnia: development and validation of a pre-screening tool. *R Soc Open Sci*. 2021;8(6):202264. doi:10.1098/rsos.202264
214. Cole BT, Roy SH, Nawab SH. Detecting freezing-of-gait during unscripted and unconstrained activity. In: *2011 Annual International Conference of the IEEE Engineering in Medicine and Biology Society*. IEEE; 2011:5649-5652. doi:10.1109/IEMBS.2011.6091367
215. Bikas T, Iakovakis D, Hadjidimitriou S, Charisis V, Hadjileontiadis LJ. DeepFoG: An IMU-Based Detection of Freezing of Gait Episodes in Parkinson's Disease Patients via Deep Learning. *Front Robot AI*. 2021;8. <https://www.frontiersin.org/journals/robotics-and-ai/articles/10.3389/frobt.2021.537384>

216. Moon S, Song HJ, Sharma VD, et al. Classification of Parkinson's disease and essential tremor based on balance and gait characteristics from wearable motion sensors via machine learning techniques: a data-driven approach. *J Neuroeng Rehabil.* 2020;17(1):125. doi:10.1186/s12984-020-00756-5
217. Hammerla N, Fisher J, Andras P, Rochester L, Walker R, Ploetz T. PD Disease State Assessment in Naturalistic Environments Using Deep Learning. *Proceedings of the AAAI Conference on Artificial Intelligence.* 2015;29(1). doi:10.1609/aaai.v29i1.9484
218. Tong L, He J, Peng L. CNN-Based PD Hand Tremor Detection Using Inertial Sensors. *IEEE Sens Lett.* 2021;5(7):1-4. doi:10.1109/LSENS.2021.3074958
219. Kim HB, Lee WW, Kim A, et al. Wrist sensor-based tremor severity quantification in Parkinson's disease using convolutional neural network. *Comput Biol Med.* 2018;95:140-146. doi:<https://doi.org/10.1016/j.combiomed.2018.02.007>
220. Eskofier BM, Lee SI, Daneault JF, et al. Recent machine learning advancements in sensor-based mobility analysis: Deep learning for Parkinson's disease assessment. In: *2016 38th Annual International Conference of the IEEE Engineering in Medicine and Biology Society (EMBC).* ; 2016:655-658. doi:10.1109/EMBC.2016.7590787
221. Pfister FMJ, Um TT, Pichler DC, et al. High-Resolution Motor State Detection in Parkinson's Disease Using Convolutional Neural Networks. *Sci Rep.* 2020;10(1):5860. doi:10.1038/s41598-020-61789-3
222. Lecun Y, Jackel LD, Bottou L, et al. Learning algorithms for classification: A comparison on handwritten digit recognition. In: Oh JH, Kwon C, Cho S, eds. *Neural Networks.* World Scientific; 1995:261-276.
223. He K, Zhang X, Ren S, Sun J. Deep Residual Learning for Image Recognition. In: *2016 IEEE Conference on Computer Vision and Pattern Recognition (CVPR).* IEEE; 2016:770-778. doi:10.1109/CVPR.2016.90
224. Vaswani A, Shazeer N, Parmar N, et al. Attention Is All You Need. *ArXiv preprint.* Published online June 12, 2017. doi:<https://doi.org/10.48550/arXiv.1706.03762>
225. Dosovitskiy A, Beyer L, Kolesnikov A, et al. An Image is Worth 16x16 Words: Transformers for Image Recognition at Scale. Published online October 22, 2020.
226. Yuan H, Chan S, Creagh AP, et al. Self-supervised learning for human activity recognition using 700,000 person-days of wearable data. *NPJ Digit Med.* 2024;7(1):91. doi:10.1038/s41746-024-01062-3
227. Ruan FY, Zhang A, Oh JY, Jin S, Jacobson NC. AI Foundation Models for Wearable Movement Data in Mental Health Research. *arXiv preprint.* Published online 2024. doi:10.48550/arXiv.2411.15240
228. Wan Z, Li M, Liu S, Huang J, Tan H, Duan W. EEGformer: A transformer-based brain activity classification method using EEG signal. *Front Neurosci.* 2023;17. doi:10.3389/fnins.2023.1148855
229. Raianan MAK, Mukta MSH, Fatema K, et al. A Review on Large Language Models: Architectures, Applications, Taxonomies, Open Issues and Challenges. *IEEE Access.* 2024;12:26839-26874. doi:10.1109/ACCESS.2024.3365742
230. Goodfellow IJ, Pouget-Abadie J, Mirza M, et al. Generative Adversarial Networks. Published online June 10, 2014. <http://arxiv.org/abs/1406.2661>
231. Ho J, Jain A, Abbeel P. Denoising Diffusion Probabilistic Models. Published online June 19, 2020.
232. Yi X, Walia E, Babyn P. Generative adversarial network in medical imaging: A review. *Med Image Anal.* 2019;58:101552. doi:<https://doi.org/10.1016/j.media.2019.101552>
233. Arjovsky M, Chintala S, Bottou L. Wasserstein Generative Adversarial Networks. In: Precup D, Teh YW, eds. *Proceedings of the 34th International Conference on Machine Learning.* Vol 70. Proceedings of Machine Learning Research. PMLR; 2017:214-223. <https://proceedings.mlr.press/v70/arjovsky17a.html>
234. Zhu JY, Park T, Isola P, Efros AA. Unpaired Image-to-Image Translation Using Cycle-Consistent Adversarial Networks. In: *Proceedings of the IEEE International Conference on Computer Vision.* Vol 2017-October. ; 2017. doi:10.1109/ICCV.2017.244

235. Karn A, Kumar S, Kushwaha SK, Katarya R. Image Synthesis Using GANs and Diffusion Models. In: *2023 IEEE International Conference on Contemporary Computing and Communications (InC4)*. Vol 1. ; 2023:1-6. doi:10.1109/InC457730.2023.10263208
236. Kazerouni A, Aghdam EK, Heidari M, et al. Diffusion models in medical imaging: A comprehensive survey. *Med Image Anal.* 2023;88:102846. doi:<https://doi.org/10.1016/j.media.2023.102846>
237. Kaplan J, McCandlish S, Henighan T, et al. Scaling Laws for Neural Language Models. Published online January 22, 2020.
238. OpenAI, Achiam J, Adler S, et al. GPT-4 Technical Report. Published online March 15, 2023.
239. Kirillov A, Mintun E, Ravi N, et al. Segment Anything. Published online April 5, 2023.
240. Krones F, Marikkar U, Parsons G, Szmul A, Mahdi A. Review of multimodal machine learning approaches in healthcare. *Information Fusion.* 2025;114:102690. doi:10.1016/j.inffus.2024.102690
241. Lopes L, Jiao F, Xue S, et al. Dopaminergic PET to SPECT domain adaptation: a cycle GAN translation approach. *Eur J Nucl Med Mol Imaging.* Published online November 19, 2024. doi:10.1007/s00259-024-06961-x
242. Saeed U, Lang AE, Masellis M. Neuroimaging Advances in Parkinson's Disease and Atypical Parkinsonian Syndromes. *Front Neurol.* 2020;11. <https://www.frontiersin.org/articles/10.3389/fneur.2020.572976>
243. Scherfler C, Schwarz J, Antonini A, et al. Role of DAT-SPECT in the diagnostic work up of Parkinsonism. *Movement Disorders.* 2007;22(9):1229-1238. doi:<https://doi.org/10.1002/mds.21505>
244. Benamer HTS, Patterson J, Grosset DG, et al. Accurate differentiation of parkinsonism and essential tremor using visual assessment of [¹²³I]-FP-CIT SPECT imaging: the [¹²³I]-FP-CIT study group. *Mov Disord.* 2000;15(3):503-510.
245. McKeith I, O'Brien J, Walker Z, et al. Sensitivity and specificity of dopamine transporter imaging with [¹²³I]-FP-CIT SPECT in dementia with Lewy bodies: a phase III, multicentre study. *Lancet Neurol.* 2007;6(4):305-313. doi:10.1016/S1474-4422(07)70057-1
246. Palermo G, Giannoni S, Bellini G, Siciliano G, Ceravolo R. Dopamine Transporter Imaging, Current Status of a Potential Biomarker: A Comprehensive Review. *Int J Mol Sci.* 2021;22(20). doi:10.3390/ijms222011234
247. Andringa G, Drukarch B, Bol JGJM, et al. Pinhole SPECT imaging of dopamine transporters correlates with dopamine transporter immunohistochemical analysis in the MPTP mouse model of Parkinson's disease. *Neuroimage.* 2005;26(4):1150-1158. doi:<https://doi.org/10.1016/j.neuroimage.2005.03.034>
248. Hirschauer TJ, Adeli H, Buford JA. Computer-Aided Diagnosis of Parkinson's Disease Using Enhanced Probabilistic Neural Network. *J Med Syst.* 2015;39(11):179. doi:10.1007/s10916-015-0353-9
249. Zhao Y, Wu P, Wu J, et al. Decoding the dopamine transporter imaging for the differential diagnosis of parkinsonism using deep learning. *Eur J Nucl Med Mol Imaging.* Published online 2022. doi:10.1007/s00259-022-05804-x
250. Calimeri F, Marzullo A, Stamile C, Terracina G. Biomedical Data Augmentation Using Generative Adversarial Neural Networks. In: Lintas A, Rovetta S, Verschure PFMJ, Villa AEP, eds. *Artificial Neural Networks and Machine Learning – ICANN 2017*. Springer International Publishing; 2017:626-634.
251. Chuquicusma MJM, Hussein S, Burt J, Bagci U. How to fool radiologists with generative adversarial networks? A visual turing test for lung cancer diagnosis. In: *2018 IEEE 15th International Symposium on Biomedical Imaging (ISBI 2018)*. ; 2018:240-244. doi:10.1109/ISBI.2018.8363564
252. Shokraei Fard A, Reutens DC, Vegh V. From CNNs to GANs for cross-modality medical image estimation. *Comput Biol Med.* 2022;146:105556. doi:10.1016/j.combiomed.2022.105556
253. Özbeý M, Dalmaz O, Dar SU, et al. Unsupervised Medical Image Translation with Adversarial Diffusion Models. Published online July 17, 2022.

254. Islam T, Hafiz MdS, Jim JR, Kabir MdM, Mridha MF. A systematic review of deep learning data augmentation in medical imaging: Recent advances and future research directions. *Healthcare Analytics*. 2024;5:100340. doi:<https://doi.org/10.1016/j.health.2024.100340>
255. Xue S, Guo R, Bohn KP, et al. A cross-scanner and cross-tracer deep learning method for the recovery of standard-dose imaging quality from low-dose PET. *Eur J Nucl Med Mol Imaging*. 2022;49(6):1843-1856. doi:10.1007/s00259-021-05644-1
256. Guo R, Xue S, Hu J, et al. Using domain knowledge for robust and generalizable deep learning-based CT-free PET attenuation and scatter correction. *Nat Commun*. 2022;13(1):5882. doi:10.1038/s41467-022-33562-9
257. Lee KW, Chin RKY. A Comparative Study of COVID-19 CT Image Synthesis using GAN and CycleGAN. In: *2022 IEEE International Conference on Artificial Intelligence in Engineering and Technology (IICAIET)*. ; 2022:1-6. doi:10.1109/IICAIET55139.2022.9936810
258. Gu J, Yang TS, Ye JC, Yang DH. CycleGAN denoising of extreme low-dose cardiac CT using wavelet-assisted noise disentanglement. *Med Image Anal*. 2021;74:102209. doi:<https://doi.org/10.1016/j.media.2021.102209>
259. Zhou L, Schaefferkoetter JD, Tham IWK, Huang G, Yan J. Supervised learning with cyclegan for low-dose FDG PET image denoising. *Med Image Anal*. 2020;65:101770. doi:<https://doi.org/10.1016/j.media.2020.101770>
260. Kalantar R, Hindocha S, Hunter B, et al. Non-contrast CT synthesis using patch-based cycle-consistent generative adversarial network (Cycle-GAN) for radiomics and deep learning in the era of COVID-19. *Sci Rep*. 2023;13(1):10568. doi:10.1038/s41598-023-36712-1
261. Heusel M, Ramsauer H, Unterthiner T, Nessler B, Hochreiter S. GANs Trained by a Two Time-Scale Update Rule Converge to a Local Nash Equilibrium. Published online June 26, 2017.
262. Manera AL, Dadar M, Fonov V, Collins DL. CerebrA, registration and manual label correction of Mindboggle-101 atlas for MNI-ICBM152 template. *Sci Data*. 2020;7(1):237. doi:10.1038/s41597-020-0557-9
263. Månnsson LG. Methods for the Evaluation of Image Quality: A Review. *Radiat Prot Dosimetry*. 2000;90(1-2):89-99. doi:10.1093/oxfordjournals.rpd.a033149
264. Fahmi R, Platsch G, Sadr AB, et al. Single-site (123)I-FP-CIT reference values from individuals with non-degenerative parkinsonism-comparison with values from healthy volunteers. *Eur J Hybrid Imaging*. 2020;4(1):5. doi:10.1186/s41824-020-0074-2
265. Tinaz S, Chow C, Kuo PH, et al. Semiquantitative Analysis of Dopamine Transporter Scans in Patients With Parkinson Disease. *Clin Nucl Med*. 2018;43(1):e1-e7. doi:10.1097/RLU.0000000000001885
266. Seibyl JP, Marek K, Sheff K, et al. Iodine-123- β -CIT and Iodine-123-FPCIT SPECT Measurement of Dopamine Transporters in Healthy Subjects and Parkinson's Patients. *Journal of Nuclear Medicine*. 1998;39(9):1500. <http://jnm.snmjournals.org/content/39/9/1500.abstract>
267. Tossici-Bolt L, Dickson JC, Sera T, et al. Calibration of gamma camera systems for a multicentre European 123I-FP-CIT SPECT normal database. *Eur J Nucl Med Mol Imaging*. 2011;38(8):1529-1540. doi:10.1007/s00259-011-1801-5
268. Buchert R, Kluge A, Tossici-Bolt L, et al. Reduction in camera-specific variability in [123I]FP-CIT SPECT outcome measures by image reconstruction optimized for multisite settings: impact on age-dependence of the specific binding ratio in the ENC-DAT database of healthy controls. *Eur J Nucl Med Mol Imaging*. 2016;43(7):1323-1336. doi:10.1007/s00259-016-3309-5
269. Tang H, Liu H, Xu D, Torr PHS, Sebe N. AttentionGAN: Unpaired Image-to-Image Translation Using Attention-Guided Generative Adversarial Networks. *IEEE Trans Neural Netw Learn Syst*. 2023;34(4):1972-1987. doi:10.1109/TNNLS.2021.3105725
270. Saharia C, Chan W, Chang H, et al. Palette: Image-to-Image Diffusion Models. In: *Special Interest Group on Computer Graphics and Interactive Techniques Conference Proceedings*. ACM; 2022:1-10. doi:10.1145/3528233.3530757

271. Takamiya K, Iwamoto Y, Nonaka M, Chen YW. CT Brain Image Synthesization from MRI Brain Images Using CycleGAN. In: *2023 IEEE International Conference on Consumer Electronics (ICCE)*. ; 2023:1-4. doi:10.1109/ICCE56470.2023.10043572
272. Hammami M, Friboulet D, Kechichian R. Cycle GAN-Based Data Augmentation For Multi-Organ Detection In CT Images Via Yolo. In: *2020 IEEE International Conference on Image Processing (ICIP)*. ; 2020:390-393. doi:10.1109/ICIP40778.2020.9191127
273. Skandarani Y, Jodoin PM, Lalande A. GANs for Medical Image Synthesis: An Empirical Study. *J Imaging*. 2021;9. <https://api.semanticscholar.org/CorpusID:234469806>
274. Hiasa Y, Otake Y, Takao M, et al. Cross-Modality Image Synthesis from Unpaired Data Using CycleGAN BT - Simulation and Synthesis in Medical Imaging. In: Gooya A, Goksel O, Oguz I, Burgos N, eds. Springer International Publishing; 2018:31-41.
275. Cohen JP, Luck M, Honari S. Distribution Matching Losses Can Hallucinate Features in Medical Image Translation. In: Frangi AF, Schnabel JA, Davatzikos C, Alberola-López C, Fichtinger G, eds. *Medical Image Computing and Computer Assisted Intervention – MICCAI 2018*. Springer International Publishing; 2018:529-536.
276. Shamsolmoali P, Zareapoor M, Granger E, et al. Image synthesis with adversarial networks: A comprehensive survey and case studies. *Information Fusion*. 2021;72:126-146. doi:<https://doi.org/10.1016/j.inffus.2021.02.014>
277. Joshi A, Koeppe RA, Fessler JA. Reducing between scanner differences in multi-center PET studies. *Neuroimage*. 2009;46(1):154-159. doi:10.1016/j.neuroimage.2009.01.057
278. Boeve BF. REM sleep behavior disorder. *Ann N Y Acad Sci*. 2010;1184(1):15-54. doi:<https://doi.org/10.1111/j.1749-6632.2009.05115.x>
279. Dauvilliers Y, Schenck CH, Postuma RB, et al. REM sleep behaviour disorder. *Nat Rev Dis Primers*. 2018;4(1). doi:10.1038/s41572-018-0016-5
280. Iranzo A, Santamaria J, Tolosa E. The clinical and pathophysiological relevance of REM sleep behavior disorder in neurodegenerative diseases. *Sleep Med Rev*. 2009;13(6):385-401. doi:<https://doi.org/10.1016/j.smrv.2008.11.003>
281. Stoessl AJ, Lehericy S, Strafella AP. Imaging insights into basal ganglia function, Parkinson's disease, and dystonia. *Lancet*. 2014;384(9942):532-544. doi:10.1016/S0140-6736(14)60041-6
282. Rahayel S, Postuma RB, Montplaisir J, et al. A Prodromal Brain-Clinical Pattern of Cognition in Synucleinopathies. *Ann Neurol*. 2021;89(2):341-357. doi:<https://doi.org/10.1002/ana.25962>
283. Albrecht F, Ballarini T, Neumann J, Schroeter ML. FDG-PET hypometabolism is more sensitive than MRI atrophy in Parkinson's disease: A whole-brain multimodal imaging meta-analysis. *Neuroimage Clin*. 2019;21:101594. doi:<https://doi.org/10.1016/j.nicl.2018.11.004>
284. Wu P, Yu H, Peng S, et al. Consistent abnormalities in metabolic network activity in idiopathic rapid eye movement sleep behaviour disorder. *Brain*. 2014;137(12):3122-3128. doi:10.1093/brain/awu290
285. Holtbernd F, Gagnon JF, Postuma RB, et al. Abnormal metabolic network activity in REM sleep behavior disorder. *Neurology*. 2014;82(7):620. doi:10.1212/WNL.0000000000000130
286. Meles SK, Renken RJ, Janzen A, et al. The Metabolic Pattern of Idiopathic REM Sleep Behavior Disorder Reflects Early-Stage Parkinson Disease. *Journal of Nuclear Medicine*. 2018;59(9):1437-1444. doi:10.2967/jnmed.117.202242
287. Shin JH, Lee JY, Kim YK, et al. Parkinson Disease-Related Brain Metabolic Patterns and Neurodegeneration in Isolated REM Sleep Behavior Disorder. *Neurology*. 2021;97(4):e378. doi:10.1212/WNL.00000000000012228
288. Kogan RV, Janzen A, Meles SK, et al. Four-Year Follow-up of [18F]Fluorodeoxyglucose Positron Emission Tomography-Based Parkinson's Disease-Related Pattern Expression in 20 Patients with Isolated Rapid

- Eye Movement Sleep Behavior Disorder Shows Prodromal Progression. *Movement Disorders*. 2021;36(1):230-235. doi:<https://doi.org/10.1002/mds.28260>
289. de Natale ER, Wilson H, Politis M. Predictors of RBD progression and conversion to synucleinopathies. *Curr Neurol Neurosci Rep.* 2022;22(2):93-104. doi:10.1007/s11910-022-01171-0
290. Bauckneht M, Chincarini A, De Carli F, et al. Presynaptic dopaminergic neuroimaging in REM sleep behavior disorder: A systematic review and meta-analysis. *Sleep Med Rev.* 2018;41:266-274. doi:10.1016/j.smrv.2018.04.001
291. Iranzo A, Lomeña F, Stockner H, et al. Decreased striatal dopamine transporter uptake and substantia nigra hyperechogenicity as risk markers of synucleinopathy in patients with idiopathic rapid-eye-movement sleep behaviour disorder: a prospective study. *Lancet Neurol.* 2010;9(11):1070-1077. doi:10.1016/S1474-4422(10)70216-7
292. Iranzo A, Santamaría J, Valldeoriola F, et al. Dopamine transporter imaging deficit predicts early transition to synucleinopathy in idiopathic rapid eye movement sleep behavior disorder. *Ann Neurol.* 2017;82(3):419-428. doi:<https://doi.org/10.1002/ana.25026>
293. Kim R, Lee JY, Kim YK, et al. Longitudinal Changes in Isolated Rapid Eye Movement Sleep Behavior Disorder-Related Metabolic Pattern Expression. *Mov Disord.* 2021;36(8):1889-1898. doi:10.1002/mds.28592
294. Feng S, Ge J, Zhao S, et al. Dopaminergic damage pattern predicts phenoconversion time in isolated rapid eye movement sleep behavior disorder. *Eur J Nucl Med Mol Imaging.* Published online 2023. doi:10.1007/s00259-023-06402-1
295. Tang CC, Nakano Y, Vo A, et al. Longitudinal network changes and phenoconversion risk in isolated REM sleep behavior disorder. *Nat Commun.* 2024;15(1):10797. doi:10.1038/s41467-024-54695-z
296. Shen D, Wu G, Suk HI. Deep Learning in Medical Image Analysis. *Annu Rev Biomed Eng.* 2017;19(1):221-248. doi:10.1146/annurev-bioeng-071516-044442
297. Ocasio E, Duong TQ. Deep learning prediction of mild cognitive impairment conversion to Alzheimer's disease at 3 years after diagnosis using longitudinal and whole-brain 3D MRI. *PeerJ Comput Sci.* 2021;7:e560-e560. doi:10.7717/peerj-cs.560
298. Zhou P, Zeng R, Yu L, et al. Deep-Learning Radiomics for Discrimination Conversion of Alzheimer's Disease in Patients With Mild Cognitive Impairment: A Study Based on (18)F-FDG PET Imaging. *Front Aging Neurosci.* 2021;13:764872. doi:10.3389/fnagi.2021.764872
299. Wu P, Zhao Y, Wu J, et al. Differential diagnosis of parkinsonism based on deep metabolic imaging indices. *Journal of Nuclear Medicine.* Published online March 1, 2022:jnumed.121.263029. doi:10.2967/jnumed.121.263029
300. Huang Z, Jiang C, Li L, et al. Correlations between dopaminergic dysfunction and abnormal metabolic network activity in REM sleep behavior disorder. *Journal of Cerebral Blood Flow and Metabolism.* 2020;40(3):552-562. doi:10.1177/0271678X19828916
301. Han X, Wu P, Alberts I, et al. Characterizing the heterogeneous metabolic progression in idiopathic REM sleep behavior disorder. *Neuroimage Clin.* 2020;27. doi:10.1016/j.nicl.2020.102294
302. McKeith IG, Boeve BF, Dickson DW, et al. Diagnosis and management of dementia with Lewy bodies: Fourth consensus report of the DLB Consortium. *Neurology.* 2017;89(1):88-100. doi:10.1212/WNL.0000000000004058
303. Gilman S, Wenning GK, Low PA, et al. Second consensus statement on the diagnosis of multiple system atrophy. *Neurology.* 2008;71(9):670-676. doi:10.1212/01.wnl.0000324625.00404.15
304. Lu J, Ge J, Chen K, et al. Consistent Abnormalities in Metabolic Patterns of Lewy Body Dementias. *Movement Disorders.* 2022;n/a(n/a). doi:<https://doi.org/10.1002/mds.29138>
305. Huang C, Tang C, Feigin A, et al. Changes in network activity with the progression of Parkinson's disease. *Brain.* 2007;130(7):1834-1846. doi:10.1093/brain/awm086

306. Cardoso MJ, Li W, Brown R, et al. MONAI: An open-source framework for deep learning in healthcare. Published online November 4, 2022.
307. Miglis MG, Adler CH, Antelmi E, et al. Biomarkers of conversion to α -synucleinopathy in isolated rapid-eye-movement sleep behaviour disorder. *Lancet Neurol*. 2021;20(8):671-684. doi:10.1016/S1474-4422(21)00176-9
308. Jiménez-Jiménez FJ, Alonso-Navarro H, García-Martín E, Agúndez JAG. Neurochemical Features of Rem Sleep Behaviour Disorder. *J Pers Med*. 2021;11(9):880. doi:10.3390/jpm11090880
309. Iranzo A, Valldeoriola F, Lomeña F, et al. Serial dopamine transporter imaging of nigrostriatal function in patients with idiopathic rapid-eye-movement sleep behaviour disorder: a prospective study. *Lancet Neurol*. 2011;10(9):797-805. doi:10.1016/S1474-4422(11)70152-1
310. Klein JC, Eggers C, Kalbe E, et al. Neurotransmitter changes in dementia with Lewy bodies and Parkinson disease dementia in vivo. *Neurology*. 2010;74(11):885. doi:10.1212/WNL.0b013e3181d55f61
311. Högl B, Stefani A, Vidovicić A. Idiopathic REM sleep behaviour disorder and neurodegeneration — an update. *Nat Rev Neurol*. 2018;14(1):40-55. doi:10.1038/nrneurol.2017.157
312. Iranzo A, Molinuevo JL, Santamaría J, et al. Rapid-eye-movement sleep behaviour disorder as an early marker for a neurodegenerative disorder: a descriptive study. *Lancet Neurol*. 2006;5(7):572-577. doi:10.1016/S1474-4422(06)70476-8
313. Smith MT, McCrae CS, Cheung J, et al. Use of Actigraphy for the Evaluation of Sleep Disorders and Circadian Rhythm Sleep-Wake Disorders: An American Academy of Sleep Medicine Systematic Review, Meta-Analysis, and GRADE Assessment. *Journal of Clinical Sleep Medicine*. 2018;14(07):1209-1230. doi:10.5664/jcsm.7228
314. Louter M, Arends JBAM, Bloem BR, Overeem S. Actigraphy as a diagnostic aid for REM sleep behavior disorder in Parkinson's disease. *BMC Neurol*. 2014;14(1):76. doi:10.1186/1471-2377-14-76
315. Liguori C, Zuccarelli V, Spanetta M, Izzi F, Biagio Mercuri N, Placidi F. Sleep-wake cycle dysregulation in idiopathic REM sleep behaviour disorder. *J Sleep Res*. 2021;30(4). doi:10.1111/jsr.13234
316. Hammad G, Reyt M, Beliy N, et al. pyActigraphy: Open-source python package for actigraphy data visualization and analysis. *PLoS Comput Biol*. 2021;17(10):e1009514. doi:10.1371/journal.pcbi.1009514
317. Van Someren Eus J W, Lijzenga Cees, Mirmiran Majid, Swaab Dick F. Long-Term Fitness Training Improves the Circadian Rest-Activity Rhythm in Healthy Elderly Males. *J Biol Rhythms*. 1997;12(2):146-156. doi:10.1177/074873049701200206
318. Witting W, Kwa IH, Eikelenboom P, Mirmiran M, Swaab DF. Alterations in the circadian rest-activity rhythm in aging and Alzheimer's disease. *Biol Psychiatry*. 1990;27(6):563-572. doi:10.1016/0006-3223(90)90523-5
319. Welch P. The use of fast Fourier transform for the estimation of power spectra: A method based on time averaging over short, modified periodograms. *IEEE Transactions on Audio and Electroacoustics*. 1967;15(2):70-73. doi:10.1109/TAU.1967.1161901
320. NHANES - National Health and Nutrition Examination Survey Homepage. Assessed on Jun 5, 2025. <https://www.cdc.gov/nchs/nhanes/index.html>.
321. Zhong G, Bolitho S, Grunstein R, Naismith SL, Lewis SJG. The Relationship between Thermoregulation and REM Sleep Behaviour Disorder in Parkinson's Disease. *PLoS One*. 2013;8(8):e72661. doi:10.1371/journal.pone.0072661
322. Peeraully T, Yong MH, Chokroverty S, Tan EK. Sleep and Parkinson's disease: A review of case-control polysomnography studies. *Movement Disorders*. 2012;27(14):1729-1737. doi:<https://doi.org/10.1002/mds.25197>
323. Yong MH, Fook-Chong S, Pavanni R, Lim LL, Tan EK. Case Control Polysomnographic Studies of Sleep Disorders in Parkinson's Disease. *PLoS One*. 2011;6(7):e22511. doi:10.1371/journal.pone.0022511

324. Litjens G, Kooi T, Bejnordi BE, et al. A survey on deep learning in medical image analysis. *Med Image Anal.* 2017;42:60-88. doi:<https://doi.org/10.1016/j.media.2017.07.005>
325. Alzubaidi L, Bai J, Al-Sabaawi A, et al. A survey on deep learning tools dealing with data scarcity: definitions, challenges, solutions, tips, and applications. *J Big Data.* 2023;10(1):46. doi:10.1186/s40537-023-00727-2
326. Kaur K, Gill JS, Bansal PK, Deshmukh R. Neuroinflammation - A major cause for striatal dopaminergic degeneration in Parkinson's disease. *J Neurol Sci.* 2017;381:308-314. doi:<https://doi.org/10.1016/j.jns.2017.08.3251>
327. Brumberg J, Blazhenets G, Bühler S, et al. Cerebral Glucose Metabolism Is a Valuable Predictor of Survival in Patients with Lewy Body Diseases. *Ann Neurol.* 2024;96(3):539-550. doi:10.1002/ana.27005
328. Schröter N, Blazhenets G, Frings L, et al. Nigral glucose metabolism as a diagnostic marker of neurodegenerative parkinsonian syndromes. *NPJ Parkinsons Dis.* 2022;8(1):123. doi:10.1038/s41531-022-00392-x
329. Arnaldi D, Chincarini A, Hu MT, et al. Dopaminergic imaging and clinical predictors for phenoconversion of REM sleep behaviour disorder. *Brain.* 2021;144(1):278-287. doi:10.1093/brain/awaa365
330. Iranzo A, Santamaría J, Valdeoriola F, et al. Dopamine transporter imaging deficit predicts early transition to synucleinopathy in idiopathic rapid eye movement sleep behavior disorder. *Ann Neurol.* 2017;82(3):419-428. doi:10.1002/ana.25026
331. Arnaldi D, Mattioli P, Raffa S, et al. Presynaptic Dopaminergic Imaging Characterizes Patients with <scp>REM</scp> Sleep Behavior Disorder Due to Synucleinopathy. *Ann Neurol.* 2024;95(6):1178-1192. doi:10.1002/ana.26902
332. Mingels C, Chung KJ, Pantel AR, et al. Total-Body PET/CT: Challenges and Opportunities. *Semin Nucl Med.* 2025;55(1):21-30. doi:<https://doi.org/10.1053/j.semnuclmed.2024.08.003>
333. Alberts I, Hünermund JN, Prenosil G, et al. Clinical performance of long axial field of view PET/CT: a head-to-head intra-individual comparison of the Biograph Vision Quadra with the Biograph Vision PET/CT. *Eur J Nucl Med Mol Imaging.* 2021;48(8):2395-2404. doi:10.1007/s00259-021-05282-7
334. Moor M, Banerjee O, Abad ZSH, et al. Foundation models for generalist medical artificial intelligence. *Nature.* 2023;616(7956):259-265. doi:10.1038/s41586-023-05881-4
335. Yang J, Soltan AAS, Clifton DA. Machine learning generalizability across healthcare settings: insights from multi-site COVID-19 screening. *NPJ Digit Med.* 2022;5(1):69. doi:10.1038/s41746-022-00614-9
336. Habib AR, Lin AL, Grant RW. The Epic Sepsis Model Falls Short—The Importance of External Validation. *JAMA Intern Med.* 2021;181(8):1040-1041. doi:10.1001/jamainternmed.2021.3333
337. Marek K, Chowdhury S, Siderowf A, et al. The Parkinson's progression markers initiative (PPMI) – establishing a PD biomarker cohort. *Ann Clin Transl Neurol.* 2018;5(12):1460-1477. doi:10.1002/acn.3644
338. Petersen RC, Aisen PS, Beckett LA, et al. Alzheimer's Disease Neuroimaging Initiative (ADNI). *Neurology.* 2010;74(3):201-209. doi:10.1212/WNL.0b013e3181cb3e25
339. He J, Baxter SL, Xu J, Xu J, Zhou X, Zhang K. The practical implementation of artificial intelligence technologies in medicine. *Nat Med.* 2019;25(1):30-36. doi:10.1038/s41591-018-0307-0
340. Ahmed MI, Spooner B, Isherwood J, Lane M, Orrock E, Dennison A. A Systematic Review of the Barriers to the Implementation of Artificial Intelligence in Healthcare. *Cureus.* Published online October 4, 2023. doi:10.7759/cureus.46454
341. European Union. Regulation (EU) 2024/1689 of the European Parliament and of the Council of 13 June 2024 laying down harmonised rules on artificial intelligence and amending Regulations (EC) No 300/2008, (EU) No 167/2013, (EU) No 168/2013, (EU) 2018/858, (EU) 2018/1139 and (EU) 2019/2144 and Directives 2014/90/EU, (EU) 2016/797 and (EU) 2020/1828 (Artificial Intelligence Act) (Text with EEA relevance). *Official Journal of the European Union.* Published online 2024. Accessed April 4, 2025. <http://data.europa.eu/eli/reg/2024/1689/oj>

342. Apostolova I, Hellwig S, Karimzadeh A, Klutmann S, Meyer PT, Buchert R. Reliable diagnosis of nigrostriatal degeneration by dopamine transporter SPECT despite drug interaction with venlafaxine or bupropion. *Eur J Nucl Med Mol Imaging*. 2025;52(4):1549-1555. doi:10.1007/s00259-024-06989-z
343. Lever J, Krzywinski M, Altman N. Model selection and overfitting. *Nat Methods*. 2016;13(9):703-704. doi:10.1038/nmeth.3968
344. Taibi DM, Landis CA, Vitiello M V. Concordance of Polysomnographic and Actigraphic Measurement of Sleep and Wake in Older Women with Insomnia. *Journal of Clinical Sleep Medicine*. 2013;09(03):217-225. doi:10.5664/jcsm.2482
345. Matarazzo M, Obeso JA. Alpha synuclein PET imaging, a step closer to *in vivo* neuropathology in Parkinson's disease and related disorders. *Neuron*. 2024;112(15):2457-2458. doi:10.1016/j.neuron.2024.07.001
346. Smith R, Capotosti F, Schain M, et al. The α -synuclein PET tracer [18F] ACI-12589 distinguishes multiple system atrophy from other neurodegenerative diseases. *Nat Commun*. 2023;14(1):6750. doi:10.1038/s41467-023-42305-3

List of Publications

First author publications

1 - Telli T, Lopes L, Karpinski M, et al. Prognostic value of [¹⁸F]FDG- and PSMA-PET in patients evaluated for [¹⁷⁷Lu]Lu-PSMA therapy of mCRPC. *European Journal of Nuclear Medicine and Molecular Imaging*. Published online 2025. doi:10.1007/s00259-025-07198-y

2 - Lopes L, Lopez-Montes A, Chen Y, et al. The Evolution of Artificial Intelligence in Nuclear Medicine. *Seminars in Nuclear Medicine*. 2025;55(3):313-327.
doi:<https://doi.org/10.1053/j.semnuclmed.2025.01.006>

3 - Lopes L, Jiao F, Xue S, et al. Dopaminergic PET to SPECT domain adaptation: a cycle GAN translation approach. *European Journal of Nuclear Medicine and Molecular Imaging*. 2025;52(3):851-863. doi:10.1007/s00259-024-06961-x

Other publications

4 - Küper AT, Kersting D, Telli T, et al. PSMA-PET follow-up to assess response in patients not receiving PSMA therapy: Is there value beyond localization of disease? *Theranostics*. 2024;14(9):3623-3633. doi:10.7150/thno.96738

5 - Hong J, Lu J, Liu F, et al. Uncovering distinct progression patterns of tau deposition in progressive supranuclear palsy using [¹⁸F]Florozolotau PET imaging and subtype/stage inference algorithm. *eBioMedicine*. 2023;97:104835. doi:10.1016/j.ebiom.2023.104835

6 - Lu J, Clement C, Hong J, et al. Improved interpretation of ¹⁸F-florzolotau PET in progressive supranuclear palsy using a normalization-free deep-learning classifier. *iScience*. 2023;26(8):107426. doi:10.1016/j.isci.2023.107426

Submitted

7 - Lopes L, Xu Q, Lu J, et al., Deep Learning-Based Prediction of Isolated REM Sleep Behaviour Disorder Progression Using PET Imaging. Submitted to *Annals of Neurology* on March 2025.

8 - Handke A*, Lopes L*, Kesch C, et al., Transcriptomic Profiling of the Tumor Immune Microenvironment Reveals Prognostic Markers in mCRPC Patients Treated with LuPSMA Therapy. Submitted to *Theranostics* on March 2025.

Declaration of Originality

Last name, First name: Serrano Lopes, Leonor

Matriculation Number: 21-137-914

I hereby declare that this thesis represents my original work and that I have used no other sources except as noted by citations.

All data, tables, figures and text citations which have been reproduced from any other source, including the internet, have been explicitly acknowledged as such.

I am aware that in case of non-compliance, the Senate is entitled to withdraw the doctorate degree awarded to me on the basis of the present thesis, in accordance with the "Statut der Universität Bern (Universitätsstatut; UniSt)", Art. 69, of 7 June 2011.

Bern, 07/04/2025,